N° d'ordre: 41489

THESE DE DOCTORAT

présentée à

L'UNIVERSITE DE LILLE 1

Ecole Doctoral Régionale Sciences Pour l'Ingénieur Lille Nord-de-France

pour obtenir le grade de

DOCTEUR EN SCIENCES

Dans la spécialité:

Micro et Nano Technologies, Acoustique et Télécommunications

par

KHANAL MANAKAMANA

FUNCTIONAL NANOPARTICLES FOR BIOLOGICAL APPLICATIONS

Soutenue le 17 OCTOBER 2014 devant le jury composé de :

Prof. Christine MENAGER	Rapporteur	Université Pierre et Marie Curie
Dr. Jean-Olivier DURAND	Rapporteur	Institut Charles Gerhardt de Montpellier
Dr. Jean DUBUISSON	Examinateur	Institut Pasteur de Lille, Lille
Prof. Tuami LASRI	Examinateur	Université Lille 1
Dr. Aloysius SIRIWARDENA	Examinateur	Université de Picardie Jules Verne
Dr. Rabah BOUKHERROUB	Invité	Institut de Recherche Interdisciplinaire
Prof. Sabine SZUNERITS	Directrice de thèse	Université Lille 1

ACKNOWLEDGEMENT

Over the past four years, I have received support and encouragement from great number of individuals to make my academic stay in France fruitful.

First of all, I would like to give my warmest gratitude to my Ph.D. supervisor Prof. Sabine Szunerits for her continued support, guidance, scientific discussion and encouragement throughout my study period and also for the suggestion while writing manuscript and having patience in correcting it. I was fortunate to find her not only as a mentor but also as a guardian thousand miles from my country, Nepal. Her guidance has made this journey thoughtful and rewarding. I am also very grateful to her for providing me opportunities to explore researches and to learn different techniques in other labs outside France.

My deepest thanks go to Dr. Rabah Boukherroub for his suggestions, sharpening my scientific thinking which is essential for research field and for organizing lab meeting every week which helped me to learn different techniques and to broaden my knowledge in material science research.

I would like to thank Dr. Aloysius Siriwardena for suggestions and scientific discussions that he shared to us *via* email and phone and being available even after his busy schedule whenever I need to discuss my work.

A special thank goes to Dr. Jean Dubuisson for his generosity and letting me to experience the research of hepatitis C virus and helping me to develop my background in HCV and current researches in anti-HCV therapeutics.

I would like to thank Dr. Alexandre Barras for his valuable suggestions during my research work and teaching me the basic concept of lipid nanocapsules which was a new topic for me, always showing an alternative way when nothing worked during experiments either in organic syntheses or in some biological assays. His scientific thinking and nature of sharing ideas while having coffee and lunch impressed me a lot. I had enjoyed those fruitful talks.

ACKNOWLEDGEMENT

My heartfelt thanks go to all my colleagues who are actually more friends than colleagues. Nadia for always being there on my troubled days, listening my problems and discussing the solutions. Many thank to Stefka and Alex (friend version of Dr. Alexandre Barras) for being so generous and supportive almost all the times. I will always cherish all those humors, stupid jokes and meaningful discussions. Beside these, I would also like to thank Nadia and Stefka helping me to deal with prefecture issues. You people have always healed my depression during my hard times. Thank you again for the support. Also, I would like to thanks Amer, Kostian, Vladimir, Mouna, Wang Qi, Wang Qian, Palain and all the lab members for maintaining the ambiance and peaceful working environment in lab and I truly appreciate the nature of sharing the ideas among lab mates.

I would also like to express my thanks to Thibaut and Lucie who had helped me on viral assays experiments, answering my naïve questions regarding HCV, giving me company and ensuring my comfort in a completely new working place.

I am indebted to my respected Prof. Purusottam Basnet and Prof. Natasa-Skalko Basnet for their guidance and encouragement while I was in Pharmacy School. The inspiration that I got from them had actually helped me to start the academic journey in France. Also, I would like to thank Erasmus Mundus Program for providing an opportunity to explore the research areas.

My special thanks go to Region Nord Pas de Calais and Université de Lille for funding my Ph.D. fellowship.

I am always grateful to my parents, brother and sister who has supported my decision to study miles away from hometown, kept patience for years, and provided continuous emotional support and inspiration.

I have no words to explain my gratitude to my beloved husband for continuous support, encouragement and keeping faith on me during my academic carrier. He has taught me to stay positive even in the worst condition. I am indebted to his unconditional love and understanding nature despite of long distance relationship. We are eagerly waiting for togetherness after past six years.

ACKNOWLEDGEMENT

At the end, I would like to thank all the Nepali friends in Lille and Paris specially; Kalyan and Kalpana for care, giving me company during my hard and good times, Nikesh and his wife Laure for creating homely environment during festive days by inviting us in their sweet home. I will definitely miss the gathering and fun with you all.

Manakamana Khanal
18th October, 2014

TABLE OF CONTENTS

ACRONYMS **a**

RESUME/ABSTRACT **I**

OBJECTIVES **II**

Chapter 1-Nanoparticles for biological applications **1**

1.1. Introduction 1

1.2. Lipid nanocapsule (LNCs) 6

1.2.1. Physical characteristics 9

1.2.2. Therapeutic loading strategies on LNCs 9

1.3. Silica nanoparticles (Silica-NPs) 13

1.4. Magnetic particles (MPs) 16

1.5. Nanodiamonds (NDs) 20

1.6. References 27

Chapter 2-Hepatitis C Virus (HCV): managing HCV infection efficiently **35**

2.1. Hepatitis C Virus (HCV) 35

2.2. Replication of HCV in host cell 36

2.3. HCV entry process 39

2.4. Experimental models for the study of HCV infection *in vitro* 41

2.4.1. HCV cell culture infection system (HCVcc) 42

2.4.2. HCV pseudotyped particles (HCVpp) 42

2.5 Boronic acid derivatives as antiviral agents 43

2.6. References 48

Chapter 3-Phenylboronic acid-modified nanoparticles as potent antiviral therapeutics **51**

3.1. Functionalization of inorganic nanostructures with boronic acid ligands 53

3.2. Physico-chemical characteristics of boronic acid modified nanoparticles 58

3.3. Effect of nanoparticles on Huh-7 cell viability 60

3.4. HCV entry inhibition assay by boronic acid-modified NPs 61

3.5. Competitive binding experiment with mannose 64

3.6. Role of triazole ring in inhibition assay 65
3.7. Conclusion 66
3.8.References 68
Chapter 4-Boronic acid-modified lipid nanocapsules as a novel class of highly efficient hepatitis C viral inhibitor 71
4.1. Synthesis of amphiphilic boronic acid (ABA) compound 72
4.2. Post-insertion of the ABA onto lipid nanocapsule (LNCs) 73
4.3. Effect of BA-LNCs on Huh-7 cell viability 77
4.4.Virus entry inhibition assay 78
4.5. Mode of action of the inhibitory effect of BA-LNCs 80
4.5.1. Competitive binding experiment with mannose /Man-9 81
4.5.2. HCV pseudotyped particles 82
4.6. Conclusion 83
4.7. References 85
Chapter 5-Nanodiamond as a nanovechicle for gene delivery 86
5.1.Gene delivery 86
5.2. Extra and intracellular barriers for gene transfer 88
5.3. Nanoparticles for cellular transfection 90
5.4. Nanodiamonds (NDs)-based gene delivery system 91
5.5. Multifunctional nanodiamonds for gene delivery 93
5.6. References 95
Chapter 6- Orthogonal surface modification strategy of nanodiamonds using dopamine anchors for gene delivery 98
6.1. Anchoring of different dopamine ligands onto NDs 100
6.2. Subsequent post-fuctionalization of ND-dop-PEG+N_3 particles 103
6.3. ND-dop-PEG-$(NH_2)_2$ based DNA delivery 105
6.3.1. Loading of plasmid DNA (pDNA) onto nanodiamonds 106
6.3.2. Effect of amine-terminated NDs on cell viability 108
6.3.3 Cellular transfection 109
6.4. Conclusion 110

6.5. References 110

Chapter 7-Conclusion and perspectives 113

APPENDIX 115

Experimental part 115

8.1. Materials. 115

8.2. Synthesis of organic compounds and nanoparticles 115

8.2.1. Copper iodide triphenylphospine ($CuI(PPh_3)$) 115

8.2.2. Boronic acid (BA)-derivative (1) 4-[(1-oxo-4-pentyn-1-yl)amino]phenylboronic acid 116

8.2.3. 2-nitrodopamine 116

8.2.4. Amphiphilic boronic acid (ABA) 117

8.2.5. 1-(6-{[2-(3,4-dihydroxyphenyl)ethyl]amino}-6-oxohexyl)triaza-1,2-dien-2-ium (4), ($DOP\text{-}N_3$) 118

8.2.5.1. 6-azidohexanoic (2) 118

8.2.5.2. 6-azidohexanoic N-hydroxysuccinimide ester (3) 118

8.2.5.3. 1-(6-{[2-(3,4-dihydroxyphenyl)ethyl]amino}-6-oxohexyl)triaza-1,2-dien-2-ium (4) 119

8.2.6. Polyethylene glycol terminated dopamine derivatives (dop-PEG) (10) 119

8.2.6.1. 2-[2-(2-azidoethoxy)ethoxy]ethanol (6) 120

8.2.6.2. 2-[2-(2-aminoethoxy)ethoxy]ethanol (7) 120

8.2.6.3. 5-({2-[2-(2-hydroxyethoxy)ethoxy]ethyl}amino)-5-oxopentanoic acid (8) 120

8.2.6.4. 5-[(2,5-dioxopyrrolidin-1-yl)oxy]-N-{2-[2-(2-hydroxyethoxy)ethoxy]ethyl}-5-oxopentan amide (9) 120

8.2.6.5. N1-(3,4-dihydroxyphenethyl)-N5-{2 [2(2hydroxyethoxy)ethoxy]ethyl} pentanediamide (10), dop-PEG 121

8.2.7. Silica particles 121

8.2.7.1. Silica-NH_2 121

8.2.7.2. Silica-N_3 121

8.2.7.3. Silica-BA 122

8.2.8. Magnetic particles 122

8.2.8.1. MP-NH_2 122
8.2.8.2. MP-N_3 122
8.2.8.3. MP-BA 122
8.2.9. Nanodiamonds (NDs) 122
8.2.9.1. ND-N_3 122
8.2.9.2. ND-BA 123
8.2.10. Lipid nanocapsule 123
8.2.10.1. Preparation of LNCs 123
8.2.10.2. Formation of boronic-acid LNCs (BA-LNCs) 124
8.2.11. Preparation of dopamine-derived nanodiamonds 124
8.2.12. Preparation of amine terminated NDs from silanization method (ND-sil-NH_2) 125
8.3. Determination of the amount of active boronic acid on the NPs-BA 125
8.3.1. ND-BA, MP-BA and Silica-BA 125
8.3.2. BA-LNCs 125
8.4. Stability study of NDs in MQ water 126
8.5. Preparation of NDs/pDNA complexes 126
8.6. Gel retardation 126
8.7. Biological assays 126
8.7.1. Cell culture 126
8.7.2. Cytotoxicity assay 127
8.7.3. Virus entry inhibition assay 127
8.7.4. Competitive assay with mannose and Man-9 128
8.7.5. HCV pseudotyped particles (HCVpp) 129
8.7.3. *In vitro* transfection studies 129
8.8. Instrumentations 130
8.8.1. Fourier transformed infrared spectroscopy 130
8.8.2. X-ray photoelectron spectroscopy 130
8.8.3. Particle size measurements 130
8.8.4. Confocal microscopy 130
8.9. References 131
LIST OF PUBLICATIONS 132

TABLE OF CONTENTS

ACRONYMS

ACN	*Acetonitrile*
APTMS	*4-aminopropyltrimethoxysilane*
ATP	*Adenosine triphosphate*
ABA	*Amphiphilic boronic acid*
BA	*Boronic acid*
BA-LNCs	*Boronic acid modified lipid nanocapsules*
BH_3.	*Boron hydride*
BSA	*Bovine serum albumin*
cAMP	*Cyclic adenosine monophosphate*
$CDCl_3$	*Deuterated chloroform*
CLDN1	*Claudin 1*
CMC	*Critical micellar concentration*
Cu (I)	*Copper iodide*
$CuI(PPh_3)$	*Copper iodide triphenylphospine*
DAPI	*4'-6-diamidino-2-phenylindole*
DCC	*N,N'-dicyclohexylcarbodiimide*
DCM	*Dichloromethane*
DMAEMA	*2-(dimethylamino)ethyl methacrylate*
DMAP	*4-dimethylaminopyridine*
DMEM	*Dulbecco modified Eagle medium*
DMF	*Dimethylforamide*
DMSO	*Dimethyl sulfoxide*
DNA	*Deoxyribonucleic acid*
DOP-N_3	*Azide-terminated dopamine derivative*
DOP-PEG	*Polyethylene glycol-terminated dopamine derivative*
DSPE	*1,2-distearoyl-sn-glycero-3-phosphoethanolamine- N-[carboxylic acid (polyethylene-glycol)]*
EDTA	*Ethylenediaminetetraacetic acid*
EDC	*N-(3-Dimethylaminopropyl)-N'-ethylcarbodiimide hydrochloride*
ER	*Endoplasmic reticulum*
EPR	*Enhanced permeability and retention*

ESI	*Electron spray ionization*
EtoAC	*Ethylacetate*
FCS	*Fetal calf serum*
FDA	*Food and Drug Administration*
FT-IR	*Fourier transformed-infrared spectroscopy*
GFP	*Green fluorescence protein*
GNPs	*Gold nanoparticles*
G-Ins	*Gluconic acid-modified insulin*
HCC	*Hepatocellular carcinoma*
HCV	*Hepatitis C Virus*
HCVcc	*HCV cell culture systems*
HCVpp	*HCV pseudotyped particles*
Hex	*Hexane*
HIV	*Human Immunodeficiency Virus*
HLB	*Hydrophilic lipophilic balance*
HNO_3	*Nitric acid*
H_2SO_4	*Sulfuric acid*
HS	*Heparin sulfate*
HTS	*High throughput screening*
Huh-7	*Hepatocyte derived cellular carcinoma cell line*
IFNα	*Interferon-alpha*
IC_{50}	*Half maximal inhibitory concentration*
IRES	*Internal ribosome entry site*
JAM	*Junction-associated adhesion molecule*
JFH	*Japenese Fulminant Hepatitis*
KBr	*Potassium bromide*
LDLR	*Low-density lipoprotein receptor*
$LiAlH_4$	*Lithium aluminium hydride*
LNCs	*Lipid nanocapsules*
MAb	*As monoclonal antibody*
Man-9	*Mannonanose-di-(N-acetyl-D-glucosamine)*
MLV	*Murin leukemia virus*
MPS	*Mesoporous silica*
MPS	*Mononuclear phagocyte system*

MPs	*Magnetic nanoparticles*
MP-NH_2	*Nitrodopamine-modified particles*
MP-N_3	*Azido-terminated magnetic particles*
MRI	*Magnetic resonance imaging*
MTS	*3-(4,5-dimethylthiazol-2-yl)-5-(3-carboxymethoxyphenyl)-2-(4-sulfophenyl)-2H tetrazolium*
MTT	*(3-(4,5-dimethylthiazol-2-yl)-2,5-diphenyltetrazolium bromide)*
nAb	*Neutralizing antibody*
NaCl	*Sodium chloride*
NaOH	*Sodium hydroxide*
NC	*Non-coding*
NDs	*Nanodiamonds*
NHS	*N-Hydroxysuccinimide*
NIH	*National Institute of Health*
NMR	*Nuclear magnetic resonance*
NPs	*Nanoparticles*
NPs-BA	*1-oxo-4-pentyn-1-yl) amino]phenylboronic acid or boronic acid derivative (**1**)*
NPC	*Nuclear pore complexes*
NS	*Non-structural*
$(N\text{-}V)^-$	*Nitrogen-vacancy center*
OCLN	*Occluding*
PBS	*Phosphate buffer saline*
pDNA	*Plasmid deoxyribonucleic acid*
PEG	*Polyethylene glycol*
PEI	*Polyethylenimine*
PET	*Positron emission tomography*
PDI	*Polydispersity index*
PIT	*Phase-inversion temperature*
pKa	*Ionization constant*
PLGA	*Poly(lactic-co-glycolic acid)*
PLL	*Poly-L-lysine*
PS-ON	*Phosphorothioate oligonucleotides*
Rcf	*Relative centrifugal force*
RISC	*RNA-induced silencing complex*

ACRONYMS

RNA	*Ribonucleic acid*
ROS	*Reactive oxygen species*
Silica-NPs	*Silica nanoparticles*
Silica-NH_2	*Amine terminated silica nanoparticles*
Silica-N_3	*Azide terminated silica nanoparticles*
siRNA	*Silencer RNA*
$SOCl_2$	*Thionyl chloride*
SRB1	*Scavenger receptor class B type 1*
SPIO	*Superparamagnetic iron oxide nanoparticle*
TEA	*Triethylamine*
TEOS	*Tetraethyl orthosilicate*
THF	*Tetrahydrofuran*
THP-1	*Human macrophage-like cells*
TNF	*Tumor necrosis factor*
UTR	*3'untranslated region*
VSVg	*Vesicular stomatitis virus glycoprotein G*
XPS	*X-ray photoelectron spectroscopy*
ZO	*Zona occludens*

RESUME

Les nanoparticules fonctionnalisées continuent de susciter beaucoup d'interêt dans les applications biomédicales et les essais biologiques. Elles sont devenues un élément clé dans la recherche en nanobiotechnologie. Un des axes primordiaux des travaux de recherche est le développement de stratégies polyvalentes de fonctionnalisation de surface pour différentes nanoparticules allant de nanostructures de diamants à des nanoparticules d'oxyde de fer, des particules de silice et des nanocapsules lipidiques.

Un des objectifs en particulier a été l'introduction de diverses fonctionnalisations sur les mêmes nanoparticules en utilisant soit des ligands dérivés de la dopamine ou soit par chimie « click » de Cu(I) catalysé. Il en résulte des nanostructures bien dispersées fonctionnalisées avec différents ligands à leurs surfaces. Les applications de ces nanostructures pour l'inhibition des infections virales et pour la délivrance de gènes ont été étudiées. En effet, l'inhibition de l'entrée du VHC a été identifiée comme étant une stratégie thérapeutique potentielle. Il a pu être démontré que différentes nanoparticules peuvent être efficacement conçues pour afficher les propriétés de lectine et se comporter donc comme des inhibiteurs efficaces d'entrée du virus *in vitro*. Les pseudo-lectines étudiées ici comprennent les nanoparticules dérivées du fer, de silice, du diamant et des nanocapsules lipidiques comportant toutes des fragments d'acide boronique attachés à leurs surfaces.Par ailleurs, le potentiel des nanoparticules de diamant pour la délivrance de gènes a été étudié. Des particules PEGylées de diamant dispersées dans l'eau et biocompatibles ont été préparées en utilisant différents ligands de dopamine et ont été testées pour leur pouvoir à transfecter des gènes *in vitro*.

Mots clés : nanoparticules fonctionnalisées, chimie « click », ligand dérivés de dopamine, nanodiamants, virus de l'hépatite C (VHC), l'acide boronique, transfection.

ABSTRACT

Functionalized nanoparticles continue to attract interest in biomedical applications and bioassays and have become a key focus in nanobiotechnology research. One of the primal focuses of the research work was the development of versatile surface functionalization strategies for different nanoparticles ranging from diamond nanostructures to iron oxide nanoparticles, silica particles and lipid nanocapsules.

One particular aim was the introduction of various functionalities onto the same nanoparticles using either dopamine-derived ligands or Cu(I) catalyzed "click" chemistry strategies. This resulted in well-dispersed nanostructures with different ligands present on the surface of the nanostructures. The possibilities to use such nanostructures for the inhibition of viral infections and for gene delivery were investigated. Indeed, inhibiting the entry of HCV has been identified as a potential therapeutic strategy. It could be demonstrated that various nanoparticles can be efficiently engineered to display "lectin-like" properties and indeed behave as effective viral entry inhibitors, *in vitro*. The pseudo-lectins investigated here include iron-, silica-, diamond-, (lipid nanocapsule)-derived nanoparticles all featuring surface-attached boronic acid moieties. In parallel to work on HCV entry inhibition, the potential of diamond nanoparticles as gene delivery system was investigated. Water dispersible and biocompatible polypegylated diamond particles were prepared using different dopamine ligands and their effect on gene delivery has been studied.

Key words: Functionalized nanoparticles, "click" chemistry, dopamine-derived ligand, nanodiamonds, hepatitis C virus (HCV), boronic acid, gene delivery

OBJECTIVES

The past decade has observed significant advancement in the field of nanobiotechnology. Functionalized nanoparticles continue to attract interest in biomedical applications and bioassays and have become a key focus in nanobiotechnology research. The use of nanomaterials in biomedical applications is of great interest since their size scale is similar to biological molecules and structures. Recent studies have shown that integrating biological components with nanomaterials can revolutionize the field of pharmacology and help to tackle diseases at a molecular level. In this thesis, different surface modification strategies have been developed. An effort was put mainly on the surface modification of nanodiamonds, (NDs), silica NPs (Silica-NPs), magnetic particles (MPs) and lipid nanocapsule (LNCs). These particles were investigated for their possibility to inhibit hepatitis C virus (HCV) cellular entry and cellular transfection.

After a general overview on nanoparticles for biological applications (**Chapter 1**), a brief description on hepatitis C virus and the importance of boronic acid ligands for viral entry will be discussed (**Chapter 2**). **Chapter 3** outlines the synthesis and characterizations of the first generation boronic acid-modified NPs and their ability to inhibit HCV entry. In this thesis, we have developed common surface modification strategies for NDs, Silica-NPs and MPs with boronic acid derivative, which has served as 'proof-of-concept' for the requirement of multivalent boronic acid derivatives for HCV entry inhibition. The NPs used in this chapter had shown the stability issues which is believed to limit the level of inhibition. Based on the result of Chapter 3, we have designed stable LNCs decorated with multiple copies of boronic acid to develop highly efficient HCV entry inhibitor (**Chapter 4**) which could be further implemented *in vivo* study.

Subsequently, versatile surface chemistry and superior biocompatible nature of inert nanodiamonds as compare to other carbon-based materials, was further explored. In **Chapter 5**, a brief introduction of gene delivery will be presented, summarizing the limiting extra and intra cellular barriers that have to be faced by nanocarriers mediated gene transfer. This will be followed by **Chapter 6,** where the development of stable multifunctional nanodiamonds

and its ability to gene delivery is described. **Chapter 7** summarizes the results and gives some perspectives of the work.

CHAPTER 1

Nanoparticles for biological applications

1.1. Introduction

The fields of nanotechnology, in which the particles of nanometer sized structures are manipulated on the molecular or atomic level, are recently gaining massive attention. One of the expanding branches of nanotechnology is nanomedicine where nanostructures are either used to carry drug for safe delivery to the targeted site or used as a contrasting agents for the various imaging techniques (**Figure 1.1**). The foremost reason for the increased interest in nanostructures is their fascinating properties which are barely found in the bulk materials.

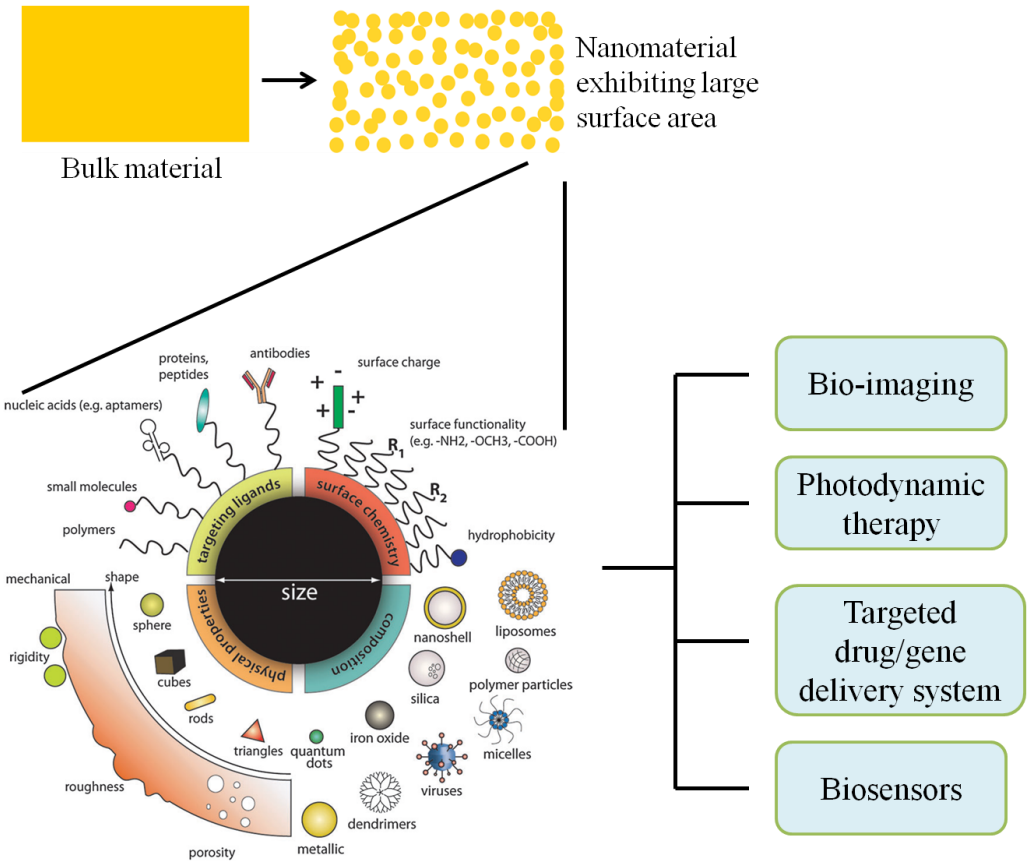

Figure 1.1. Use of nanoparticles for various bioapplications [1].

Nanoparticles (NPs) can be assembled from various material compositions with different physical and chemical properties and functionalized with numerous ligands for biological targeting. Such flexibility in designing nanomaterials enables researchers to tailor nanoparticle for specific intracellular applications as contrast agents, drug delivery vehicles, and therapeutics [1-3]. In addition, NPs loaded with therapeutics or diagnostics are considered 'value-added' in that they are jointly capable of more than the sum of each component individually. The power of NPs lies in its large surface to volume ratio that allows huge loading of therapeutics and/or specific receptor recognizing agent well on the surface of NPs These smartly designed NPs have proved to prolong the shelf-life of potent drugs, able to target the site of action and thus minimize the possible side-effects of the drugs, to diminish the solubility issues of hydrophobic drug and therefore, help to improve the efficacy of drug by increasing the bioavailability of therapeutic agents [4-6]. For instance, an important characteristic of tumors is the enhanced permeability and retention (EPR) effect. This is often exploited in NP-based therapies as the small size of the nanostructures allow them to pass through fenestrate and the comprised lymphatic drainage causes them to accumulate, thereby passively targeting tumors [7]. A large number of NPs-based products (**Table 1.1 and Table 1.2**) have been approved and used for both diagnostic and therapeutic purposes, and are recently under clinical trials [8-10]. These uncountable NPs products actually reflect the extended area of intended applications and the vibrancy underlying on this field.

Generally, NPs are categories into two groups i.e. inorganic and organic NPs [11] and some of the commonly used nanoparticles under these groups are summarized in **Figure 1.2**. Inorganic nanoparticles comprise metal, metal oxides and semiconductors. These inorganic NPs often possess unique electric, magnetic, optical, and plasmonic properties due to the quantum mechanical effects at nanoscale level [12]. Tremendous efforts have been put into the fabrication of inorganic nanomaterials with controlled size, shape, and compositions [13, 14]. Most of these inorganic materials are indeed commercialized and some of them are listed in **Table 1.1** along with applications and the diseases that are targeted by them.

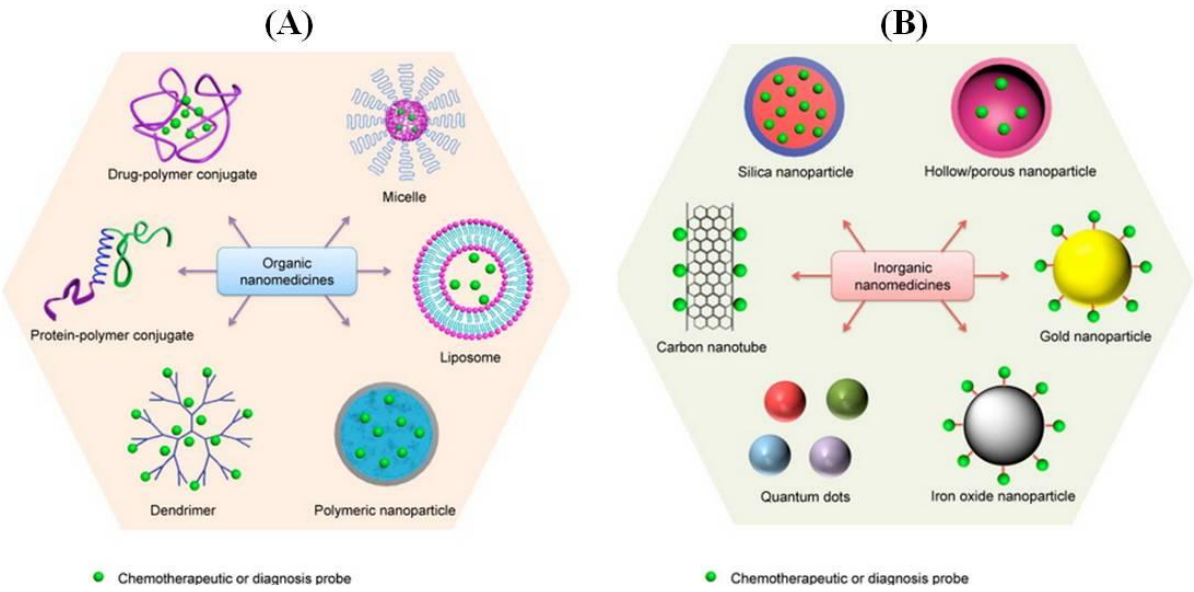

Figure 1.2. Classification of nanomaterials that are commonly used as nanomedicine. Some examples of widely used organic (A) and inorganic nanomedicines (B) [15].

Table 1.1. Inorganic nanoparticles and their current development stage [11].

Commercial name	Material	Application	Target disease	Development stage
Feridex I.V.®	Dextran-coated SPIO	MRI contrast agent	Liver tumors	FDA approval in 1996
GastroMARK™	Silicone-coated SPIO	MRI contrast agent	Gastrointestinal forms of cancer	FDA approval in 1996
Resovist R®	Carboxydextrane-coated SPIO	MRI contrast agent	Liver tumors	EU approval in 2001
Acticoat	Silver nanoparticles	Antimicrobial barrier dressing	Wound healing	FDA approval in 2005
NanoTherm	Aminosilane-coated SPIO	Magnetic thermotherapy	Brain tumors	EU approval in 2010
			Prostate and pancreatic carcinoma	Phase I
NBTXR3	Hafnium oxide	Radiation therapy	Soft-tissue	Phase 1

	nanoparticle		sarcoma	
-	Silica-gold nanoparticles	Photothermal ablation of atherosclerotic plaques	Atherosclerosis	Phase 1/phase 2
AuroShell®	Gold@silica nanoshells	Photothermal therapy	Refractory head and neck cancers	Phase 1
			Primary and metastatic tumors in the lung	Approved by FDA for clinical trials in 2012
Aurimmune	TNF-α-bound PEGylated colloidal gold particles	Targeted delivery of TNF-α	Solid tumors	Completed phase 1
Cornell dots	Silica nanoparticles embedded with fluorophores or radioactive iodine	Fluorescence/PET contrast agents	Cancer	Approved by FDA for clinical trials in 2011

Abbreviations: US Food and Drug Administration (FDA), positron emission tomography (PET), clinical trial phases (phase 1/2), superparamagnetic iron oxide nanoparticle (SPIO), tumor necrosis factor (TNF).

Among inorganic nanomaterials, gold, magnetic and silica nanoparticles are often used in biology for bio-imaging and targeted drug delivery systems. In this thesis, we have exploited different strategies of surface modifications of two metal oxides particles namely, magnetic nanoparticles (MPs) and silica nanoparticles (Silica-NPs) for grafting multiple copies of chemically synthesized small organic molecules, which have been investigated further for the inhibition of hepatitis C virus (HCV) entry in the targeted cells.

Another class of nanoparticles that is broadly used for biomedical purposes like diagnosis, imaging and therapeutic delivery are organic nanoparticles [16, 17] which consist of wide range of nanoparticles like polymeric particles, liposomes, lipid nanocapsules (LNCs), dendrimers, hydrogels and so on [16]. Different size of nanoparticles have been prepared using various kinds of biodegradable polymers like polylactide-polyglycolide, polycaprolactones and also proteinous materials like albumin and collagen [18]. Some

examples of organic nanomaterials and their current development stages are grouped in **Table 1.2.**

Table 1.2. Organic nanoparticles and their current development stage [19].

Commercial name	Material	Application	Target	Development stage
Abraxane	Protein	Cancer therapy	Breast	FDA approved
Doxil/Caelyx	Liposome	Cancer therapy	Various forms	FDA approved
Oncaspar	Polymer	Cancer therapy	Acute lymphoblastic Leukemia	FDA approved
CALAA-01		Cancer therapy	Various forms	In phase 2 clinical trials
VivaGel	Dendrimer	Microbicide	Cervicovaginal	In phase 2 clinical trials
Genexol-PM	Micelle	Cancer therapy	Various forms	In phase 4 clinical trials
Leuprolide Depot (Lutrate)	*PLGA	Cancer therapy	Prostrate Cancer	In phase 3 clinical trials

*PLGA = Poly (lactide-co-glycolide)

Organic NPs differ theoretically from inorganic NPs in terms of the principles of production and the materials used. Inorganic NPs are normally formed by the precipitation of inorganic salts. Only clustering of a few atoms is required sometimes for the formation of inorganic NPs. The nature of binding among atoms can be different: covalent, metallic, etc, but in any case, the inorganic structure forms a three-dimensional arrangement with linked atoms. Regarding this, the closest organic NPs to an inorganic one would be a dendrimer, which is a single-molecule NP [20]. Most of the organic NPs are formed by several organic molecules which are driven together by self-organization or chemical binding [21]. For the synthesis of organic NPs, with an exception of dendrimers and some other polymer NPs, organic molecules that can arrange themselves three-dimensionally are generally required. Also another important difference from inorganic NPs is that many of the organic NPs, due to the weak nature of the interactions holding them together, have a dynamic character, for instance, micelles and vesicles can fuse and generate larger particles. Moreover, the continuous addition of surfactant to a micellar solution can indeed increase the size of the micelles and even change shape from spherical to cylindrical over the second critical micellar

concentration (CMC) [22]. In case of micelles that are considered as the smallest organic NPs, the size can be controlled by the length of surfactant and moreover, the smallest size that could be achieved are that of the sphere with a radius equal to the length of the surfactant in the micellar phase [23]. Again, dendrimers, as a single-molecule NPs, are an exception and can have a controllable size from 1-100 nm [24].

One of the most important features of organic NPs is that they offer relatively simple routes for the encapsulation of materials. This together with the fact that the molecules used for the fabrication of the organic NPs can be biodegradable makes organic NPs the most appealing systems for drug delivery and biomedical applications. In this thesis, we have worked on lipid nanocapsules (LNCs) that fall under the organic nanomaterials. All the ingredients of LNC formulation are derived from organic materials and are bio-degradable.

In this thesis, lipid nanocapsules (LNCs) were used next to inorganic nanostructures such as silica (Silica-NPs), magnetic particles (MPs), and detonated nanodiamonds (NDs). A particular emphasis was placed on the use of nanoscale diamond particles, one of the highly promising nanomaterials [25]. Before discussing our results on the application of these nanomaterials, some general outline about these nanostructures are given below.

1.2. Lipid nanocapsules (LNCs)

During the period when nanoparticles were investigated more for the development of passive/active targeting of drug delivery system, Heurtault et al. for the first time designed and patented LNC [26]. LNCs are biomemetic carriers that mimic lipoproteins. Their size ranges from 20-100 nm, and they are recognized as a hybrid structure between polymer nanocapsule and liposomes. Compared to liposomes, LNC possesses many advantages regarding stability and excipients. For instance, liposomes are manufactured by using organic solvent and are more prone to be leaky and unstable in biological fluids, where as LNCs are prepared by solvent-free, soft energy procedure and present a great stability (with physical stability up to 18 months) [26].

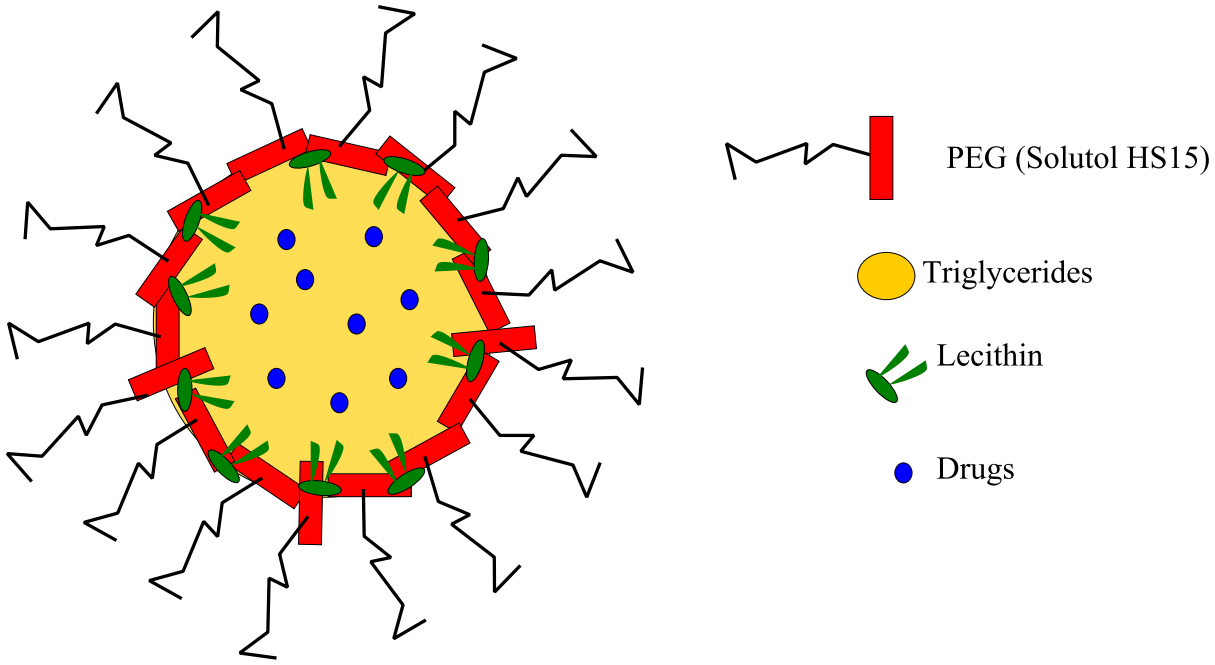

Figure 1.3. Schematic depiction of LNC prepared by the phase inversion temperature method.

LNCs (**Figure 1.3**) comprise of an oily core, corresponding to medium-chain triglycerides surrounded by a membrane made from a mixture of lecithin and a pegylated surfactant. The formulation of LNCs basically relies on the phase-inversion temperature (PIT) phenomenon of an emulsion leading to LNCs with good mono-dispersion.

The principal components of LNC are based on an oily phase, an aqueous phase and a nonionic surfactant. The oily phase comprises of triglycerides of capric and caprylic acids which is commercially recognized as Labrafac® WR 1349. Likewise, the hydrophilic surfactant is the mixture of free PEG 660 and PEG 660 hydroxystearate, commercially available as Solutol® and the aqueous phase consists of MiliQ® water and sodium chloride. In addition to these, another surfactant Lipoid® composed of 69 % phosphatidylcholine soya bean lecithin is also used in small proportion to increase the LNC stability [27, 28]. All these inactive pharmaceutical ingredients are approved by Food and Drug Administration (FDA). The ratios of different constituents have different influences on LNCs formulation and stability which are demonstrated in **Table 1.3.**

Table 1.3. Factors influencing the formulation and stability of LNC prepared by PIT method.

Components/Factors	Effects	References
Solutol®	Major influence on LNC formation and stability	[29-31]
Temperature cycles	Favoring LNC formulation and improving the quality of LNC dispersion	[31, 32]
Labrafac®	Increase of LNC size	[30]
NaCl	Decrease of PIT	[26, 33]
Lipoid®	Stabilizing the LNC rigid shell	[28, 34]

According to the patent filed by Heurtault et al. in 2002, the preparation process involves two steps wherein, first step consists in mixing all the components (proportion may vary as per to the study) under magnetic stirring and heating from room temperature to T2 temperature, above the PIT, to obtain a w/o emulsion (**Figure 1.4**). This is further followed by a cooling process to the T1 temperature, below PIT, forming o/w emulsion. Several temperature cycles crossing the phase-inversion zone between T2 and T1 are then performed.

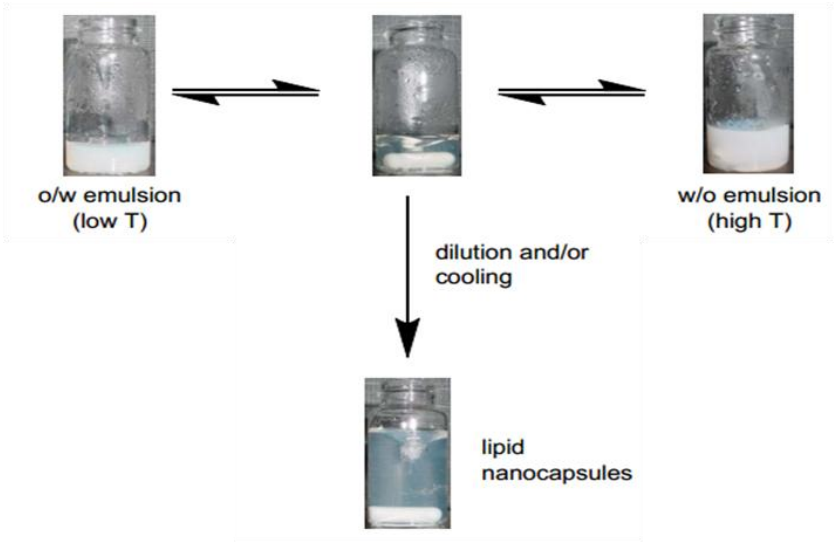

Figure 1.4. Preparation of LNC using low-energy method based on phase inversion induced by temperature change [26].

Accordingly, second step is an irreversible shock which is induced by sudden dilution with cold water added to the mixture that has been maintained at the previously defined temperature. Three temperatures cycle of heating and cooling at the rate of 4 °C/min are usually applied between 85 and 60 °C [26, 35].

1.2.1. Physical characteristics

As mentioned earlier, the LNC size and dispersity are highly reliant on the proportion of the components used. The average volume size of LNC ranges from 20 to 100 nm and exhibits a very narrow range of dispersity (PDI < 0.3). Percentage of Solutol® plays a major role in determining the LNC diameters and it's inversely proportional to the diameter of LNC. It means the higher proportion of Solutol® results in the considerable decrease in the average particle diameter. On the other hand, the increased proportion of oil leads to larger LNC diameter while the proportion of water has no effect on the diameter. Moreover, it has been revealed that an increasing number of cycles can improve the size and dispersion of LNC. In case of lower surfactant used in the formulation, the higher number of cycle is required to stabilize LNC dispersion [31]. Generally, LNCs have negative surface charge due to the negative contribution of phospholipids molecules and the presence of PEG dipoles in their shell [28].

1.2.2. Therapeutics loading strategies on LNC

Therapeutics loading on LNC can be done in two ways, either by encapsulating the lipophilic drug into the capsule during the LNC preparation process or by modifying the rigid shell of LNC by post-insertion technique. In the case of encapsulation of hydrophobic drug, an efficient drug-loading mechanism with encapsulation rates has been reported over 90 % [36], which is much higher than compare to liposomes [37]. Both passive and active targeting is possible with LNCs because of their rigid shell that allows the surface modification. Colloidal drugs are rapidly removed from the blood circulation by the mononuclear phagocyte system (MPS), mostly by Kuffer cells in liver, macrophage in spleen and bone marrow [38] considering colloidal drugs as foreign bodies. Nanoparticles coated with PEG and its derivatives are proven to decrease the opsonization and increase the half-life of those PEGyated colloidal systems in the blood circulation [39, 40]. LNC improves passive targeting due to the shell consisting of a PEG at high density [41]. While passive targeting concerns with MPS and increasing half-life of colloidal system in bloodstream, active targeting involves the attachment of a homing moieties, such as monoclonal antibody (MAb) or a ligand, in order to deliver a drug to pathological sites or to cross biological barriers based on molecular recognition process. The development of immune-nanocapsule is possible due to the rigid shell that facilitates the post-insertion.

Post-formulation strategies have been gaining popularity where nanoparticles are considered as platform for interfacial modification. Organic chemistry offers several ways to achieve the post-formulation goal [42, 43] but most of coupling reactions have to be carried out in organic solvent or need organo-metallic compounds and to remove these undesired components extra effort is required. Recently, the water-solvent based copper catalyzed 'click' reaction has facilitated the modification of NPs [44, 45]. However, the physical methods without addition of any reagent are always preferable and particularly, a method called post-insertion has been widely used to modify the surface of liposomes [46, 47]. The method is based on the incubation of liposomes with a micellar suspension of the added surfactant which results in transfer of the surfactant inside the lipidic bilayer of liposome. The commonly used surfactant is PEG due to its ability to increase colloidal stability and enhance blood circulation time by decreasing macrophase up-take [48, 49].

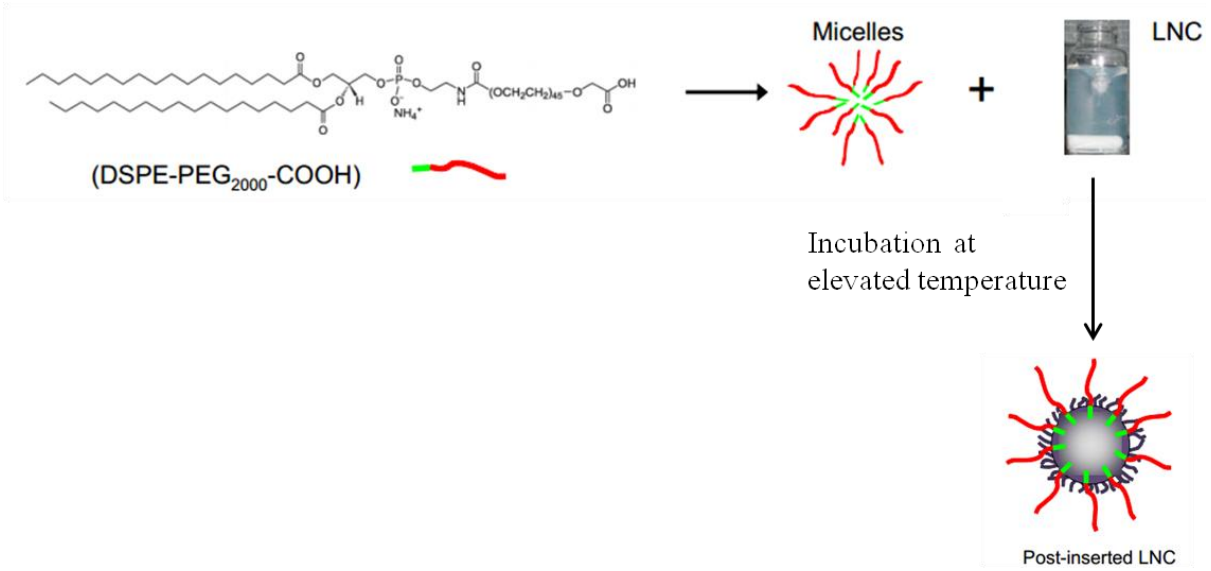

Figure 1.5. Post-insertion of amphiphilic phosopholipids-PEG i.e. 1,2-distearoyl-sn-glycero-3-phosphoethanolamine- N-[carboxylic acid (polyethylene-glycol)].

Pierrier and co-workers successfully applied the similar method to LNCs using amphiphilic phospholipids-PEG [50]. The study was generally focused on the feasibility of post-insertion (**Figure 1.5**) into LNCs and the effect of the length of the hydrophilic part. The study showed that the post-insertion process depends on temperature and conformation of PEG chains from Solutol HS-15 which is supposed to favor the transfer of micellar amphiphilic phospholipids-PEG to LNCs. Beside these, post-insertion also depends on the

concentration of amphiphilic phospholipids-PEG and the result obtained has suggested that the molecules have to be associated into micelles in order for post-insertion to occur. Relation between the time and temperature for post-insertion process is showed in **Table 1.4.**

Table 1.4. Relation between temperature and post-insertion duration [50].

Post-insertion temperature (°C)	Time for completion of the process (min)
25	No post-insertion
37	240
45	180
60	90

It has been shown in the **Table 1.4** that the post-insertion process can also be applied to the thermo-sensitive groups by increasing the incubation duration. Though both low-HLB (hydrophilic lipophilic balance) and high-HLB amphiphiles are acceptable for post-insertion, highly hydrophilic molecules are speculated to result reversible and incomplete post-inserted LNCs. Moreover, PEG with a length of 2000 or 3000 $gmol^{-1}$ is considered to be more suitable as longer PEG lengths are required to protect LNCs from external medium [50].

LNCs have thus become emerging nanoparticles in the field of nanomedicine due to its excellent encapsulating capacity of lipophilic drugs into its cavity and capability of both passive and active targetings. LNCs surpass the liposomes in terms of dynamic stability which allows absolutely no leaking of the encapsulated drug. This nanomaterial has shown remarkable feasibility for development of sustainable release of the payloads. In a study carried out by the Lamprecht et al., LNCs of different sizes encapsulated with amiodarone, an antiarrythmic agent had shown to have a tremendous drug loading and slow sustained release profile of amiodarone as compared to the PLGA nanoparticles [51]. This could be of interest to develop sustained release drug delivery for topical or systemic applications. Subsequently, many lipophilic as well as hydrophilic drugs have been formulated with LNCs. For example, indinavir, an inhibitor of HIV-1 protease [52], hydrophobic anti-cancer agents like paclitaxel [53], derivatives of 4-hydroxy tamoxifen combined with ferrocen [54]. Moreover, LNCs loaded with radionuclides like ^{188}Re, [36] was used for bio-imaging and radiotherapy. These examples reveal that LNC helps to improve the efficacy of poor water soluble drugs by

encapsulating in a higher rate and contribute for sustain release of the loaded drug. Passive targeting is another interesting feature that makes LNC a promising nanoparticle for *in vivo* applications. LNCs formulation with post-inserted longer PEG chains, DSPE-PEG 2000 on its surface along with encapsulated docetaxel (more than 98 %), had shown significant and substantial accumulation of these LNCs in tumor than conventional LNCs and control Taxotere®, docetaxel formulation in *in vivo* study. The half-life of this formulation was found to be more than 5 h while for conventional LNCs, half-life was less than 21 min [55]. Moreover, also because of superficial way to graft targeting agents like antibodies on the surface of LNC facilitates the active targeting, LNC is gaining popularity. A study was done recently to prepare folate-modified LNC encapsulated quercetin that can enhance the solubility of quercetin and also can offer folate-mediated active targeting to treat H22 tumor-bearing mice having over expressed folate receptor [56]. This study uncovers the fact that LNC's formulation is comparatively more effective than quercetin alone.

As LNCs are formulated using pharmaceutically accepted organic excipients which are biodegradable, LNCs are considered as safe and non-toxic formulation. However, surfactant dependent toxicity has been reported by Maupas and co-workers [57] in HaCaT cells. The study was carried out by formulating LNCs with different non-ionic surfactants. They have found the correlation between the LNCs and the pure respective surfactant in term of toxicity. Consequently, it seems to be possible to estimate the toxicological behavior of LNCs by evaluating the surfactant component alone. The peculiar features of LNCs have allowed them to be used as potential drug delivery system in many therapeutic applications not only for cancer diagnosis and therapy as drug carrier for highly potent drugs that are generally unfit for oral use, but also for gene therapy. Moreover, their compatibility for large-scale industrial production, through pilot scale up production was carried out in 2013 by increasing 50 folds the materials used for laboratory batches [58] which has already facilitated for the commercialization of LNCs. However, further studies are being required to elucidate the benefits of this formulation compare to other conventional drug formulations and to study the long-term toxicity both *in vitro* and *in vivo*.

1.3. Silica nanoparticles (Silica-NPs)

Drug delivery and controlled release using silica materials has been reported already in 1983. Since then, the rapid advancement in the synthesis and surface modification techniques enables silica to be used extensively as drug carriers, owing to their biocompatibility and easy formulation with drugs [59]. Generally, Silica-NPs used in nanomedicine are categorized as mesoporous and non-porous silica and both of them bear amorphous silica structure. Meso-pores of pore size 2-50 nm containing mesoporous silica (MPS) are commonly used to deliver the active pharmaceutics payloads based on physical and chemical adsorption [60, 61]. However, nonporous Silica-NPs delivery is carried out through either encapsulation or conjugation manner. Therapeutics release from MPS can be controlled by 'gate-keeping' strategy or simply by modifying the inner core to control the binding affinity with loaded materials [62], while payloads release in case of nonporous is controlled by means of chemical linkers or the degradation of silica matrix [15]. Since, we have worked on the grafting of chemically synthesized molecule on the surface of nonporous silica, the details of MPS are avoided. Thus, here the non porous silica particles are described in detail.

Synthesis of size-controlled Silica-NPs was first reported by Stober et al., where monodisperse silica spheres with uniform diameters ranging from 50 nm to 2 µm were successfully prepared in a reaction mixture of water, alcoholic solvent, ammonia, and tetraalkoxysilane [63]. The particle formation is actually proceeds through an aggregation process of siloxane substructures (**Figure 1.6**). The final particle size depends on the stability of thus formed Silica-NPs in the reaction mixture (alcohol, water, and ammonia) and the stability of the reaction mixture depends on rate constants of hydrolysis and condensation [64]. Hartlen et al. and Yokai et al. introduced another method to prepare monodisperse Silica-NPs with diameters as small as 12 nm in a heterogeneous reaction with lysine or arginine instead of ammonia as a basic catalyst in the aqueous medium and tetraethoxysilane in the organic layer. [65, 66]. Moreover, diameter ranging from 10~100 nm monodispersed Silica-NPs was also synthesized by using reverse microemulsions, in which particles form in inverse micelles are separated with a help of suitable surfactant in a nonpolar organic solvent [67]. This method facilitates the easy encapsulation of active molecules in the reverse miscelles during NPs formation. Similarly like size, there are various studies done for the preparation of one-dimensional silica nanorods/nanotubes [68, 69] and other nanostructures [70]. Shapes are controlled mainly by using templates, including anodic aluminium oxide membranes [71], cylindrical polymer brushes [72] and nickel-hydrazine complex nanorods [73].

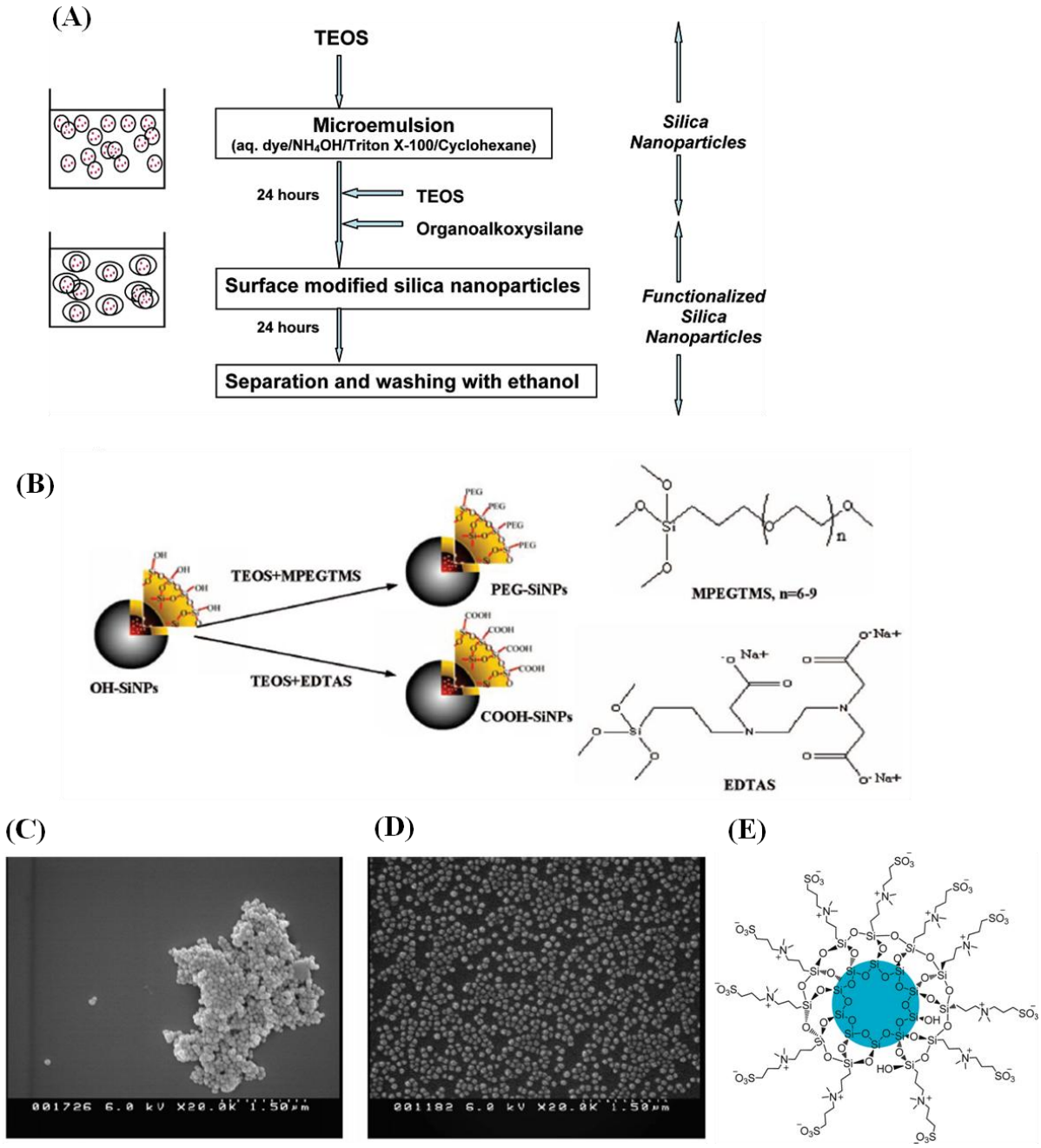

Figure 1.6. Schematic representation of the procedure for the surface modification of dye-doped Silica-NPs using a w/o microemulsion. Following 24 h of synthesis, the surface of the silica nanoparticles is modified via co-hydrolysis of tetraethyl orthosilicate and organosilane reagents in an additional 24 h post-coating step (A) [74], Different strategies for surface modification of Silica-NPs (B) [75], SEM images of amine-modified dye-doped Silica-NPs; Amine-modified particles. (C) and Amine/phosphonate-modified particles (D) [74]. It shows that the overall charge and concentration of functional groups on the surface of the NPs greatly affect the tendency of the NPs to aggregate. Silica-NPs decorated with sulfobetaine siloxane , zwitterions (E) [76].

Surface properties of NPs are assumed to determine the interactions between NPs and biological system like cellular internalization and trafficking, biodistribution and tumor penetration of NPs [77, 78]. Thus, to obtain efficient disease targeting and improved effectiveness of nanosystem, modulation of surface properties in nanomedicine is essential and the surface properties of Silica-NPs can be controlled with addition of 3-aminopropyltriethoxylsilane to create positive charges, 3- (trihydroxysilyl)-propylmethylphosphonate to form negative charges or carboxyethyl- silanetriol, or zwitter-ion silanes to create zwitter-ionic surface charge (**Figure 1.6E**), while following the formulation of Silica-NPs [74-76]. Moreover, surface functionalization of Silica-NPs can be carried out either chemically, through covalent bonding or physically by physical adsorption

Silica-NPs have been already entered into preclinical studies for therapeutic and diagnosis purposes. The potential clinical translation of these NPs is possible only after the complete evaluation of safety and potential toxicity. Numerous study *in vitro* toxicity of Silica-NPs have been carried out and majority of these studies suggest that the Silica-NPs-related toxicity is associated strongly with particle size [79-82], shape, porosity, chemical purity, surface chemistry and solubility [83, 84]. Regarding the particle size toxicity, investigators found that cells viability and mitochondrial potential are strongly affected by smaller NPs than lager NPs, where Silica-NPs of particle size 80 nm and 500 nm were studied [82]. Subsequently, Passagne et al. had reported that 20 nm Silica-NPs are more toxic than 100 nm. Here, the cytoxocity is associated to oxidative stress with up-production of reactive oxygen species (ROS) and lipid peroxidation [79]. Likewise, regarding surface chemistry related toxicity, Morishige et al. compared interleukin-1b production levels in THP-1 human macrophage-like cells treated with 1000 nm Silica-NPs with or without surface functional groups (-COOH, $-NH_2$, $-SO_3H$, -CHO) and found that all the modifications significantly suppress interleukin-1b production by reducing ROS level [85]. In addition, positively charged NPs are reported to be more toxic than negatively charged NPs [80, 86]. However, studies done *in vivo* revealed that positively charged Silica-NPs are rapidly excreted from liver into gastrointestinal tract, while negatively charged NPs remain concealed in the liver [87].

Therefore**,** Silica-NPs can be considered as promising alternatives to organic drug carriers as it exhibits many unique features like controllable size, shape and surface chemistry.

Therefore, it has been used in numerous bio-applications for delivery of drugs, proteins, genes and also for imaging. Nevertheless, for the implementation of Silica-NPs into the clinical use, some of the major challenges should be addressed and overcome. Major challenges include the improved drug loading, spatial and temporal control release of payloads, long-term stability, and well-understood biocompatibility and potential toxicity. An alternate way to overcome most of these problems could be the organo-silica hybrid [88, 89].

1.4. Magnetic nanoparticles (MPs)

Magnetic nanoparticles are the most widely studied metal oxide nanoparticles and falls under inorganic nanomaterials that actively contribute to the recent advancement in the field of nanomedicine. MPs are composed of mainly iron oxides (magnetite; Fe_3O_4 or maghemite; γ-Fe_2O_3) [13] and is popular because of its unique magnetic properties, which arises due to its smaller size than the magnetic domain wall width (typically less than 100 nm) [90].

MPs are considered as biocompatible nanomaterial since they can be readily metabolized by the liver adding them as part of body's iron pool [21]. Induction of ROS is typically a transient effect that highly depends on the stability of the coating agent, in its nature of producing ROS, and in the concentration of MPs that have been internalized by cells. The biodegradation of the MPs is responsible for the generation of free ferric iron and further complete dissolution of the magnetic core. Free ferric iron was found in some cases to induce high levels of ROS, apoptosis or inflammation and to alter transferring receptor [91]. Though long-term studies in animal have not been performed yet, clearance mechanisms of MPs in humans have been studied with MRI. The study showed that MPs (dextran coated) of hydrodynamic diameter of 62 and 150 nm were rapidly cleared after intravenous (i.v) injection by macrophages. Thus the half-life in blood was measured to be 6 minutes. Being macrophage-rich organ, peak concentration of MPs in liver and spleen were found to be after 2 hours and 4 hours respectively. In lysosome MPs were enzymatically degraded and free iron were subsequently released into metabolic pool of iron [92].

MPs can be prepared by various well-established methods like co-precipitation, solvothermal/hydrothermal synthesis, flame spray pyrolysis, micro-emulsion and high-thermal decomposition [93]. Amongst, the co-precipitation technique is the easiest and widely implemented chemical route for the synthesis of MPs. The technique is based on aging a

stoichiometric mixture of ferrous and ferric salts under basic conditions, yielding magnetite in the absence of oxygen. But, this magnetite is unstable in air and is quickly transformed into maghemite. This method is popular due to the fact that a large amount of material is possible to synthesize in short period of time with a good control over shape and particle size (2-50 nm) by adjusting the pH, ionic strength and concentration of the growth solution. However, the problem lies on the agglomeration of particles when exposed to both water and physiological environment and are likely to degrade through oxidation process. Thus, surface stabilization processes are essential for the further use of MPs. A varied of methods have been developed as demonstrated in **Figure 1.7** and some of the examples of commonly used coating agents and their applications and advantages are summarized in **Table 1.5.**

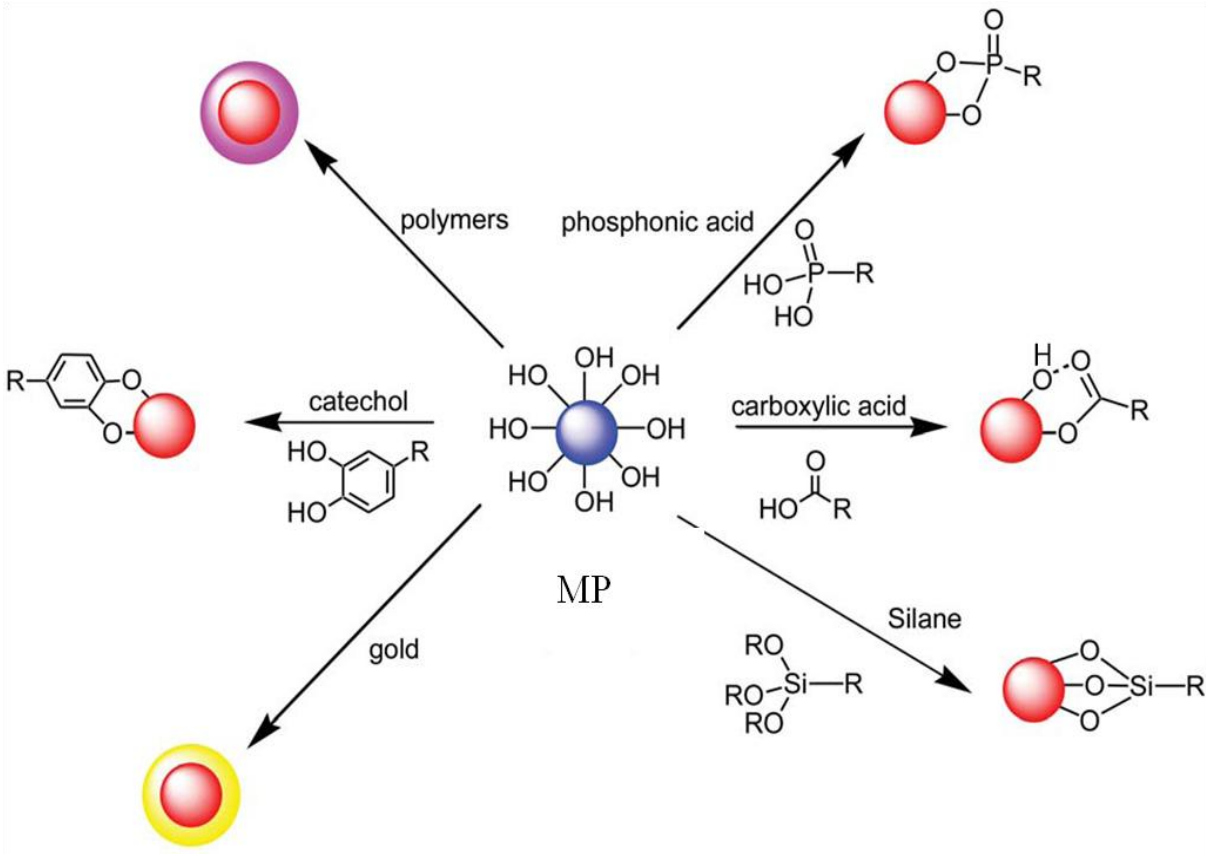

Figure 1.7. Schematic depiction of commonly used stabilization strategies used for the protection and stabilization of MPs. Three main approaches mainly coating (polymer, gold, and silica), catechol co-ordination and other monomeric stabilizers like carboxylates, phosphates, and phosphonates, have been applied to stabilize the MPs [93].

Table 1.5. Some examples of commonly used different coating agents in fabrication of MPs.

Coating agent	Advantages/applications	References
Dextran	Stabilizer and enhances blood circulation	[94, 95]
Polyethylene glycol (PEG)	Protein repellent, nonimmunogenic and nonantigenic. Long-term circulation capability in blood vessels.	[96-98]
Silica	Stabilizer exhibiting biocompatibility and optical transparency. Useful in fabrication of multifunctional MPs.	[99-101]

A versatile approach for the anchoring of different functions is based on catechol linkers. The catechol approach simply relies on the fact that the simple alcohols bind weakly to MP surfaces. However, the limited reactivity of these simple alcohols hinders any further conjugation. In contrast, diols bind quite strongly to MP surfaces and been implemented successfully in quite range of conjugation protocol [102-104]. Xu and co-worker first reported a general strategy to use dopamine as a stable anchor to graft functional molecules onto the surface of MPs [105]. Mazur et al. has recently demonstrated that different catechol ligands can actually be used simultaneously to generate the multifunctional nanostructures in a facile and reproducible way (**Figure 1.8A)** [103]. This finding has opened up various options to conjugate different functional molecules on the same nanoparticle. Though dopamine derivatives are extensively used linkers for the conjugation onto MPs, the use of dopamine has been considered as uncertain since the MPs-catechol complex tends to dissociate at pH 6 and reported to be oxidized to a quinine-like structure in the presence of Fe^{3+} [106-108] as shown in (**Figure 1.8Ba**). Moreover, the amine-function of dopamine is also considered as highly reactive that could result in the formation of 5, 6-dihydroxylindole as an intermediate leading to polydopamine (**Figure 1.8Bb**) [109]. Thus, the problems associated with dopamine derivatives on coating MPs are revealed to be overcome by attaching electronegative nitro-groups to the aromatic catechol system (**Figure 1.8c**).

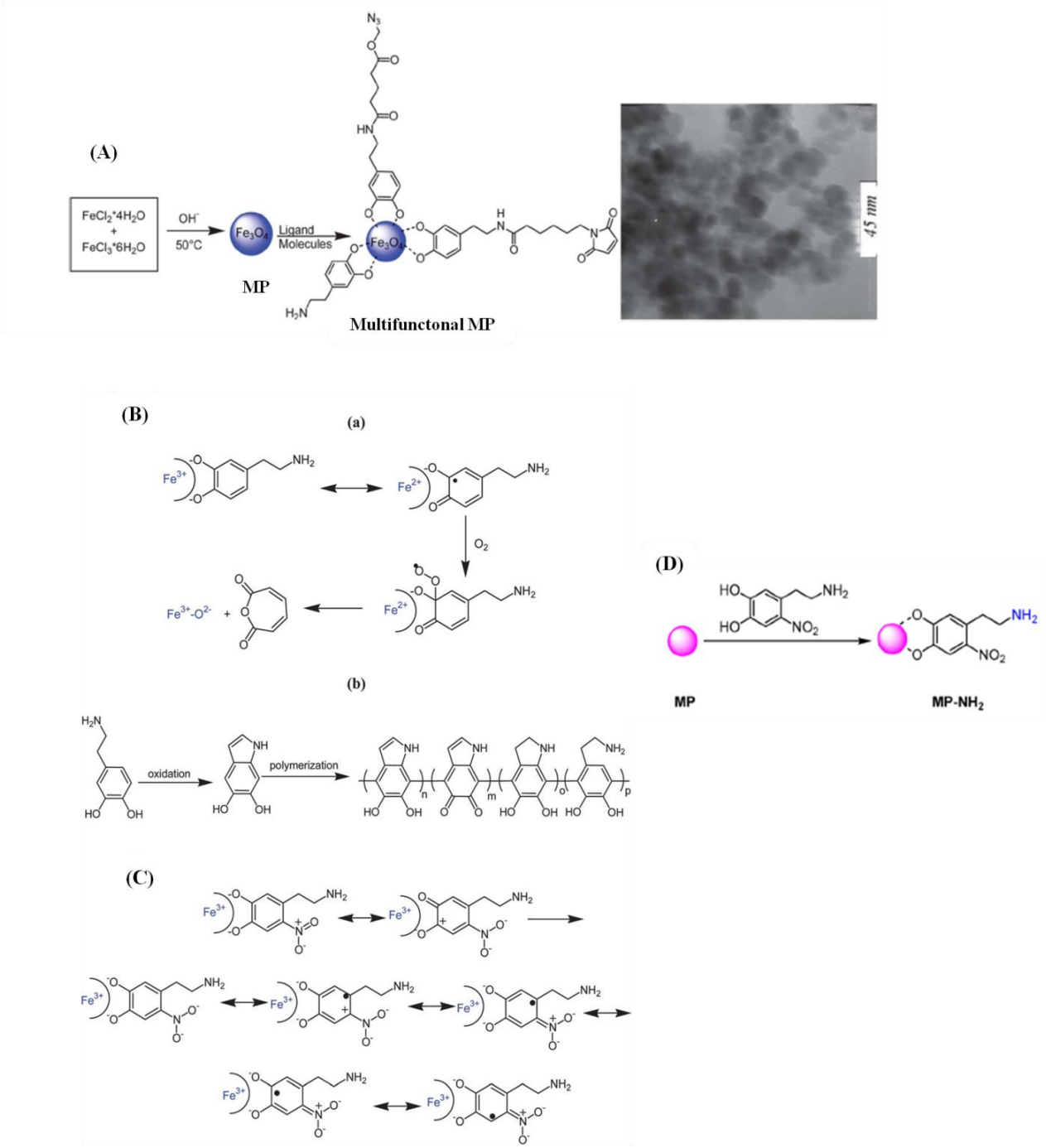

Figure 1.8. (A) Schematic illustration and TEM image of multifunctional IONPs formed by simultaneous modification of co-precipitated MPs with differently functionalized dopamine derivatives [93]; (B) (a) Iron-catalyzed catechol degradation: Fe^{3+} complexed catechols are oxidized to semiquinones while Fe^{3+} is reduced to Fe^{2+} before semiquinones are further degraded through reactions with oxygen, (b) polymerization of dopamine; (C) Proposed binding mechanism of 2-nitrocatechols with initial binding to Fe^{3+} ions [110]. (D) Formation of amine coated MPs using chemically synthesized 2-nitrodopamine [111].

The stability of 2-nitrocatechol has already been demonstrated by Reimhult and co-workers [107]. Beside stability, 2-nitrocatechol has an additional advantage of being less neurotoxic than compare to other metabolites of dopamine, including 6-hydroxydopamine [110]. Thus this approach was used in this thesis where, chemically synthesized 2-nitrodopamine (**Figure 1.8 D**) has been used to coat MPs to create stable MPs.

Therefore, smartly coated MPs possess a wide scope in diagnostic and therapeutic applications. MPs based on superparamagnetic iron oxide are not only being accepted for clinical purposes in human for MRI diagnosis but in near future are expected to be used for therapeutic issues and thus develop in theranostic agents. The peculiar properties, like easy synthesis of huge amount of MPs in the cost-effective ways, biomolecules conjugation by the surface modification of the covering shell of MPs and the magnetic property that can be used to drive NPs inside the organism by applying an external magnetic field gradient to the targeted area of the body, make MPs popular in nanotechnology. Regardless the good tolerance that some shielded MPs has shown, the study on long-term outcome of the MPs in the body is still need to be carried out. In addition, potential risks associated with intensive use of MPs have to be proceeded immediately.

1.5. Nanodiamonds (NDs)

NDs have been currently gaining massive attention in the field of nanomedicine due to its superior biocompability than compared to other carbon nanomaterials [112]. Single crystals of cubic diamond particles was discovered in 1963 by a group of Soviet scientists in a soot produced by detonating an oxygen-deficient TNT/hexogen composition in inert media without using any extra carbon sources [113]. The average size of this nanocrystal is 4-5 nm. The discovery of this particle was kept secret for long under Soviet military regime due to security reasons [114]. NDs started to get recognition and researches commenced soon after the first report got published in 1988 [114]. However, the industrial production in the western part of the world got suspended shortly due to the problem in disintegrating the ND aggregates into primary particles of 4-5 nm. Some of the involved ND's researchers had also discussed about the presence of extremely tight core that makes the primary particles into the ND aggregates [115]. Despite of aggregation problem, multitude of commercially available methods make the production of large quantities of NDs at rather low-cost possible [116].

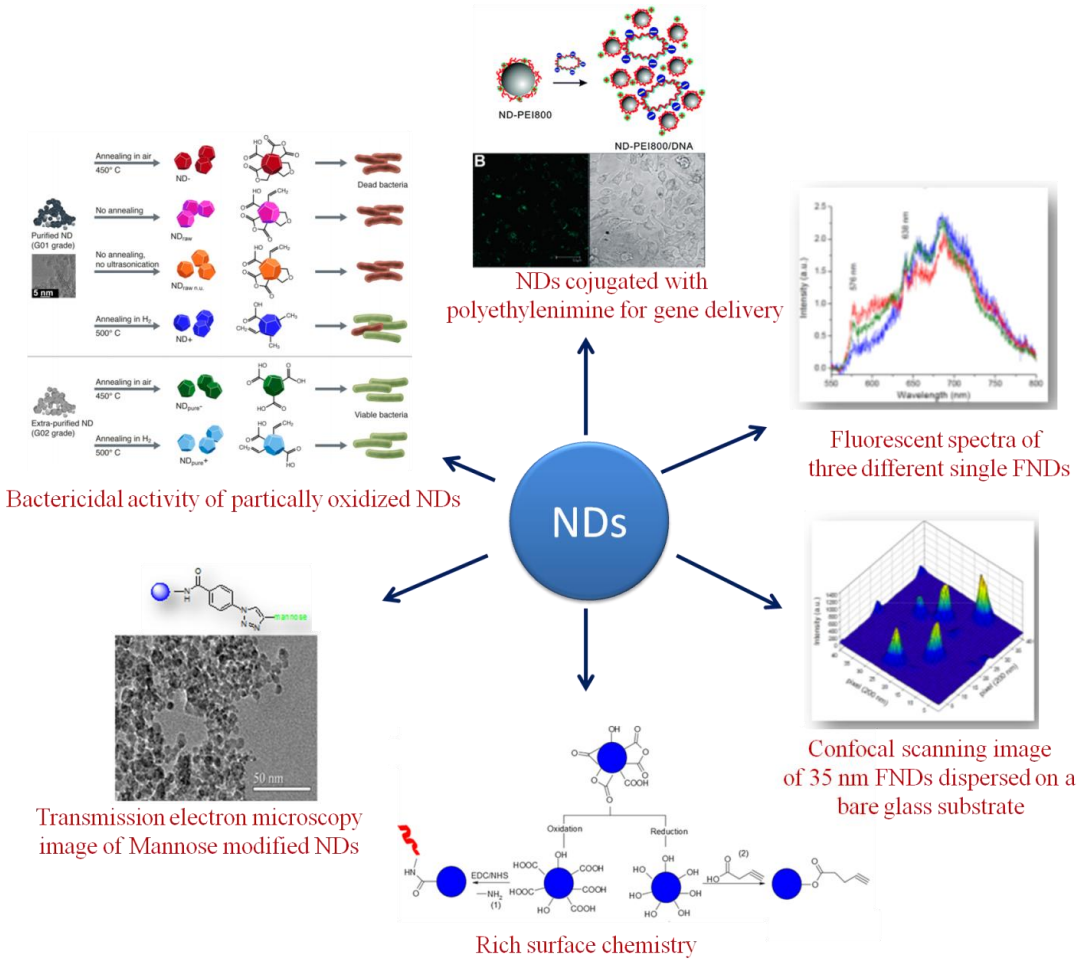

Figure 1.9. Interest of NDs for various biological application, gene delivery image is taken from reference [117], confocal scanning image and fluorescent spectra are from reference [118], bactericidal properties of partially oxidized NDs from reference [119], Transmission electron microscopy image (TEM) is taken from reference [120].

Currently, NDs is gaining immense attention not only because of commercialized of highly purified colloidal suspension of NDs with particle diameter of 4-10 nm but also due to another attracting feature of NDs i.e. biological imaging. Bio-imaging with NDs is possible owing to its intrinsic fluorescent property of producing stable fluorescence from color centers after surface treatment with strong oxidative acids [121]. The fluorescence of NDs is actually originated from point defects embedded in the crystal lattice and among all the defects negatively charged nitrogen-vacancy center $(N\text{-}V)^-$ is the most remarkable one which is the dominant end product of thermal annealing of irradiation-damaged diamond containing atomically dispersed nitrogen atoms [118]. **Figure 1.9** highlights the important features and application of NDs.

Detonated NDs contain both graphitic carbon and incombustible metals and oxides as impurities either inside the agglomerates or attached to the outer surface [122]. Therefore, various purification techniques have been applied to remove the impurities from ND aggregates and enhance the ease of surface chemistry. Mostly applied techniques used strong oxidants like nitric acid (HNO_3) or a mixture of sulfuric acid (H_2SO_4) and HNO_3 to remove non-diamond carbon [123].

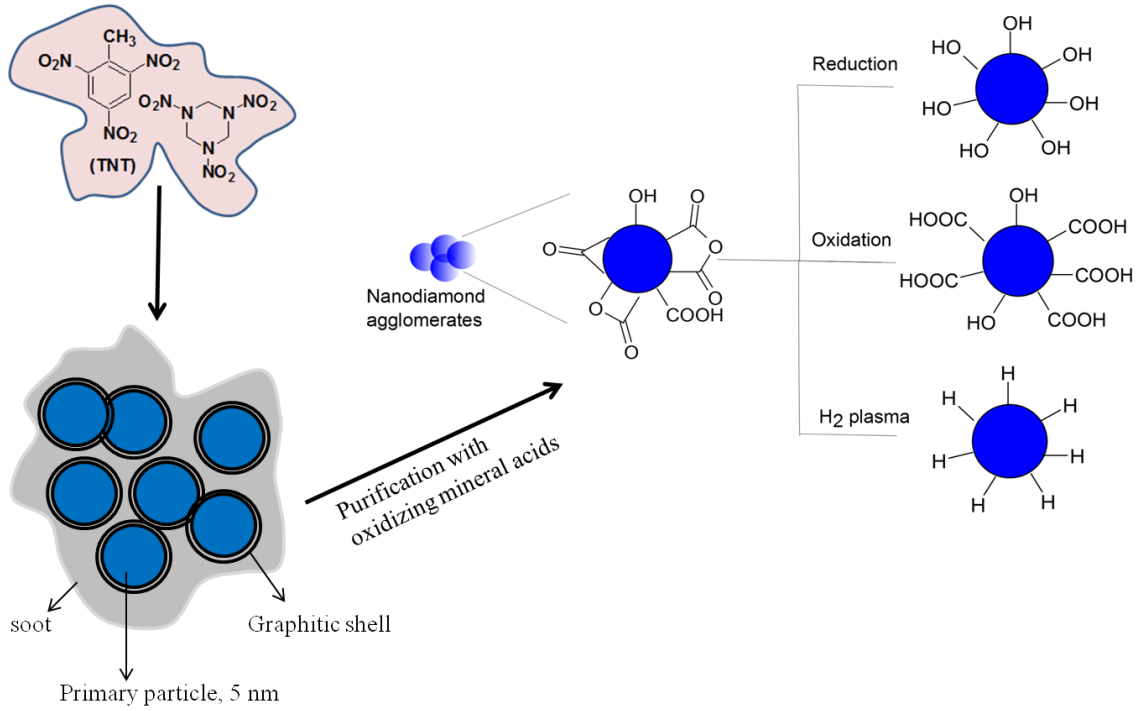

Figure 1.10. Formation of detonated NDs from TNT/hexogen composition in inert media forming surface functional groups on pristine nanodiamond and various treatment like oxidation (O_3, mixture of concentrated HNO_3 and H_2SO_4), reduction (with boron hydride (BH_3).tetrahydrofuran (THF) solution or lithium aluminium hydride ($LiAlH_4$)) or reduction with plasma treatment [123] to homogenize the surface functions and can be later used for surface modifications.

During the pretreatment/purification process, the surface of particles and particle aggregates covered by the various functional groups like carboxyl, lactone, ketone, hydroxyl and sometimes alkyl groups (**Figure 1.10**) get reduced or oxidized to form the enough number of hydroxide/hydride and carboxylic groups respectively depending on the form of treatments. Various kinds of functional nanodiamonds, like hydroxylated, carboxylated, amine terminated etc have been commercialized recently which facilitates researchers to tune the surface with

the help of surface chemistry and thus to create its practical utility in the field of nanomedicine.

Before discussing about different pre-existing and possible strategies for surface modifications, it is important to understand about the aggregations of primary particles. Aggregation of nanodiamonds is a major problem that limits its applications. Therefore, de-aggregation processes are equally imperative that usually improve stability of colloidal solution and increase the volume of surface functional groups. De-aggregation of nanodiamond can be carried out by milling with ceramic beads like zirconia or silica or by microbead-assisted ultrasonic disintegration that was established by Osawa and co-workers [124]. Moreover, the fractionation of particles by utilizing centrifugation speed also contributes to separate different particle sizes [125]. Surface modifications of NDs mostly rely on the carboxylic and hydroxyl functions which are thoroughly described under covalent and uncovalent method of modifications.

Oxidative-acid treated NDs provide the best platform for the physical adsorption of proteins [126] and gene delivery [117]. It has higher affinity for proteins, thus this suitable property was utilized by Nguyen and co-worker to immobilize lysozyme for biotechnological application [126]. For the gene delivery, carboxylic acid-functionalized NDs was exposed to a positive polymer like polyethylenimine (PEI) to create enough positive charges on the surface of NDs and later using electrostatic interaction, plasmid DNA [117] or siRNA [127] were conjugated on NDs. Subsequently, carboxylic acid-functionalized NDs had been used to improve the delivery of various water insoluble therapeutics like doxorubicin, purvalanol A, 4-hydroxytamoxifen and dexamethasone by complexing with drug molecules [128, 129].

The carbonyl group usually present on the surface of detonated NDs, under strong acids treatment, can be converted into carboxylic acid groups (**Figure 1.11A**). These acid groups are often employed to covalently conjugate biomolecules like bovine serum albumin (BSA) [130], poly-L-lysine (PLL) [130], polyethylene glycol (PEG) and DNA through electrostatic interaction with PLL present on ND's surface [118]. Likewise, the carbonyl functions can also be reduced to hydroxyl group under either by borone mediated reduction [131] or special treatment called Fenton treatment, where ND reacts with hydrogen peroxide (H_2O_2) and iron (II) sulfate ($FeSO_4$) under strong acidic conditions.

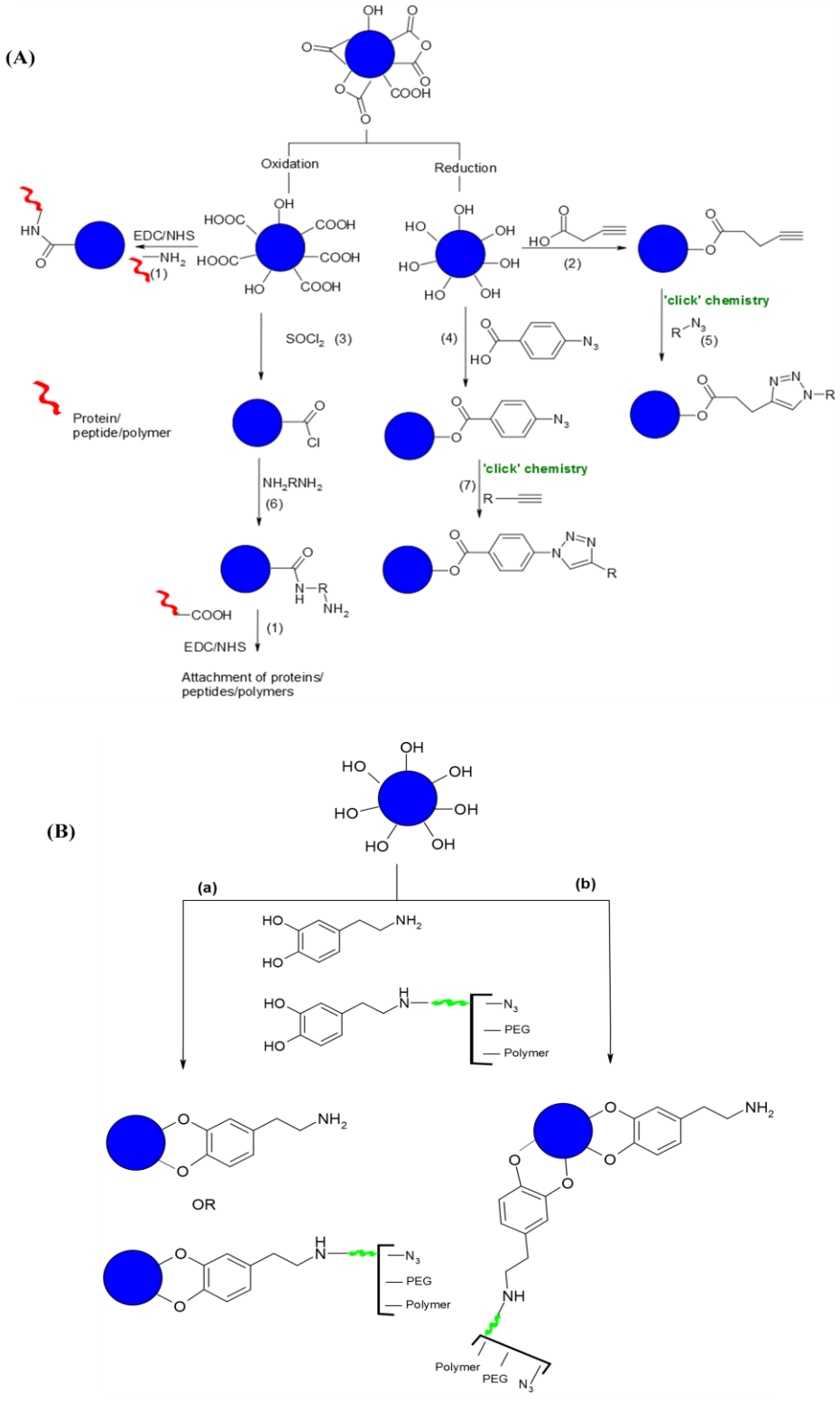

Figure 1.11. Basic strategies used for surface modification of ND. Carboxylic and hydroxyl group have been utilize to perform different surface chemistries from amide, ester to 'click chemistry' (A); Direct surface modification strategy using dopamine derivatives to form either single functional or multifunctional NDs (B).

This process also somehow removes the undesirable soot matter and at the same time, increases the density of hydroxyl groups that facilitates further modification process [132, 133]. Thus created enough hydroxyl groups are used by Barras and co-workers to create azido/alkynyl terminated NDs using 4-azidobenzoic acid/4-pentynoic acid and thus introduced azido/alkynyl groups can be utilized to 'click' various other molecules containing alkynyl/azido group via copper catalysed 'click reaction' [134]. Amine group can be added to NDs surface through thionyl chloride ($SOCl_2$) chemistry on which carbonyl chloride was introduced first which is supposed to be more reactive than carboxylic acid functional and thus formed carbonyl chlorides were reacted to di-amine compounds to create amine functions on NDs [112]. Silanization of subsequent hydroxyl group is another popular method to introduce amine groups to the surface of NDs that can be later utilized to conjugates biomolecules through the amide linkage [117]. In addition to these, Barras and co-workers have reported different strategy for the first time to create azide groups directly onto the surface of the hydroxylated NDs by using dopamine derivatives containing terminal azide functional group [135]. This direct and facile way of grafting dopamine derivatives on NDs opens up the possibility of creating novel multifunctional NDs which could behave as multifunctional particles. For instance, on the same particles, use of azide terminated dopamine derivate could create possibility to 'click chemistry' and at the same time polyethylene glycol (PEG) terminated dopamine derivate could improve the stability issues of NDs. This could be achieved by using different ratios of either two or three different dopamine derivatives (**Figure 1.11B)**. This multifunctional strategy has been successfully used in magnetic nanoparticle [103]. We have utilized this approach to create multifunctional NDs in this thesis for gene delivery *in vitro*. In addition to these, aromatic diazonium salts have also been shown to react with ND surface and introduce new functionalities such as carboxylic acids and NHS-esters [136]. Dahoumane and co-workers used similar approach to demonstrate the improvement of overall stability of NDs after modification with protein bovine serum albumin (BSA). Recently, in contrast to traditional ways, hydroxyled NDs are thiolated by Hsu and co-worker [137] and successfully conjugated with gold nanoparticles (GNPs). This approach introduces a new approach towards surface modification of detonated NDs and provides a new platform for the application of NDs.

NDs are considered to be highly up-taken [138] via clathrin-mediated endocytosis pathway [139] and a highly biocompatible nanomaterial. For the safety assessment *in vitro*, cellular toxicity can be performed by various ways. Out of these, first report on the NDs

cellular compatibility was made by Schrand and co-workers by using MTT (3-(4,5-dimethylthiazol-2-yl)-2,5-diphenyltetrazolium bromide) assay and ATP (adenosine triphosphate) production assay and found that NDs do not induce significant toxicity on a variety of cell lines [140]. They have found that the NDs are the most biocompatible nanomaterials among the carbon nanomaterials tested like carbon black, multi-walled carbon nanotubes and single-walled carbon nanotubes. The study also focused on the generation of reactive oxygen species (ROS) in two cell lines (macrophage and neuroblastoma) by different carbon nanomaterials on which NDs was revealed to be compatible to both cell lines by not generating ROS whereas rest of the carbon nanomaterials were found to generate comparatively high amount of ROS. Endocytic carboxylated NDs are considered to be non-toxic during cell division and differentiation since they did not interfere with the gene and protein expressions on the regulation of cell cycle progression of various cancer cell lines [139]. However, study done on oxidized NDs done by Xing and co-workers has shown slight increase on expression of DNA repair proteins (p53 and MOGG-1) in mouse cells ES cells and more DNA damage as compare to raw/pristine NDs. Therefore, the toxicity depends on the chemical functional groups on the surface of NDs that are introduced during surface modification. However, compare to carbon nanotubes, DNA damages caused by oxidized NDs are less severe [141]. The biocompatibility of NDs is further supported by *in vivo* toxicity analysis in animal model. Wang group has revealed that NDs does not cause noticeable adverse effects in lungs through histopathological and ultrastructural investigations [142]. Moreover, long-term of toxicity of ND hydrosols on mice and the offspring was studied by replacing water in the mice's diet by 0.002 to 0.05 wt. % ND hydrosols for three to six months and the results compared to the control mice had shown that NDs neither caused death nor affected the growth or the internal organs weight dynamics. Moreover, the substitutions of water did not affect the mouse's reproductive ability [138]. The biodistribution of NDs are tracked by the radiolabeled NDs. By the help of PET, it has been found that the intravenously injected NDs were distributed in various organs of mice, mainly in lungs, spleen and liver and excreted into the urinary tract and the addition of surfactant agents did not show any changes in distribution except slight reduction in the urinary excretion rate [143]. Both *in vitro* and *in vivo* studies show that NDs have no or a small toxic side effect on biological systems and provides an important basis for designing a ND-based drug delivery system.

Due to NDs superior physical and chemical properties including ultrahigh hardness, high thermal conductivity, low friction coefficient, and excellent resistance against corrosive chemicals, they are widely used in industries. Interestingly, as mentioned earlier, the foremost advantage of NDs is its super biocompatibility nature and the fact that its surface can be easily tuned with carboxyl and amino groups has opened up many possibilities for developing NDs as a nanocarrier in the field of nanobiotechnology. Moreover, nano-sized NDs exhibits large specific surface area and oxidative acid-treated NDs has shown exceptionally high affinity for proteins in aqueous solution. Likewise, NDs containing isolated nitrogen vacancy defect centers can be used as a non-toxic, nonphotobleaching fluorescent probe of biological cells [112]. Despite of all these excellent properties, NDs has aggregation issue that limits the bio-applications. Some of the approaches proposed are microbeads (zircionia)-assisted ultrasonic disintegration and dry milling using cheap milling media (such as water-soluble salts and sugars) that do not introduce contaminants. Subsequently, using different centrifugation speed can help to fractionate particles by weight and size. Surface coating with polymer, high zeta potentials or protein like bovine serum albumin (BSA) can be used to improve overall stability of NDs.

1.6. References

1. Chou, L.Y., K. Ming, and W.C. Chan, *Strategies for the intracellular delivery of nanoparticles.* Chem Soc Rev, 2011. **40**(1): p. 233-45.
2. Wissing, S.A., O. Kayser, and R.H. Muller, *Solid lipid nanoparticles for parenteral drug delivery.* Adv Drug Deliv Rev, 2004. **56**(9): p. 1257-72.
3. Popovtzer, R.A., A.; Kotov, N.A.; Aron Popovtzer, A.; Balter, A.; Carey, T.E.; Raoul K. , *Targeted Gold Nanoparticles Enable Molecular CT Imaging of Cancer.* Nano Letters, 2008. **8**(12): p. 4593-4596.
4. Kim, J., et al., *Targeted delivery of nanoparticles to ischemic muscle for imaging and therapeutic angiogenesis.* Nano Lett, 2011. **11**(2): p. 694-700.
5. Choi, H.S. and J.V. Frangioni, *Nanoparticles for biomedical imaging: fundamentals of clinical translation.* Mol Imaging, 2010. **9**(6): p. 291-310.
6. Soppimath, K.S., et al., *Biodegradable polymeric nanoparticles as drug delivery devices.* J Control Release, 2001. **70**(1-2): p. 1-20.
7. Portney, N.G. and M. Ozkan, *Nano-oncology: drug delivery, imaging, and sensing.* Anal Bioanal Chem, 2006. **384**(3): p. 620-30.
8. Davis, M.E., Z.G. Chen, and D.M. Shin, *Nanoparticle therapeutics: an emerging treatment modality for cancer.* Nat Rev Drug Discov, 2008. **7**(9): p. 771-82.
9. Hrkach, J., et al., *Preclinical development and clinical translation of a PSMA-targeted docetaxel nanoparticle with a differentiated pharmacological profile.* Sci Transl Med, 2012. **4**(128): p. 128ra39.
10. Peer, D., et al., *Nanocarriers as an emerging platform for cancer therapy.* Nat Nanotechnol, 2007. **2**(12): p. 751-60.

11. Bao, G., S. Mitragotri, and S. Tong, *Multifunctional nanoparticles for drug delivery and molecular imaging.* Annu Rev Biomed Eng, 2013. **15**: p. 253-82.
12. Alivisatos, P., *The use of nanocrystals in biological detection.* Nat Biotechnol, 2004. **22**(1): p. 47-52.
13. Jana, N.R.C., Y.; Peng, X., *Size- and Shape-Controlled Magnetic (Cr, Mn, Fe, Co, Ni) Oxide Nanocrystals via a Simple and General Approach.* Chem. Mater., 2004. **16**: p. 3931-3935.
14. Champion, J.A., Y.K. Katare, and S. Mitragotri, *Particle shape: a new design parameter for micro- and nanoscale drug delivery carriers.* J Control Release, 2007. **121**(1-2): p. 3-9.
15. Tang, L. and J. Cheng, *Nonporous Silica Nanoparticles for Nanomedicine Application.* Nano Today, 2013. **8**(3): p. 290-312.
16. Doshi, N. and S. Mitragotri, *Designer Biomaterials for Nanomedicine.* Advanced Functional Materials, 2009. **19**(24): p. 3843-3854.
17. Liechty, W.B., et al., *Polymers for drug delivery systems.* Annu Rev Chem Biomol Eng, 2010. **1**: p. 149-73.
18. Panyam, J. and V. Labhasetwar, *Biodegradable nanoparticles for drug and gene delivery to cells and tissue.* Advanced Drug Delivery Reviews, 2003. **55**(3): p. 329-347.
19. Kim, B.Y.S.R.J.T.C., W. C. W. , *Nanomedicine.* Th e new england journal of medicine, 2010. **363**(25): p. 2434-2443.
20. Wolinsky, J.B. and M.W. Grinstaff, *Therapeutic and diagnostic applications of dendrimers for cancer treatment.* Adv Drug Deliv Rev, 2008. **60**(9): p. 1037-55.
21. Sapsford, K.E., et al., *Functionalizing nanoparticles with biological molecules: developing chemistries that facilitate nanotechnology.* Chem Rev, 2013. **113**(3): p. 1904-2074.
22. Fuente, J.M.G., V., *Nanobiotechnology: Inorganic Nanoparticles Vs Organic Nanoparticles.* 2012. **4**.
23. Nagarajan, R., *Theory of Surfactant Self -Assembly: A Predictive Molecular Thermodynamic Approach* Langmuir, 1991(7): p. 2934-2969.
24. Kesharwani, P., K. Jain, and N.K. Jain, *Dendrimer as nanocarrier for drug delivery.* Progress in Polymer Science, 2014. **39**(2): p. 268-307.
25. Krueger, A., *Beyond the shine: recent progress in applications of nanodiamond.* J. Mater. Chem., 2011. **21**: p. 12571.
26. Heurtault, B., et al., *A novel phase inversion-based process for the preparation of lipid nanocarriers.* Pharm Res, 2002. **19**(6): p. 875-80.
27. Minkov, I., et al., *Reorganization of lipid nanocapsules at air-water interface: Part 2. Properties of the formed surface film.* Colloids Surf B Biointerfaces, 2005. **44**(4): p. 197-203.
28. Vonarbourg, A., et al., *Electrokinetic properties of noncharged lipid nanocapsules: influence of the dipolar distribution at the interface.* Electrophoresis, 2005. **26**(11): p. 2066-75.
29. Heurtault, B., et al., *Properties of polyethylene glycol 660 12-hydroxy stearate at a triglyceride/water interface.* Int J Pharm, 2002. **242**(1-2): p. 167-70.
30. Heurtault, B., et al., *The influence of lipid nanocapsule composition on their size distribution.* Eur J Pharm Sci, 2003. **18**(1): p. 55-61.
31. Anton, N., et al., *Nano-emulsions and nanocapsules by the PIT method: an investigation on the role of the temperature cycling on the emulsion phase inversion.* Int J Pharm, 2007. **344**(1-2): p. 44-52.

32. Anton, N., J.P. Benoit, and P. Saulnier, *Design and production of nanoparticles formulated from nano-emulsion templates-a review.* J Control Release, 2008. **128**(3): p. 185-99.
33. Anton, N., et al., *Salting-out effect induced by temperature cycling on a water/nonionic surfactant/oil system.* J Phys Chem B, 2007. **111**(14): p. 3651-7.
34. Dulieu, C. and D. Bazile, *Influence of lipid nanocapsules composition on their aptness to freeze-drying.* Pharm Res, 2005. **22**(2): p. 285-92.
35. Saulnier, P.A., N.; Heurtault, B.; Benoit, J.-P., *Liquid crystals and emulsions in the formulation of drug carriers.* Comptes Rendus Chimie, 2008. **11**: p. 221–228.
36. Allard, E., et al., *188Re-loaded lipid nanocapsules as a promising radiopharmaceutical carrier for internal radiotherapy of malignant gliomas.* Eur J Nucl Med Mol Imaging, 2008. **35**(10): p. 1838-46.
37. Huynh, N.T., et al., *Lipid nanocapsules: a new platform for nanomedicine.* Int J Pharm, 2009. **379**(2): p. 201-9.
38. Moghimi, S.M., A.C. Hunter, and J.C. Murray, *Long-circulating and target-specific nanoparticles: theory to practice.* Pharmacol Rev, 2001. **53**(2): p. 283-318.
39. Moghimi, S.M. and J. Szebeni, *Stealth liposomes and long circulating nanoparticles: critical issues in pharmacokinetics, opsonization and protein-binding properties.* Prog Lipid Res, 2003. **42**(6): p. 463-78.
40. Mosqueira, V.C., et al., *Biodistribution of long-circulating PEG-grafted nanocapsules in mice: effects of PEG chain length and density.* Pharm Res, 2001. **18**(10): p. 1411-9.
41. Ballot, S., et al., *99mTc/188Re-labelled lipid nanocapsules as promising radiotracers for imaging and therapy: formulation and biodistribution.* Eur J Nucl Med Mol Imaging, 2006. **33**(5): p. 602-7.
42. Acharya, S., F. Dilnawaz, and S.K. Sahoo, *Targeted epidermal growth factor receptor nanoparticle bioconjugates for breast cancer therapy.* Biomaterials, 2009. **30**(29): p. 5737-50.
43. Ljubimova, J.Y., et al., *Poly(malic acid) nanoconjugates containing various antibodies and oligonucleotides for multitargeting drug delivery.* Nanomedicine (Lond), 2008. **3**(2): p. 247-65.
44. Hein, C.D., X.M. Liu, and D. Wang, *Click chemistry, a powerful tool for pharmaceutical sciences.* Pharm Res, 2008. **25**(10): p. 2216-30.
45. Lutz, J.F. and Z. Zarafshani, *Efficient construction of therapeutics, bioconjugates, biomaterials and bioactive surfaces using azide-alkyne "click" chemistry.* Adv Drug Deliv Rev, 2008. **60**(9): p. 958-70.
46. Iden, D.L. and T.M. Allen, *In vitro and in vivo comparison of immunoliposomes made by conventional coupling techniques with those made by a new post-insertion approach.* Biochim Biophys Acta, 2001. **1513**(2): p. 207-16.
47. Moreira, J.N., et al., *Use of the post-insertion technique to insert peptide ligands into pre-formed stealth liposomes with retention of binding activity and cytotoxicity.* Pharm Res, 2002. **19**(3): p. 265-9.
48. Vonarbourg, A., et al., *Parameters influencing the stealthiness of colloidal drug delivery systems.* Biomaterials, 2006. **27**(24): p. 4356-73.
49. Vonarbourg, A., et al., *Evaluation of pegylated lipid nanocapsules versus complement system activation and macrophage uptake.* J Biomed Mater Res A, 2006. **78**(3): p. 620-8.
50. Perrier, T., et al., *Post-insertion into Lipid NanoCapsules (LNCs): From experimental aspects to mechanisms.* Int J Pharm, 2010. **396**(1-2): p. 204-9.

51. Lamprecht, A., Y. Bouligand, and J.P. Benoit, *New lipid nanocapsules exhibit sustained release properties for amiodarone.* J Control Release, 2002. **84**(1-2): p. 59-68.
52. Pereira de Oliveira, M., et al., *Tissue distribution of indinavir administered as solid lipid nanocapsule formulation in mdr1a (+/+) and mdr1a (-/-) CF-1 mice.* Pharm Res, 2005. **22**(11): p. 1898-1905.
53. Lacoeuille, F., et al., *In vivo evaluation of lipid nanocapsules as a promising colloidal carrier for paclitaxel.* Int J Pharm, 2007. **344**(1-2): p. 143-9.
54. Allard, E., et al., *Lipid nanocapsules loaded with an organometallic tamoxifen derivative as a novel drug-carrier system for experimental malignant gliomas.* J Control Release, 2008. **130**(2): p. 146-53.
55. Khalid, M.N., et al., *Long circulating poly(ethylene glycol)-decorated lipid nanocapsules deliver docetaxel to solid tumors.* Pharm Res, 2006. **23**(4): p. 752-8.
56. Ding, B., et al., *Preparation and evaluation of folate-modified lipid nanocapsules for quercetin delivery.* J Drug Target, 2014. **22**(1): p. 67-75.
57. Maupas, C., et al., *Surfactant dependent toxicity of lipid nanocapsules in HaCaT cells.* Int J Pharm, 2011. **411**(1-2): p. 136-41.
58. Thomas, O.L., F., *Lipid nanocapsules: a nanocarrier suitable for scale-up process.* J. DRUG DEL. SCI. TECH, 2013. **23**(6): p. 555-559.
59. Unger, K.R., H.; Valentin, B.; Kircher, W., *The use of porous and surface modified silicas as drug delivery and stabilizing agents.* Drug Development and Industrial Pharmacy, 1983. **9**(1-2): p. 69-91.
60. Slowing, II, et al., *Mesoporous silica nanoparticles as controlled release drug delivery and gene transfection carriers.* Adv Drug Deliv Rev, 2008. **60**(11): p. 1278-88.
61. Suteewong, T., et al., *Multicompartment mesoporous silica nanoparticles with branched shapes: an epitaxial growth mechanism.* Science, 2013. **340**(6130): p. 337-41.
62. Zhao, Y., et al., *Mesoporous silica nanoparticle-based double drug delivery system for glucose-responsive controlled release of insulin and cyclic AMP.* J Am Chem Soc, 2009. **131**(24): p. 8398-400.
63. Stober, W.F., A.; Bohn E., *Controlled Growth of Monodisperse Silica Spheres in the Micron Size Range.* Journal of Colloid and Interface Science 1968. **26**: p. 62-69
64. Blaaderen, A.V.G., J. V.; Vrij A. , *Monodisperse Colloidal Silica Spheres from Tetraalkoxysilanes: Particle Formation and Growth Mechanism* Journal of Colloid and Interface Science, 1992. **154**(2): p. 481-501.
65. Hartlen, K.D.A., A. P. T.; Kitaev, V., *Facile Preparation of Highly Monodisperse Small Silica Spheres (15 to >200 nm) Suitable for Colloidal Templating and Formation of Ordered Arrays.* Langmuir, 2008. **24**: p. 1714-1720.
66. Yokoi, T.S., Y.; Terasaki, O.; Kubota, Y.; Okubo, T.; Tatsumi, T., *Periodic Arrangement of Silica Nanospheres Assisted by Amino Acids.* J. AM. CHEM. SOC., 2006. **128**: p. 13664-13665.
67. Roy, I., et al., *Ceramic-based nanoparticles entrapping water-insoluble photosensitizing anticancer drugs: a novel drug-carrier system for photodynamic therapy.* J Am Chem Soc, 2003. **125**(26): p. 7860-5.
68. Kwon, N.H., et al., *Nanowire-based delivery of Escherichia coli O157 shiga toxin 1 A subunit into human and bovine cells.* Nano Lett, 2007. **7**(9): p. 2718-23.
69. Mitchell, D.T., et al., *Smart nanotubes for bioseparations and biocatalysis.* J Am Chem Soc, 2002. **124**(40): p. 11864-5.

70. Deng, Z., et al., *Hollow chitosan-silica nanospheres as pH-sensitive targeted delivery carriers in breast cancer therapy.* Biomaterials, 2011. **32**(21): p. 4976-86.
71. Son, S.J., et al., *Template synthesis of multifunctional nanotubes for controlled release.* J Control Release, 2006. **114**(2): p. 143-52.
72. Mullner, M., et al., *Water-soluble organo-silica hybrid nanotubes templated by cylindrical polymer brushes.* J Am Chem Soc, 2010. **132**(46): p. 16587-92.
73. Gao, C., Z. Lu, and Y. Yin, *Gram-scale synthesis of silica nanotubes with controlled aspect ratios by templating of nickel-hydrazine complex nanorods.* Langmuir, 2011. **27**(19): p. 12201-8.
74. Bagwe, R.P.H., L. R.; Tan, W., *Surface Modification of Silica Nanoparticles to Reduce Aggregation and Nonspecific Binding.* Langmuir, 2006. **22**: p. 4357-4362.
75. He, X.N., H.; Wang, K.; Tan, W.; Wu, X.; Zhang, P., *In Vivo Study of Biodistribution and Urinary Excretion of Surface-Modified Silica Nanoparticles.* Anal. Chem. , 2008. **80**: p. 9597–9603.
76. Estephan, Z.G., J.A. Jaber, and J.B. Schlenoff, *Zwitterion-stabilized silica nanoparticles: toward nonstick nano.* Langmuir, 2010. **26**(22): p. 16884-9.
77. Albanese, A., P.S. Tang, and W.C. Chan, *The effect of nanoparticle size, shape, and surface chemistry on biological systems.* Annu Rev Biomed Eng, 2012. **14**: p. 1-16.
78. Verma, A., et al., *Surface-structure-regulated cell-membrane penetration by monolayer-protected nanoparticles.* Nat Mater, 2008. **7**(7): p. 588-95.
79. Passagne, I., et al., *Implication of oxidative stress in size-dependent toxicity of silica nanoparticles in kidney cells.* Toxicology, 2012. **299**(2-3): p. 112-24.
80. Oh, W.K., et al., *Cellular uptake, cytotoxicity, and innate immune response of silica-titania hollow nanoparticles based on size and surface functionality.* ACS Nano, 2010. **4**(9): p. 5301-13.
81. Quignard, S., et al., *Long-term fate of silica nanoparticles interacting with human dermal fibroblasts.* Biomaterials, 2012. **33**(17): p. 4431-42.
82. Zhang, Y., et al., *Influence of silica particle internalization on adhesion and migration of human dermal fibroblasts.* Biomaterials, 2010. **31**(32): p. 8465-74.
83. Yu, T., et al., *Influence of geometry, porosity, and surface characteristics of silica nanoparticles on acute toxicity: their vasculature effect and tolerance threshold.* ACS Nano, 2012. **6**(3): p. 2289-301.
84. Yu, T., A. Malugin, and H. Ghandehari, *Impact of silica nanoparticle design on cellular toxicity and hemolytic activity.* ACS Nano, 2011. **5**(7): p. 5717-28.
85. Morishige, T., et al., *The effect of surface modification of amorphous silica particles on NLRP3 inflammasome mediated IL-1beta production, ROS production and endosomal rupture.* Biomaterials, 2010. **31**(26): p. 6833-42.
86. Nan, A., et al., *Cellular uptake and cytotoxicity of silica nanotubes.* Nano Lett, 2008. **8**(8): p. 2150-4.
87. Souris, J.S., et al., *Surface charge-mediated rapid hepatobiliary excretion of mesoporous silica nanoparticles.* Biomaterials, 2010. **31**(21): p. 5564-74.
88. Tang, L., et al., *Synthesis and biological response of size-specific, monodisperse drug-silica nanoconjugates.* ACS Nano, 2012. **6**(5): p. 3954-66.
89. Ohulchanskyy, T.Y., et al., *Organically modified silica nanoparticles with covalently incorporated photosensitizer for photodynamic therapy of cancer.* Nano Lett, 2007. **7**(9): p. 2835-42.
90. Krishnan, K.M., et al., *Nanomagnetism and spin electronics: materials, microstructure and novel properties.* Journal of Materials Science, 2006. **41**(3): p. 793-815.

91. Lunov, O., et al., *Lysosomal degradation of the carboxydextran shell of coated superparamagnetic iron oxide nanoparticles and the fate of professional phagocytes.* Biomaterials, 2010. **31**(34): p. 9015-22.
92. Weissleder, R., et al., *Superparamagnetic iron oxide: pharmacokinetics and toxicity.* AJR Am J Roentgenol, 1989. **152**(1): p. 167-73.
93. Turcheniuk, K., et al., *Recent advances in surface chemistry strategies for the fabrication of functional iron oxide based magnetic nanoparticles.* Nanoscale, 2013. **5**(22): p. 10729-52.
94. Berry, C.C., et al., *Dextran and albumin derivatised iron oxide nanoparticles: influence on fibroblasts in vitro.* Biomaterials, 2003. **24**(25): p. 4551-7.
95. Lunov, O., et al., *The effect of carboxydextran-coated superparamagnetic iron oxide nanoparticles on c-Jun N-terminal kinase-mediated apoptosis in human macrophages.* Biomaterials, 2010. **31**(19): p. 5063-71.
96. Tromsdorf, U.I., et al., *A highly effective, nontoxic T1 MR contrast agent based on ultrasmall PEGylated iron oxide nanoparticles.* Nano Lett, 2009. **9**(12): p. 4434-40.
97. Xie, J., et al., *Controlled PEGylation of Monodisperse Fe3O4 Nanoparticles for Reduced Non-Specific Uptake by Macrophage Cells.* Advanced Materials, 2007. **19**(20): p. 3163-3166.
98. Chen, T., et al., *Smart multifunctional nanostructure for targeted cancer chemotherapy and magnetic resonance imaging.* ACS Nano, 2011. **5**(10): p. 7866-73.
99. Ruiz-Hernandez, E., A. Baeza, and M. Vallet-Regi, *Smart drug delivery through DNA/magnetic nanoparticle gates.* ACS Nano, 2011. **5**(2): p. 1259-66.
100. Huang, C.C., et al., *Enhancing transversal relaxation for magnetite nanoparticles in MR imaging using Gd(3)+- chelated mesoporous silica shells.* ACS Nano, 2011. **5**(5): p. 3905-16.
101. El-Boubbou, K., C. Gruden, and X. Huang, *Magnetic glyco-nanoparticles: a unique tool for rapid pathogen detection, decontamination, and strain differentiation.* J Am Chem Soc, 2007. **129**(44): p. 13392-3.
102. Bakandritsos, A., G.C. Psarras, and N. Boukos, *Some physicochemical aspects of nanoparticulate magnetic iron oxide colloids in neat water and in the presence of poly(vinyl alcohol).* Langmuir, 2008. **24**(20): p. 11489-96.
103. Mazur, M., et al., *Iron oxide magnetic nanoparticles with versatile surface functions based on dopamine anchors.* Nanoscale, 2013. **5**(7): p. 2692-702.
104. Mahmoudi, M., et al., *Optimal design and characterization of superparamagnetic iron oxide nanoparticles coated with polyvinyl alcohol for targeted delivery and imaging.* J Phys Chem B, 2008. **112**(46): p. 14470-81.
105. Xu, C., et al., *Dopamine as a robust anchor to immobilize functional molecules on the iron oxide shell of magnetic nanoparticles.* J Am Chem Soc, 2004. **126**(32): p. 9938-9.
106. Xie, J., et al., *Linking Hydrophilic Macromolecules to Monodisperse Magnetite (Fe(3)O(4)) Nanoparticles via Trichloro-s-triazine.* Chem Mater, 2006. **18**(23): p. 5401-5403.
107. Amstad, E., et al., *Ultrastable iron oxide nanoparticle colloidal suspensions using dispersants with catechol-derived anchor groups.* Nano Lett, 2009. **9**(12): p. 4042-8.
108. Shultz, M.D., et al., *Reactive nature of dopamine as a surface functionalization agent in iron oxide nanoparticles.* J Am Chem Soc, 2007. **129**(9): p. 2482-7.
109. Lei, C., et al., *Dopamine as the coating agent and carbon precursor for the fabrication of N-doped carbon coated Fe3O4 composites as superior lithium ion anodes.* Nanoscale, 2013. **5**(3): p. 1168-75.
110. Palumbo, A., et al., *Nitrite- and peroxide-dependent oxidation pathways of dopamine: 6-nitrodopamine and 6-hydroxydopamine formation as potential contributory*

mechanisms of oxidative stress- and nitric oxide-induced neurotoxicity in neuronal degeneration. Chem Res Toxicol, 1999. **12**(12): p. 1213-22.
111. Khanal, M., et al., *Phenylboronic-acid-modified nanoparticles: potential antiviral therapeutics.* ACS Appl Mater Interfaces, 2013. **5**(23): p. 12488-98.
112. Mochalin, V.N., et al., *The properties and applications of nanodiamonds.* Nat Nanotechnol, 2012. **7**(1): p. 11-23.
113. Danilenko, V.V., *On the History of the Discovery of Nanodiamond Synthesis.* Physics of the Solid State, 2004. **46**(4): p. 581–584.
114. Krüger, A., et al., *Unusually tight aggregation in detonation nanodiamond: Identification and disintegration.* Carbon, 2005. **43**(8): p. 1722-1730.
115. Ōsawa, E., *Recent progress and perspectives in single-digit nanodiamond.* Diamond and Related Materials, 2007. **16**(12): p. 2018-2022.
116. Ho, D., *Nanodiamonds: Applications in Biology and Nanoscale Medicine.* Springer, 2009.
117. Zhang, X.Q., et al., *Polymer-functionalized nanodiamond platforms as vehicles for gene delivery.* ACS Nano, 2009. **3**(9): p. 2609-16.
118. Fu, C.C., et al., *Characterization and application of single fluorescent nanodiamonds as cellular biomarkers.* Proc Natl Acad Sci U S A, 2007. **104**(3): p. 727-32.
119. Wehling, J., et al., *Bactericidal Activity of Partially Oxidized Nanodiamonds.* ACS Nano, 2014.
120. Barras, A., et al., *Glycan-functionalized diamond nanoparticles as potent E. coli anti-adhesives.* Nanoscale, 2013. **5**(6): p. 2307-16.
121. Yu, S.J., et al., *Bright fluorescent nanodiamonds: no photobleaching and low cytotoxicity.* J Am Chem Soc, 2005. **127**(50): p. 17604-5.
122. Osswald, S., et al., *Control of sp2/sp3 carbon ratio and surface chemistry of nanodiamond powders by selective oxidation in air.* J Am Chem Soc, 2006. **128**(35): p. 11635-42.
123. Krueger, A., *The structure and reactivity of nanoscale diamond.* Journal of Materials Chemistry, 2008. **18**: p. 1485–1492.
124. Ozawa, M., et al., *Preparation and Behavior of Brownish, Clear Nanodiamond Colloids.* Advanced Materials, 2007. **19**(9): p. 1201-1206.
125. Williams, O.A., et al., *Size-dependent reactivity of diamond nanoparticles.* ACS Nano, 2010. **4**(8): p. 4824-30.
126. Nguyen, T.T.-B., H.-C. Chang, and V.W.-K. Wu, *Adsorption and hydrolytic activity of lysozyme on diamond nanocrystallites.* Diamond and Related Materials, 2007. **16**(4-7): p. 872-876.
127. Alhaddad, A., et al., *Nanodiamond as a vector for siRNA delivery to Ewing sarcoma cells.* Small, 2011. **7**(21): p. 3087-95.
128. Chen, M., et al., *Nanodiamond-mediated delivery of water-insoluble therapeutics.* ACS Nano, 2009. **3**(7): p. 2016-22.
129. Huang, H., et al., *Active nanodiamond hydrogels for chemotherapeutic delivery.* Nano Lett, 2007. **7**(11): p. 3305-14.
130. Mohan, N., et al., *In vivo imaging and toxicity assessments of fluorescent nanodiamonds in Caenorhabditis elegans.* Nano Lett, 2010. **10**(9): p. 3692-9.
131. Krueger, A., *New carbon materials: biological applications of functionalized nanodiamond materials.* Chemistry, 2008. **14**(5): p. 1382-90.
132. Martin, R., et al., *Fenton-treated functionalized diamond nanoparticles as gene delivery system.* ACS Nano, 2010. **4**(1): p. 65-74.

133. Martin, R., et al., *Nano-jewels in biology. Gold and platinum on diamond nanoparticles as antioxidant systems against cellular oxidative stress.* ACS Nano, 2010. **4**(11): p. 6957-65.
134. Barras, A., et al., *Functionalization of diamond nanoparticles using "click" chemistry.* Langmuir, 2010. **26**(16): p. 13168-72.
135. Barras, A., et al., *Direct functionalization of nanodiamond particles using dopamine derivatives.* Langmuir, 2011. **27**(20): p. 12451-7.
136. Dahoumane, S.A., et al., *Protein-functionalized hairy diamond nanoparticles.* Langmuir, 2009. **25**(17): p. 9633-8.
137. Hsu, M.H., et al., *Directly Thiolated Modification onto the Surface of Detonation Nanodiamonds.* ACS Appl Mater Interfaces, 2014.
138. Zhu, Y., et al., *The biocompatibility of nanodiamonds and their application in drug delivery systems.* Theranostics, 2012. **2**(3): p. 302-12.
139. Liu, K.K., et al., *Endocytic carboxylated nanodiamond for the labeling and tracking of cell division and differentiation in cancer and stem cells.* Biomaterials, 2009. **30**(26): p. 4249-59.
140. Schrand, A.M., et al., *Are diamond nanoparticles cytotoxic?* J Phys Chem B, 2007. **111**(1): p. 2-7.
141. Xing, Y., et al., *DNA damage in embryonic stem cells caused by nanodiamonds.* ACS Nano, 2011. **5**(3): p. 2376-84.
142. Yuan, Y.W., X.; Jia, G.; Liu, J. H.; Wang, T.; Gu, Y.; Yang, S. T.; Zhen, S.; Wang, H.; Liu, Y., *Pulmonary toxicity and translocation of nanodiamonds in mice.* Diamond & Related Materials, 2010. **19**: p. 291–299.
143. Rojas, S., et al., *Biodistribution of amino-functionalized diamond nanoparticles. In vivo studies based on 18F radionuclide emission.* ACS Nano, 2011. **5**(7): p. 5552-9.

CHAPTER 2

Hepatitis C Virus (HCV): managing HCV infection efficiently

2.1. Hepatitis C Virus (HCV)

Though HCV was identified first in 1989 [1], its impact on public health was known only in the past few years. It is considered a major cause of chronic liver diseases leading to fibrosis, cirrhosis and hepatocellular carcinoma over the course of several years [2]. Humans are natural hosts for HCV and the virus is generally transmitted by blood through medical and surgical procedures and intravenous drug use. According to the consensus panel of the National Institute of Health (NIH), HCV infection starts with acute hepatitis in which 20-80 % is self resolving; in 50-80 % cases , HCV infection develops into a chronic desease (**Figure 2.1**), causing hepatitis, cirrhosis (in ~10-20 % of cases after 10-20 years), and hepatocellular carcinoma (HCC). The incidence rate is 1-4 % per year in patients with HCV-related cirrhosis [3].

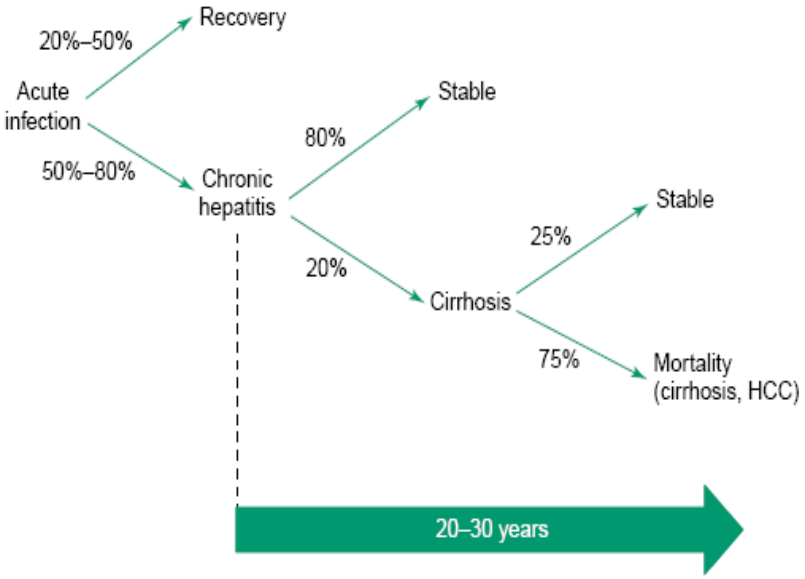

Figure 2.1. Schematic depiction of natural history of HCV infection. HCV infection starts with acute infection and through chronic hepatitis can lead to cirrhosis to mortality [4].

HCV is a small envelope virus of size 40-60 nm with positive stranded RNA genome and belongs to the Hepacivirus genus in the *Flaviviridae* family. HCV genotypes are identified from the phylogenetic analysis of full-length or partial sequence of HCV strains isolated in various regions of world. The strains include six main groups generally numbered from 1 to 6 and referred as 'types' or 'clades' and various subtypes or subclades had been also identified which are indicated by lower-case letters, for instance 1a, 1b, 1c, …., 2a, 2b, 2c,…, and so on [4].

Currently used standard therapies including pegylated interferon and ribavirin (**Figure 2.2B/C**) have raised the hope of managing HCV infection efficiently in countries with adequate medical infrastructures. Most of the recently available therapeutic molecules are shown to inhibit the replication step by targeting protease and polymerase [5]. However, due to the fact of existence of the genetic diversity during replication in the host, development of drug-resistant virus mutants usually cause significant limitations for the development of anti-HCV drug [6]. Therefore, combinations of drugs targeting various steps of viral life cycle along with virus entry can improve the effectiveness of therapeutics.

2.2. Replication of HCV in host cell

HCV genome codes two envelope glycoproteins, E1 and E2, which play a key role in virus entry into the hepatocyte. HCV entry is a complex process which initiates with the attachment of virus on the receptor present on hepatocytes following the endocytosis. After possible receptor-mediated endocytosis, HCV envelope glycoproteins are thought to mediate fusion of the virus envelope with endosomal membrane through a pH-dependent mechanism. The viral nucleocapsid is thought to be uncoated after its release into cytoplasm (**Figure 2.2A**). HCV RNA later serves as a template for viral replication and as messenger RNA (mRNA) for HCV protein synthesis. Binding of ribosomal 40S subunit mediates polyprotein translation to the internal ribosome entry site (IRES). The resolved 3D structure of IRES [7] has opened the possibility to develop the IRES inhibitor strategies to inhibit the HCV infection. Polyprotein translation is ensured by the 80S functional ribosome, and 3'untranslated region (UTR) of HCV genome plays the regulatory role in this process. The cellular and viral proteases further co- and post- translate the polyprotein precursor to yield 10 mature proteins [8].

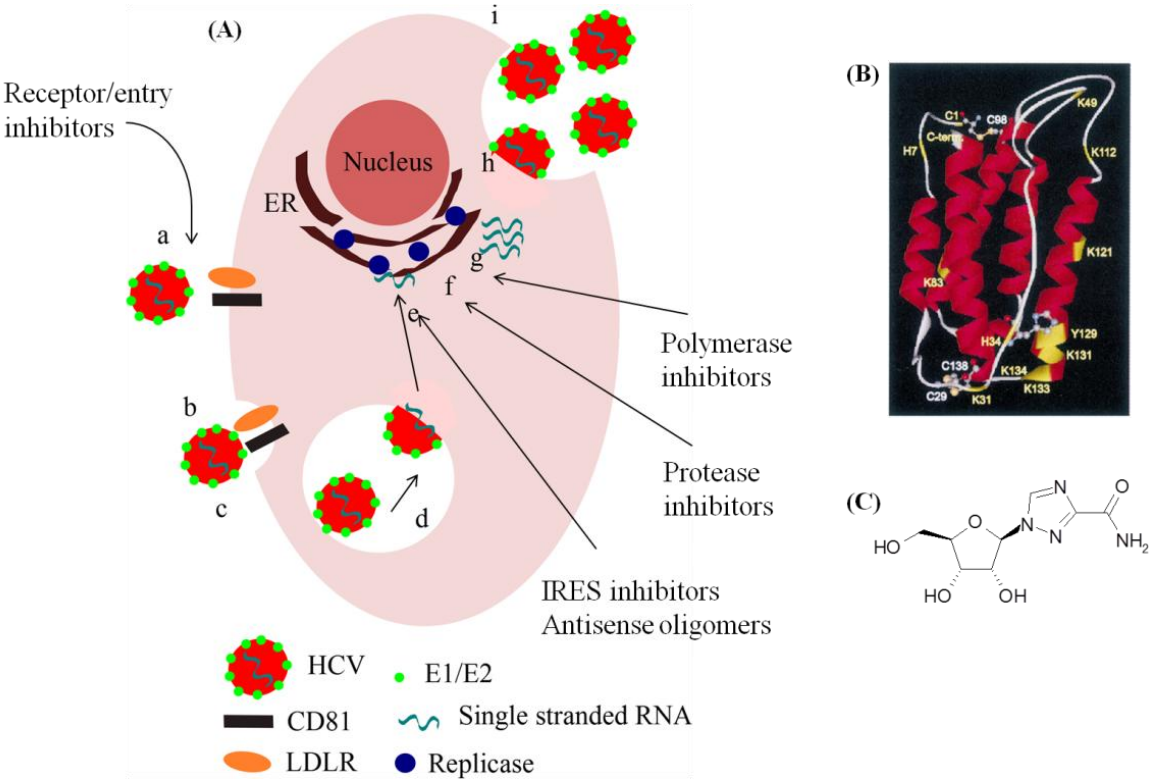

Figure 2.2. Schematic representation of life cycle of HCV showing several specific steps that could be the targets for antiviral drugs. a. attachment; b. endocytosis; c. virion-membrane fusion; d. uncoating; e-g. translation and polyprotein processing, replicase assembly, RNA replication, viral assembly and ER budding; h. vesicle transport and glycoprotein maturation; i. vesicle fusion and virions release (A). Abbreviations: endoplasmic reticulum (ER), internal ribosome-entry site (IRES), low-density lipoprotein receptor (LDLR), Ribbon structure of crystal structure of Interferon-alpha2b (B) [9] and Chemical structure of ribavirin (C).

Among these 10 proteins, the three structural proteins (C, E1 and E2) (**Figure 2.3**) are released by the action of host-cell signal peptidase. A small membrane polypeptide designated p7 separates those structural proteins from non-structural proteins. The matured form of the core protein (C), in conjunction with the genomic RNA, forms the HCV nucleocapsid. In addition to its role in nucleocapsid formation, HCV core protein has experimentally been suggested to play a role in the pathogenesis of liver disease by modulating host-cell gene transcription, cell proliferation, cell death and cell signaling, lipid metabolism, and host immune responses [10]. The p7 protein currently was reported to belong to the viroporin family and to form an ion channel, thus strongly considered to play an important role in viral particle release and maturation [11, 12].

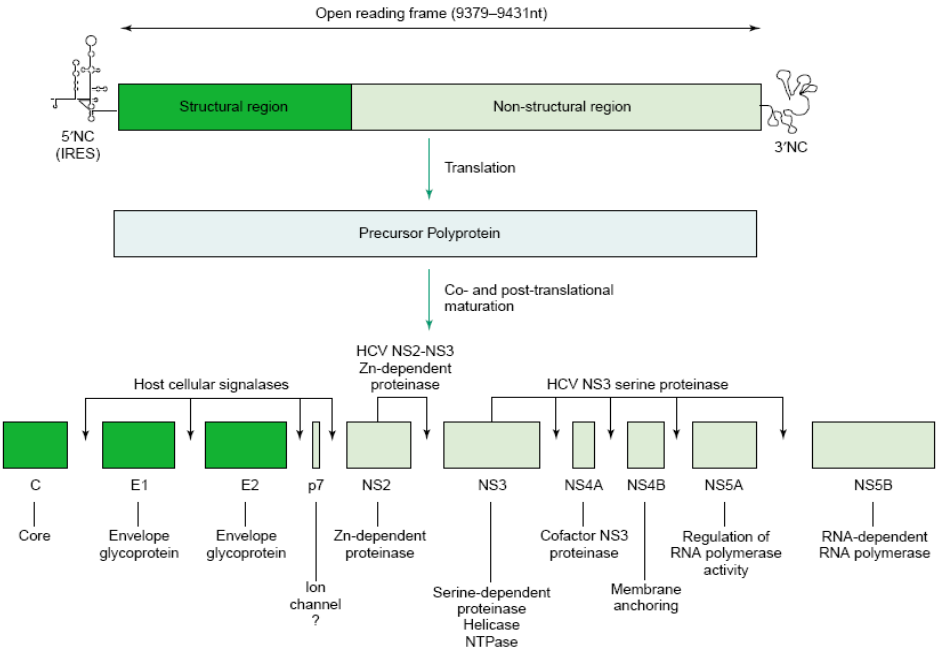

Figure 2.3. Hepatitis C virus (HCV) polyprotein translation and post-translational cleavage leading to the production of functional HCV proteins. IRES, internal ribosome entry site; NC, non-coding.

The non-structural (NS) proteins are referred as NS2, NS3, NS4A, NS4B, NS5A and NS5B (**Figure 2.3**). Among them, the NS2–NS3 junction has a zinc-dependent autocatalytic proteinase function, which separates NS2 from the N-terminus of NS3 [10]. The N-terminal one-third of NS3 is a serine proteinase and its association with NS4A is responsible for downstream cleavage of the HCV polyprotein. The 3D structure of NS3 serine proteinase, both free and complexed with NS4A, was recently determined, opening the way to develop the specific inhibitors. The C-terminal two-thirds of NS3 possess helicase and NTPase functions. The 3D structure of this domain has also been determined, both free and complexed with DNA, again providing hope to the discovery of specific inhibitors. NS4B is an integral membrane protein that appears to play a role in the formation of the replication complex. NS5A plays an important, but unknown, role in the regulation of NS5B, the RNA-dependent RNA polymerase (RdRp). The 3D structure of RdRp was recently resolved, revealing several potential target sites for specific inhibitors [10].

2.3. HCV entry process

Entry of virus into host cell is required for initiation, spread and maintenance of infection and thus could be a promising target for antiviral therapy. HCV entry is a complex process mediated by both viral and host cells factors (**Figure 2.4**). Though viral envelope glycoproteins are considered as key factor for entry process of HCV, as a result of its association with low- or very low-density lipoproteins, the lipoprotein moiety can also play a role in the entry process of HCV particles. Series of specific cellular entry factors have been shown to be essentials in the early multisteps HCV life cycle. These molecules include the scavenger receptor class B type 1 (SRB1), the tetraspanin CD81, tight junction proteins claudin 1 (CLDN1) and occludin (OCLN), and receptor tyrosine kinase-like epidermal growth factor receptor. After interaction of envelope glycoprotein, HCV particle is internalized by clathrin-mediated endocytosis [13]. Fusion between viral and endosomal membranes is followed by release of the viral genome into the cytosol where translation and replication take place. HCV particles are then assembled and released from the host cell.

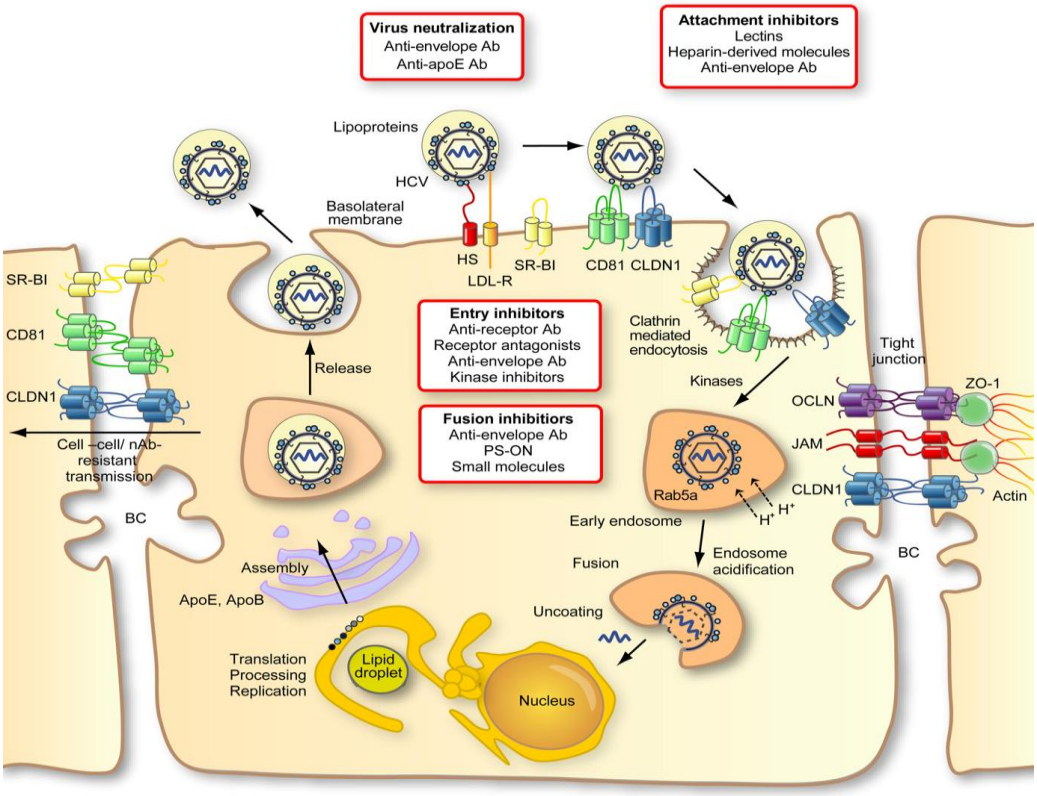

Figure 2.4. HCV entry into hepatocytes: molecular mechanisms and targets for antiviral therapies [14]. HCV is believed to first interact with HS and LDLR on the basolateral membrane surface of hepatocytes to allow concentration of the virion. Subsequently,

interaction with other host factors such as SR-BI, CD81, CLDN1, and OCLN ultimately leads to viral internalization via clathrin-mediated endocytosis.
Abbreviations: Ab, antibody; apo, apolipoprotein; BC, bile canaliculi; CLDN1, claudin 1; HCV, Hepatitis C Virus; HS, hepran sulfate; JAM, junction-associated adhesion molecule; LDLR, low-density lipoprotein receptor; nAb, neutralizing antibody; OCLN, occludin; PS-ON, phosphorothioate oligonucleotides; SR-BI, scavenger receptor class B type I; ZO, zona occludens.

An alternative route of viral entry is direct cell-cell transmission which is resistant to neutralizing antibodies. Entry inhibitors can potentially interfere with the viral life cycle at different steps, i.e. viral binding, post-binding and fusion. Some of the compounds that targets within the HCV entry process and their stage of development are summarized in **Table 2.1**. Current clinical model and HCV-infected patients have demonstrated that the virus has developed multiple strategies to escape host neutralizing immune responses during viral entry process. These includes evasion from neutralizing antibodies and viral spread by cell-cell transmission [14]. These challenges have to be taken into consideration for design of efficient antiviral strategies. The well-conserved receptors and (co) receptors were considered to be more promising targets to overcome the high variability of the viral envelope proteins. Also, blockage of CD81, SR-B1, claudin 1 with monoclonal antibodies or small molecules could be the efficacious ways to prevent the HCV infection in a genotype-independent manner [15-18]. However, by interfering to the natural functions of these host receptors could lead to undesired side effects. Without interfering the host's receptor cells, another way of preventing HCV is to target envelope glycoprotein using small compounds [19]. Nevertheless, those small compounds have found to be genotype-specific. Therefore, the concept of alternative way to block the interaction between virus and its receptors has been developed taking advantage of highly glycosylated nature of the viral envelope proteins E1 and E2. These glycosylation, upto 5 in E1 and 11 in E2, are located in specific sites and are well-conserved in different genotypes. Moreover, the glycans play major role in protein folding, HCV entry [20], and protection of the virus from antibody-dependent neutralization [21].

Table 2.1. Examples of compounds targeting viral entry and their stage of development. [14].

Target	Examples of compounds	Stage of development
HCV E1E2	Neutralizing antibodies	
	Polyclonal HCV IgG (civacir)	Phase II
	HCV-Ab^{XTL}68	Phase II
	Human mAB AR3	Mouse model
	CBH and HC antibodies	Cell culture
	IGH antibodies	Cell culture
	AP33	Cell culture
	3/11	Cell culture
	Fab e137	Cell culture
	HCV1 and HCV 95-2	Cell culture
	Heparin and HS analogues	Cell culture
	Lectins	Cell culture
HCV particle	Anti-apoE mAb	Cell culture
SR-BI	Anti-SR-BI pAb and mAb	Cell culture
	Serum amyloid A	Cell culture
CD81	Anti-CD81 mAb	Cell culture Mouse model
	Imidazole based compounds	Cell culture
CLDN1	Anti-CLDN1 pAB and mAb	Cell culture
Internalization/fusion	PS-ON	Mouse model
	Arbidol	Cell culture
	Chloroquine	Cell culture
	Silymarin	Cell culture

Abbreviations: CLDN, claudin; mAb, monoclonal antibody; pAb, polyclonal antibodies; SR-BI, scavenger receptor class B type I; PS-ON: phosphorothioate oligonucleotides

Natural lectins are gaining recognition currently that specifically targets glycan of envelope glycoproteins and has successfully revealed to inhibit the early stage of HCV entry *in vitro* [22, 23] and *in vivo* [23]. However, expenses on the large-scale production and purification of these protein-based anti-viral agents along with their stability issues, susceptible to be cleaved by proteolytic enzyme, make them less preferable for the eventual use. Therefore, small synthetic compounds like boronic acid derivatives that bind glycans selectively and strongly could be the better alternatives to antiviral lectins.

2.4. Experimental models for the study of HCV infection *in vitro*

The HCV's lifecycle and host-virus interactions that determine the infection outcomes are difficult to study because of rarely available suitable HCV cell culture infection systems

and small animal models. Consequently, the development of the preventive vaccines and anti-HCV therapeutics has been hindered severely. However, different experimental models have been developed eventually that facilitates the understanding of HCV lifecycle and further help to accelerate the anti-HCV drug development. These experimental models include HCV replicons, infectious HCV cell culture systems (HCVcc) and HCV pseudotyped particles (HCVpp). We have worked mostly on HCVcc and HCVpp experimental models in this thesis that are discussed in detail below.

2.4.1. HCV cell culture infection systems (HCVcc)

Several groups reported robust HCV infection and production of infectious progeny HCV (HCVcc) in Huh 7 human hepatoma cell cultures using the HCV genotype 2a JFH-1 consensus genome cloned from a Japenese Fulminant Hepatitis (JFH) patient or derivative thereof [24-26]. Thus, based on these reports, the ability to recapitulate the entire lifecycle *in vitro* was finally achieved in 2005. This system yields viral titre between 10^4 -10^6 units/mL and allows spreading of viral infection throughout a cell culture within days of inoculation. Most importantly, the HCVcc is infectious in primary hepatocytes transplanted into SCID-uPA mice, and virus recovered from it is infectious too *in vitro* [27]. By the help of this experimental model, high throughput screening (HTS) assays are being developed as means to discover new HCV-specific therapeutics targeting on the aspects of infection. Currently, HCVcc encoding a luciferase reporter gene for luciferase assay [28] and HCVcc having mutation in E1 glycoprotein to reconstitute the A4 epitope; for immuno-fluorescence assay are widely used for HTS assay to study the efficiency of anti-HCV therapeutics [29].

2.4.2. HCV pseudotyped particles (HCVpp)

HCV entry studies have been accelerated following the development of HCVpp that incorporates the HCV E1/E2 glycoproteins on murin leukemia virus (MLV) or HIV-1 retroviral core particles [13, 30]. Although HCVpp only resemble HCV at the level of surface glycoprotein expression, their ability to mimic HCV entry has helped to track and analyze the HCV entry process through identifying various cellular entry factors and simultaneously the possible targets [31-33]. In this context, only the early steps of the viral life cycle, i.e. virus interaction with receptors, uptake and fusion, are HCV specific, whereas all later steps are dependent on the retroviral nucleocapsid elements. These pseudoparticles are defective for reinfection since they do not contain the genetic information to express envelope

glycoproteins in their genome. All the six HCV genotypes psudotyped particles are now available encoding for various reporter proteins like GFP and luciferase and thus prove to be a strong tool to study HCV entry and development of the HCV entry inhibition drug [34].

2.5. Boronic acid derivatives as antiviral agents

Boronic acid derivatives are being highly recognized in the field of medicinal chemistry because of its peculiar property to form tetravalent boronate di-ester cyclic complexes selectively and reversibly with either 1,2- or 1,3 cis-diols that are specifically present in the glycans [35, 36] (**Figure 2.5B**). These derivates are often called "pseudo-lectins" or "borono-lectins" because of their affinity for carbohydrates and are previously investigated for the specific capture of glycoproteins from unfractionated protein mixtures [2, 37]. In o numerous studies, boronic acid derivatives have been used for the development of glucose-responsive sensors for release of insulin and cyclic adenosine monophosphate (cAMP) from boronic acid modified mesoporous silica nanoparticles (MSN) as shown in **Figure 2.5A** [38]. Gluconic acid-modified insulin (G-Ins) is immobilized on the exterior surface of MSN through a diol ester bond between boronic acid and gluconic acid and at the same time, also serve as caps to encapsulate cAMP molecules inside the mesopores of MSN. The release of both G-Ins and cAMP from MSN was then triggered by introducing glucose that displaces the G-Ins from boronic acid and thus uncapped MSN, leading to release if cAMP. So, the idea is to control the release of both insulin and cAMP by the blood glucose level of the patient itself. Likewise, in another study, 4-aminophenylboronic acid modified reduced graphene oxide was utilized for sugar detection [39] where the boronic acid sensing system showed a remarkable stability and proved to be a suitable sugar detector for the detection of sugar content of complex matrixes like apple juice. Similarly, one interesting study was carried out in fullerene to study the target-selective photodegradation of oligosaccharides by fullerene-boronic acid hybrids upon visible light irradiation [40].

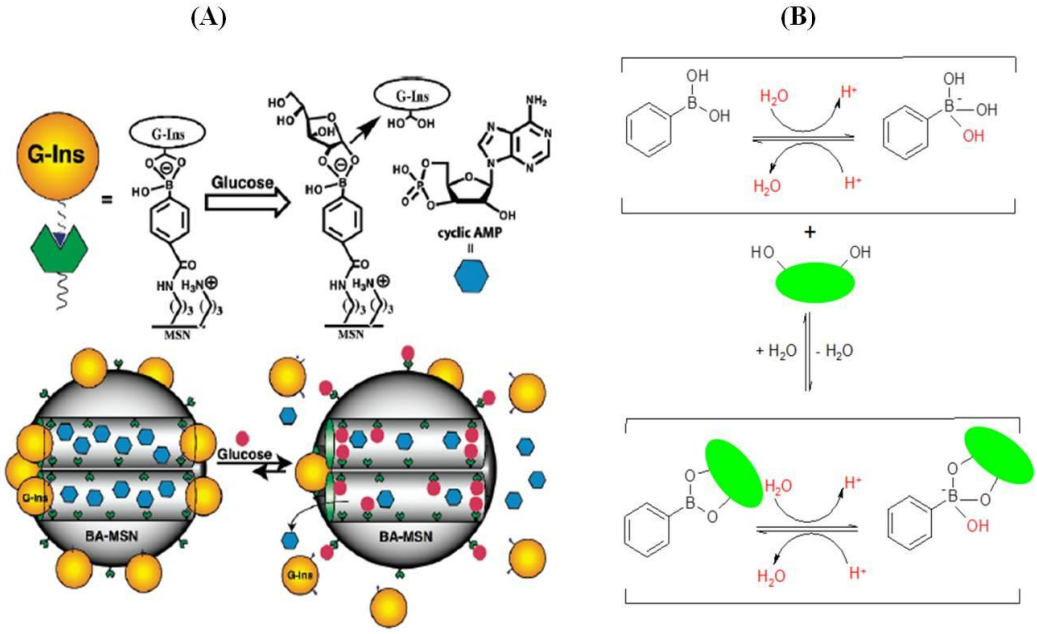

Figure 2.5. (A) Schematic representation of the glucose-responsive MSN-based delivery system for controlled release of bioactive G-Ins (gluconic acid-modified insulin) and cAMP [38], (B) Structural representation of binding equilibrium of phenylboronic acid with a diol. In either of cases, binding constant depends on pKa of boronic acid and optimum pH for binding boronic acid compounds to diol is above the pKa of boronic acid [41].

One exceptional property of boronic acid is that it is a strong Lewis acid and interacts with all nucleophiles/Lewis bases including diols on the formation of a six-membered ring under appropriate conditions [42]. The binding affinity between sugars and boronic acid is highly dependent on ionization constant (pKa) of boronic acid. The pKa of most phenylboronic acid varies from 4.5 to 8.8 [43] depending upon the phenyl substitution [44] and some of the examples are listed on **Table 2.2.** This indicates that with an appropriate substitution, boronic acid can made conversion from a neutral and trigonal planar sp^2 boron to an anionic tetrahedral (**Figure 2.5B**) under physiological conditions.

Table 2.2. Ionization constant (pKa) for selected boronic acids derivatives.

Boronic acid, $RB(OH)_2$	pKa
Boric acid, $B(OH)_3$	9.0
Methyl	10.4
Phenyl	8.9

3,5-Dichlorophenyl	7.4
3,5-Bis(trifluoromethyl)phenyl	7.2
2-Methoxyphenyl	9.0
3-Methoxyphenyl	8.7
4-Methoxyphenyl	9.3
4-Carboxyphenyl	8.4
2-Nitrophenyl	9.2
4-Nitrophenyl	7.1
4-Bromophenyl	8.6
4-Fluorophenyl	9.1
2-Methylphenyl	9.7
3-Methylphenyl	9.0
4-Methylphenyl	9.3
3,5-Dimethylphenyl	9.1
3-Methoxycarbonyl-5-nitrophenyl	6.9
2-Fluoro-5-nitrophenyl	6.0
3-Pyridyl (15)	4.0, 8.2
3-Benzyl-3-pyridylium	4.2
8-Quinolinyl	4.0

The rate of formation/dissociation of phenylboronate di-ester complexes is pH-dependent and occurs most rapidly in tetrahedral state of boron, which is mostly favored at pH value higher than the pKa of the boronic acid [42, 45]. Moreover, the pKa value further depends on variations in structures of phenylboronic acid unit and these analogs can provide improved affinity and selectivity towards a given saccharide as well as analogs with modulated pH optimal, better adapted for sequestering sugars under physiological conditions [36, 41, 46, 47]. Realizing that the process of cleaving an amide bond also requires the conversion of sp^2 carbonyl carbon to a tetrahedral sp^3 carbon, it is easy to understand that boronic acid compounds would make good transition state analogs for the inhibition of hydrolytic enzymes and it has been used as serine protease inhibitor to develop potent anti-coagulant agent [41].

Besides the development of boronic acid-sugar sensing devices, the concept of forming reversible diol complexes between boronic acid derivatives and sugars has also been

largely applied in therapeutic strategies for the treatment of Human Immunodeficiency virus (HIV) and the activity of these boronic acid derivatives are due to their affinity to the highly glycosylated envelope of HIV [48-50]. However, investigations have shown lack of activity of monovalent phenylboronic acid derivatives to decrease the infection level of HIV [35]. In contrary, significant boronic acid moieties present on a polymeric scaffold i.e. multivalent have been demonstrated to be more effective on interfering the interaction between HIV and its target host cells and thereby reduce viral infections [50-52]. The multiple copies of boronic acid polymers has been put forward the ability to have multivalent interactions with glycan present in the envelope glycoprotein of virus (**Figure 2.6**). The study has shown that the polymer bearing multiple copies of boronic acid can form multiple phenylboronate di-ester complexes with several cis-diol units of glycans reducing the viral infection whereas corresponding monovalent unit shows no any significant inhibition effect on the viral infection.

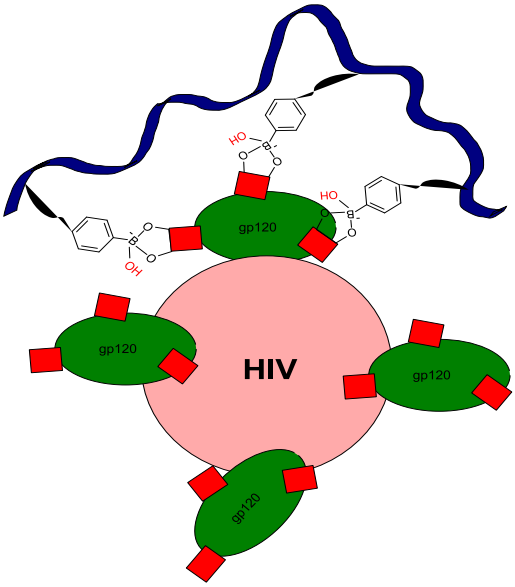

Figure 2.6. Hypothetical scheme of the binding chemistry: multivalent polymer bound boronic acid (represented as blue ribbon) binding due to complexation with a high mannose region (red box) of gp120 (green eclipse) through interaction with the 4,6-diols of mannopyranose residues present in envelope gp120 of HIV [51].

Therefore, it is unambiguous that multiple copies of boronic acid moieties are essential to inhibit the viral infection. Biocompatible and inert nanomaterials could be the best alternatives for creation of multivalent boronic acid.

Nanomaterials have been effectively studied in past few years against HCV and other viral infections. Mostly, researcher used nanomaterials as an artificial RNA silencing machinery [53], that were used as targeted delivery system to deliver either interferon-alpha (IFNα) [54] or DNAzyme [55], which can reduce the possible side effects of these therapeutics while inhibiting HCV infection both *in vitro* and *in vivo*. Lee and co-worker used hybrid material of gold nanoparticle and hyaluronic acid to load IFNα and to specifically target liver tissue. In another study carried out by Wang et al., gold nanoparticle was utilized to design nanozyme that mimics RNA-cleavage function of the active RNA-induced silencing complex (RISC)-the cellular machinery that mediates RNA interference pathways. This nanozyme is reported to decrease 99 % HCV RNA levels in mice [53]. Similarly, Ryoo and co-workers had reported iron oxide nanoparticles-assisted functional delivery of therapeutic DNAzyme for treatment of HCV by inducing knockdown of hepatitis C virus (HCV) gene, NS3 which encodes helicase and protease essential for the virus replication [55]. These nanoparticles-based studies are mostly focused on targeting the replication of virus, thus there is no any report till date on using nanoparticle-based HCV entry inhibitors which are associated with multivalent boronic acid forming diol complexes with glycans present on the envelope glycoprotein. Thus, nanoparticles can create the best platform for making multivalent boronic moieties that could be useful for inhibition of HCV entry into the targeted hepatocyte. Also, in medicinal chemistry, use of boronic acids as enzyme inhibitors to a large degree reflects the usefulness of boron as a carbon analog in the binding process, but not in terms of reactions, which is the essence of a good enzyme inhibitor. Likewise, several researches have been carried out for investigation of boronic acid as protease enzyme inhibitor to reduce the infection of hepatitis C virus (HCV) [56, 57] where a series of peptide boronic acids containing residues were investigated as inhibitors of HCV NS3 protease, a viral non-structural protein, in viral replicon assay. Though there are few studies done on the boronic acid compounds as anti-viral agents, these studies mostly focus on the inhibition of non-structural protein that is essential for viral replication but not on entry of virus.

Therefore, taking advantages of nanoparticle's features to have multiple boronic acid moieties on its surface and properties of boronic acid to form reversible diol complex with glycans present on envelope glycoprotein of HCV have been put together, to develop the stable and efficient HCV entry inhibitors.

The ability of boronic acid modified nanostructures to block HCV entry by forming reversible diol complex with envelope glycoprotein of HCV is investigated in details in the next two chapters. The multivalency of boronic acid can be achieved by utilizing the large surface-to-volume ratio of nanoparticles whose surface can be easily modified by various surface functionalization techniques. These nanostructures could be a cost-effective way, to treat HCV infection along with combinations of drugs targeting various steps of viral cell life cycle.

2.6. References

1. Choo, Q.L., et al., *Isolation of a cDNA clone derived from a blood-borne non-A, non-B viral hepatitis genome.* Science, 1989. **244**(4902): p. 359-62.
2. Tan, S.L., et al., *Hepatitis C therapeutics: current status and emerging strategies.* Nat Rev Drug Discov, 2002. **1**(11): p. 867-81.
3. Panel, C., *National institute of health consensus development conference statement: Management of hepatitis C: 2002-June 10-12, 2002.* Hepatology, 2002. **36**: p. S3-S20.
4. Pawlotsky, J.M., *Pathophysiology of hepatitis C virus infection and related liver disease.* Trends Microbiol, 2004. **12**(2): p. 96-102.
5. Asselah, T. and P. Marcellin, *New direct-acting antivirals' combination for the treatment of chronic hepatitis C.* Liver Int, 2011. **31 Suppl 1**: p. 68-77.
6. Sarrazin, C. and S. Zeuzem, *Resistance to direct antiviral agents in patients with hepatitis C virus infection.* Gastroenterology, 2010. **138**(2): p. 447-62.
7. Kieft, J.S., et al., *Crystal structure of an RNA tertiary domain essential to HCV IRES-mediated translation initiation.* Nat Struct Biol, 2002. **9**(5): p. 370-4.
8. Grakoui, A., et al., *Expression and identification of hepatitis C virus polyprotein cleavage products.* J Virol, 1993. **67**(3): p. 1385-95.
9. Wang, Y.S., et al., *Structural and biological characterization of pegylated recombinant interferon alpha-2b and its therapeutic implications.* Adv Drug Deliv Rev, 2002. **54**(4): p. 547-70.
10. Penin, F., et al., *Structural biology of hepatitis C virus.* Hepatology, 2004. **39**(1): p. 5-19.
11. Pavlovic, D., et al., *The hepatitis C virus p7 protein forms an ion channel that is inhibited by long-alkyl-chain iminosugar derivatives.* Proc Natl Acad Sci U S A, 2003. **100**(10): p. 6104-8.
12. Xu, Z., et al., *Hepatitis C virus f protein is a short-lived protein associated with the endoplasmic reticulum.* J Virol, 2003. **77**(2): p. 1578-83.
13. Blanchard, E., et al., *Hepatitis C virus entry depends on clathrin-mediated endocytosis.* J Virol, 2006. **80**(14): p. 6964-72.
14. Zeisel, M.B., et al., *Hepatitis C virus entry into hepatocytes: molecular mechanisms and targets for antiviral therapies.* J Hepatol, 2011. **54**(3): p. 566-76.
15. Fofana, I., et al., *Monoclonal anti-claudin 1 antibodies prevent hepatitis C virus infection of primary human hepatocytes.* Gastroenterology, 2010. **139**(3): p. 953-64, 964 e1-4.
16. Meuleman, P., et al., *Anti-CD81 antibodies can prevent a hepatitis C virus infection in vivo.* Hepatology, 2008. **48**(6): p. 1761-8.

17. Meuleman, P., et al., *A human monoclonal antibody targeting scavenger receptor class B type I precludes hepatitis C virus infection and viral spread in vitro and in vivo.* Hepatology, 2012. **55**(2): p. 364-72.
18. Syder, A.J., et al., *Small molecule scavenger receptor BI antagonists are potent HCV entry inhibitors.* J Hepatol, 2011. **54**(1): p. 48-55.
19. Baldick, C.J., et al., *A novel small molecule inhibitor of hepatitis C virus entry.* PLoS Pathog, 2010. **6**(9): p. e1001086.
20. Goffard, A., et al., *Role of N-linked glycans in the functions of hepatitis C virus envelope glycoproteins.* J Virol, 2005. **79**(13): p. 8400-9.
21. Helle, F., et al., *The neutralizing activity of anti-hepatitis C virus antibodies is modulated by specific glycans on the E2 envelope protein.* J Virol, 2007. **81**(15): p. 8101-11.
22. Helle, F., et al., *Cyanovirin-N inhibits hepatitis C virus entry by binding to envelope protein glycans.* J Biol Chem, 2006. **281**(35): p. 25177-83.
23. Meuleman, P., et al., *Griffithsin has antiviral activity against hepatitis C virus.* Antimicrob Agents Chemother, 2011. **55**(11): p. 5159-67.
24. Kato, T., et al., *Sequence analysis of hepatitis C virus isolated from a fulminant hepatitis patient.* J Med Virol, 2001. **64**(3): p. 334-9.
25. Lindenbach, B.D., et al., *Complete replication of hepatitis C virus in cell culture.* Science, 2005. **309**(5734): p. 623-6.
26. Zhong, J., et al., *Robust hepatitis C virus infection in vitro.* Proc Natl Acad Sci U S A, 2005. **102**(26): p. 9294-9.
27. Lindenbach, B.D., et al., *Cell culture-grown hepatitis C virus is infectious in vivo and can be recultured in vitro.* Proc Natl Acad Sci U S A, 2006. **103**(10): p. 3805-9.
28. Zhang, Y., et al., *Novel chimeric genotype 1b/2a hepatitis C virus suitable for high-throughput screening.* Antimicrob Agents Chemother, 2008. **52**(2): p. 666-74.
29. Goueslain, L., et al., *Identification of GBF1 as a cellular factor required for hepatitis C virus RNA replication.* J Virol, 2010. **84**(2): p. 773-87.
30. Hsu, M., et al., *Hepatitis C virus glycoproteins mediate pH-dependent cell entry of pseudotyped retroviral particles.* Proc Natl Acad Sci U S A, 2003. **100**(12): p. 7271-6.
31. Helle, F. and J. Dubuisson, *Hepatitis C virus entry into host cells.* Cell Mol Life Sci, 2008. **65**(1): p. 100-12.
32. Keck, Z.Y., et al., *Therapeutic control of hepatitis C virus: the role of neutralizing monoclonal antibodies.* Curr Top Microbiol Immunol, 2008. **317**: p. 1-38.
33. Zeisel, M.B., et al., *Hepatitis C virus entry: molecular mechanisms and targets for antiviral therapy.* Front Biosci (Landmark Ed), 2009. **14**: p. 3274-85.
34. Yang, J.P., D. Zhou, and F. Wong-Staal, *Screening of small-molecule compounds as inhibitors of HCV entry.* Methods Mol Biol, 2009. **510**: p. 295-304.
35. Trippier, P.C., C. McGuigan, and J. Balzarini, *Phenylboronic-acid-based carbohydrate binders as antiviral therapeutics: monophenylboronic acids.* Antivir Chem Chemother, 2010. **20**(6): p. 249-57.
36. Yan, J., et al., *The relationship among pKa, pH, and binding constants in the interactions between boronic acids and diols—it is not as simple as it appears.* Tetrahedron, 2004. **60**(49): p. 11205-11209.
37. Lin, Z.-A., et al., *Synthesis of magnetic nanoparticles with immobilized aminophenylboronic acid for selective capture of glycoproteins.* Journal of Materials Chemistry, 2011. **21**(2): p. 518.
38. Zhao, Y., et al., *Mesoporous silica nanoparticle-based double drug delivery system for glucose-responsive controlled release of insulin and cyclic AMP*. J Am Chem Soc, 2009. **131**(24): p. 8398-400.

39. Wang, Q., et al., *Sensitive sugar detection using 4-aminophenylboronic acid modified graphene.* Biosens Bioelectron, 2013. **50**: p. 331-7.
40. Takahashi, D., S. Hirono, and K. Toshima, *Target-selective photodegradation of oligosaccharides by a fullerene-boronic acid hybrid upon visible light irradiation.* Chem Commun (Camb), 2011. **47**(42): p. 11712-4.
41. Yang, W., X. Gao, and B. Wang, *Boronic acid compounds as potential pharmaceutical agents.* Med Res Rev, 2003. **23**(3): p. 346-68.
42. Cheng, Y., et al., *A new class of fluorescent boronic acids that have extraordinarily high affinities for diols in aqueous solution at physiological pH.* Chemistry, 2010. **16**(45): p. 13528-38.
43. Liu, X.C.H., J.L.; Scouten, W.H. , *Synthesis and structural investigation of two potential boronate affinity chromatography ligands catechol [2-(diisopropylamino) carbonyl]phenylboronate and catechol [2-(diethylamino)carbonyl, 4-methyl]phenylboronate.* J Organomet Chem, 1995. **493**: p. 91-94.
44. Springsteen, G.W., B. , *A detailed examination of boronic acid–diol complexation.* Tetrahedron, 2002. **58**: p. 5291-5300.
45. Wiskur, S.L., et al., *Thermodynamic analysis of receptors based on guanidinium/boronic acid groups for the complexation of carboxylates, alpha-hydroxycarboxylates, and diols: driving force for binding and cooperativity.* Chemistry, 2004. **10**(15): p. 3792-804.
46. Cai, S.X. and J.F. Keana, *o-acetamidophenylboronate esters stabilized toward hydrolysis by an intramolecular O-B interaction: potential linkers for selective bioconjugation via vicinal diol moieties of carbohydrates.* Bioconjug Chem, 1991. **2**(5): p. 317-22.
47. Dowlut, M. and D.G. Hall, *An improved class of sugar-binding boronic acids, soluble and capable of complexing glycosides in neutral water.* J Am Chem Soc, 2006. **128**(13): p. 4226-7.
48. Balzarini, J., *Targeting the glycans of gp120: a novel approach aimed at the Achilles heel of HIV.* Lancet Infect Dis, 2005. **5**(11): p. 726-31.
49. Balzarini, J., *Targeting the glycans of glycoproteins: a novel paradigm for antiviral therapy.* Nat Rev Microbiol, 2007. **5**(8): p. 583-97.
50. Trippier, P.C., J. Balzarini, and C. McGuigan, *Phenylboronic-acid-based carbohydrate binders as antiviral therapeutics: bisphenylboronic acids.* Antivir Chem Chemother, 2011. **21**(3): p. 129-42.
51. Jay, J.I., et al., *Modulation of Viscoelasticity and HIV Transport as a Function of pH in a Reversibly Crosslinked Hydrogel.* Adv Funct Mater, 2009. **19**(18): p. 2969-2977.
52. Mahalingam, A., et al., *Activity and safety of synthetic lectins based on benzoboroxole-functionalized polymers for inhibition of HIV entry.* Mol Pharm, 2011. **8**(6): p. 2465-75.
53. Wang, Z., et al., *Nanoparticle-based artificial RNA silencing machinery for antiviral therapy.* Proc Natl Acad Sci U S A, 2012. **109**(31): p. 12387-92.
54. Lee, M.Y., et al., *Hyaluronic acid-gold nanoparticle/interferon alpha complex for targeted treatment of hepatitis C virus infection.* ACS Nano, 2012. **6**(11): p. 9522-31.
55. Ryoo, S.R., et al., *Functional delivery of DNAzyme with iron oxide nanoparticles for hepatitis C virus gene knockdown.* Biomaterials, 2012. **33**(9): p. 2754-61.
56. Priestley, E.S., et al., *P1 Phenethyl peptide boronic acid inhibitors of HCV NS3 protease.* Bioorg Med Chem Lett, 2002. **12**(21): p. 3199-202.
57. Boloor, A., et al., *Synthesis and antiviral activity of HCV NS3/4A peptidomimetic boronic acid inhibitors.* Bioorg Med Chem Lett, 2009. **19**(19): p. 5708-11.

CHAPTER 3

Phenylboronic acid-modified nanoparticles as potent antiviral therapeutics

Hepatitis C Virus (HCV) entry is a complex process which initiate with the attachment of virus on the receptor present on hepatocytes following the endocytosis, replication, assembly and release of viral particles from the host cell [1]. Like Human Immunodeficiency Virus (HIV), HCV also features highly glycosylated envelope proteins [2]. Majority of the compounds targeting HCV entry are various glycan recognizing proteins either lectins [3], including natural product like pradimicin [4, 5]. Proteins like cyanovirin-N and griffithsin have been proved to be active on blocking the entry and ultimately the level of infection by interacting with high-mannose glycans present on HCV glycoproteins [1, 4]. Nevertheless, expenses on the large-scale production and purification of these protein-based anti-viral agents along with their stability issues, likely to be cleaved by proteolytic enzyme make them less preferable for the eventual use.

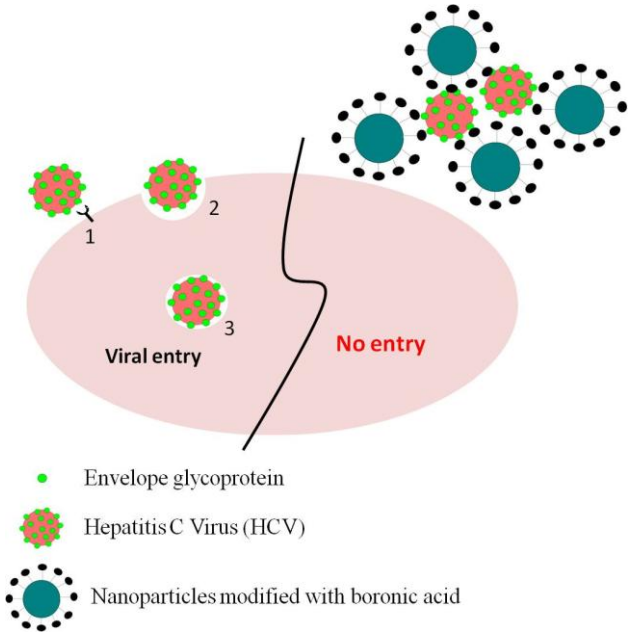

Figure 3.1. Schematic representation of the underlying concept of using boronic acid modified nanoparticles as HCV entry inhibitors. Three steps of viral entry are shown in the figure. Recognition of receptor present on the hepatocyte by glycans present on viral envelope protein (1) followed by the adherence (2) and encapsulation of viral particles by hepatocyte

(3). On the other hand in the presence of the multiple copies of BA on nanoparticle inhibits the entry of HCV by forming diol complexes with glycans of viral envelope protein.

Therefore, the carbohydrate binding synthetic compounds that bind glycans selectively and strongly could be the better alternatives to antiviral lectins. Our idea is thus to identify if simple organic ligands, such as phenylboronic acid moieties, when liked to nanostructures would allow the development of a new potential therapeutic strategy to interfere with entry of hepatitis C virus (**Figure 3.1**). The concept of forming reversible diol complexes between boronic acid derivatives and sugars has also been largely applied in therapeutic strategies for the treatment of HIV and the activity of these boronic acid derivatives are due to their affinity to bind to the highly glycosylated envelope of HIV [6-8]. However, investigation has shown lack of activity of monovalent phenylboronic acid derivatives to decrease the infection level of HIV [9]. In contrary, significant boronic acid moieties present on a polymeric scaffold i.e. multivalent have been demonstrated to be more effective on interfering the interaction between HIV and its target host cells and thereby reduce viral infections [8, 10, 11]. Likewise, several researches have been carried out for investigation of boronic acid as protease enzyme inhibitor to reduce the infection of hepatitis C virus (HCV) [12, 13] where a series of peptide boronic acids containing residues were investigated as inhibitors of HCV NS3 protease, a viral non-structural protein, in viral replicon assay. Though there are few studies done on the boronic acid compounds as anti-viral agents, these studies mostly focus on the inhibition of non-structural protein that is essential for the viral replication but not on entry of virus. This approach of inhibition of HCV entry by using multivalent boronic acid moieties on nanoparticles has not been studied yet.

Therefore, the main objective of this chapter is to investigate and develop potential nanoparticle-based HCV entry blocking therapeutic agent by utilizing phenylboronic acid-modified various nanoparticles and to compare the efficacy of those nanoparticles in the inhibition of HCV infection by blocking HCV entry into Huh-7 target cells.

Boronic acid based nanoparticles are supposed to have number of advantages over other current lectin-based HCV inhibitors like less expensive to produce and ease on purification, modification of nanoparticles, more stable over a long time as well as eliminate the mitogenic problem. Moreover, most importantly, the multiple copies of boronic acid moieties grafted on nanoparticles are supposed to increase the affinity to the glycosylated enveloped virus significantly than compare to monomer having single unit of boronic acid. In

this chapter, the first example of nanoparticles, specifically designed to behave as HCV entry inhibitors are studied thoroughly. Three kinds of inorganic particles, namely, nanodiamond (NDs), silica (Silica-NPs) and magnetic nanoparticles (MPs) were used in this study to form the multivalent boronic acid moieties. However, neither magnetic property of MP nor fluorescence property of NDs was used in this study since the main motive was to develop common surface strategy for the formation of NP-based borono-lectins and to validate the 'proof-of-concept' of using multivalent boronic acid moieties to inhibit the HCV entry.

3.1. Functionalization of inorganic nanostructures with boronic acid ligands

Three kinds of particles, namely, nanodiamonds (NDs), silica (Silica-NPs) and magnetic nanoparticles (MPs) were used as scaffolds for an integration of boronic acid derivative. Silica-NPs [14], NDs [15] and MPs [16-18] featuring multiple surface-conjugated boronic acid groups have already been investigated for their ability to capture glycoproteins for purification purpose but are never studied and considered as HCV entry inhibitors. In all kind of nanomaterials, the common strategy used for modification to graft the boronic acid (BA) is featured in **Figure 3.2**. In this study, hydroxyl-groups present on commercially available NDs were directly modified by 4-azidobenzoic acid to create azido group, necessary for "click" reaction, in presence of N,N'-dicyclohexylcarbodiimide (DCC) and a catalytic amount of 4-dimethylaminopyridine(DMAP). Likewise, commercially available silicon dioxide was silanized first with 4-aminopropyltrimethoxysilane (APTMS) to create amine terminated particles (Silica-NH_2) and these amine groups were further reacted with 4-azidobenzoic acid to create azido group in the same reaction conditions as in NDs. In case of MPs, first amine terminated MPs were formed by grafting 2-nitrodopamine, on to the surface of MPs and then followed by the conjugation of amine groups with 4-azidobenzoic acid groups with DCC and DMAP protocol as used in NDs and Silica-NPs. 2-nitrodopamine for functionalization of MPs, was motivated by the consideration of reported irreversible binding of this ligand compared with that observed for the more classically used iron oxide ligand that is referred as dopamine. This irreversibility is associated to the presence of the electronegative nitro group, which leads to the enhanced interactions of phenolic functions with the MPs surface leading to its lower rate of oxidation and enhanced stability as compared with dopamine ligand [19-21]. It was also observed that 2-nitrodopamine ligand have pKa values near pH 6.5, lower when compared to dopamine ligands with pKa around pH 9 [19-21].

The success of formation of azide groups on surface of nanoparticles was characterized by using Fourier transformed-infrared spectroscopy (FT-IR) and further verified by X-ray photoelectron spectroscopy (XPS) (**Figure 3.3**). FT-IR transmission spectra of both azide terminated nanostructures are almost identical.

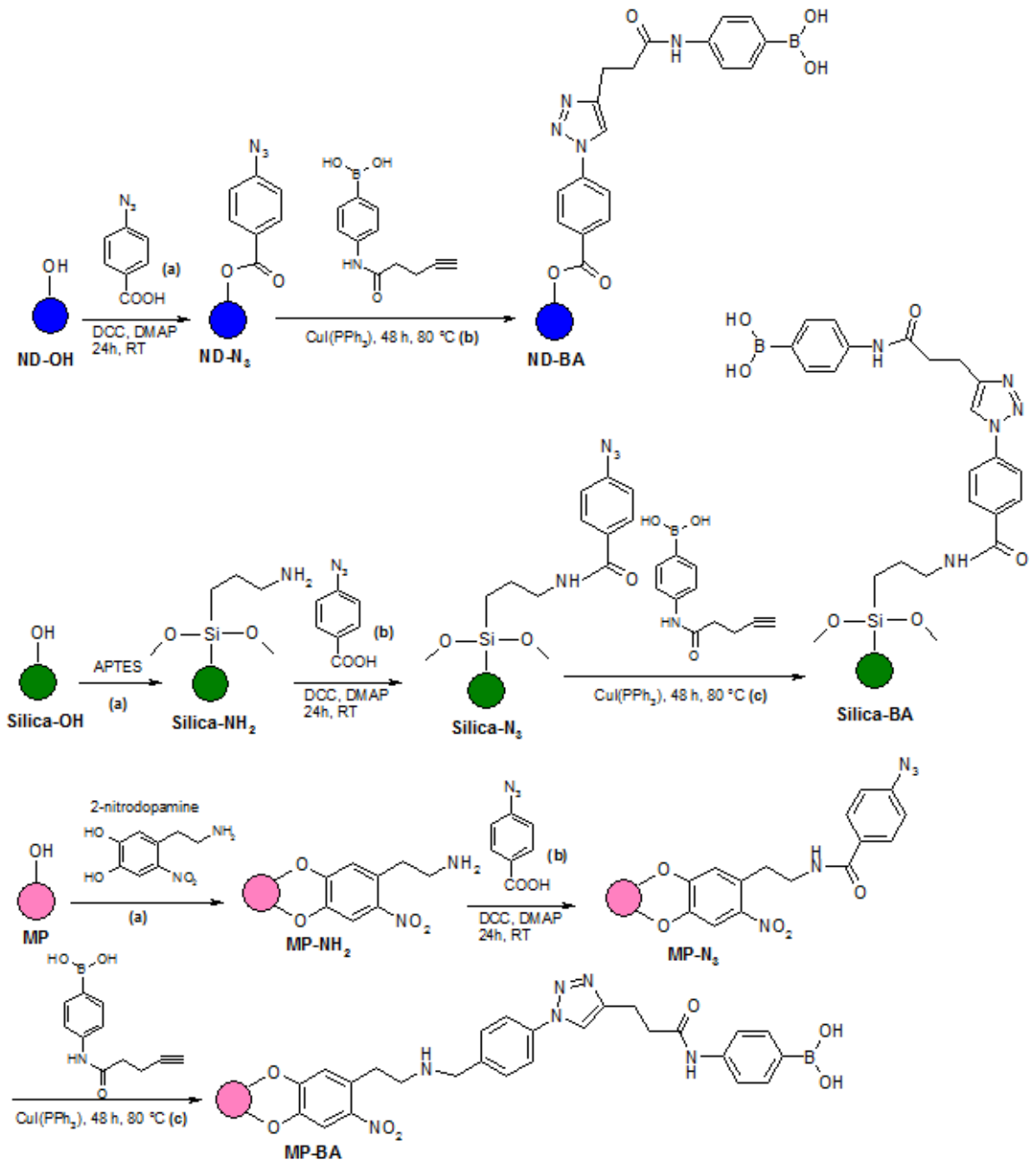

Figure 3.2. Surface modification steps involved in the preparation of BA grafted NDs, Silica-NPs and MPs. In both particles, common strategy 'click' was applied to form BA-grafted particles.

An identical band at 2125 cm^{-1} (**Figure 3.3A**) corresponds to the ν_{as} (N_3) stretching mode which is observed in all particles serves as a proof of successful grafting of azide group on nanoparticles. A broad band at 3447 cm^{-1} assigned to the stretching mode of unreacted surface hydroxyl group or could be more because of adsorbed water molecules. Likewise, band at 2936 cm^{-1} is characteristic of the presence of C-H bonds. In case of azide terminated ND, band at 1730 cm^{-1} which corresponds to carbonyl (C=O) group further validates the formation of an ester linkage. Similarly, band at 1286 cm^{-1} can be attributed to C-O stretching on ND surface, being rather intense when compared to other ND spectra [22].

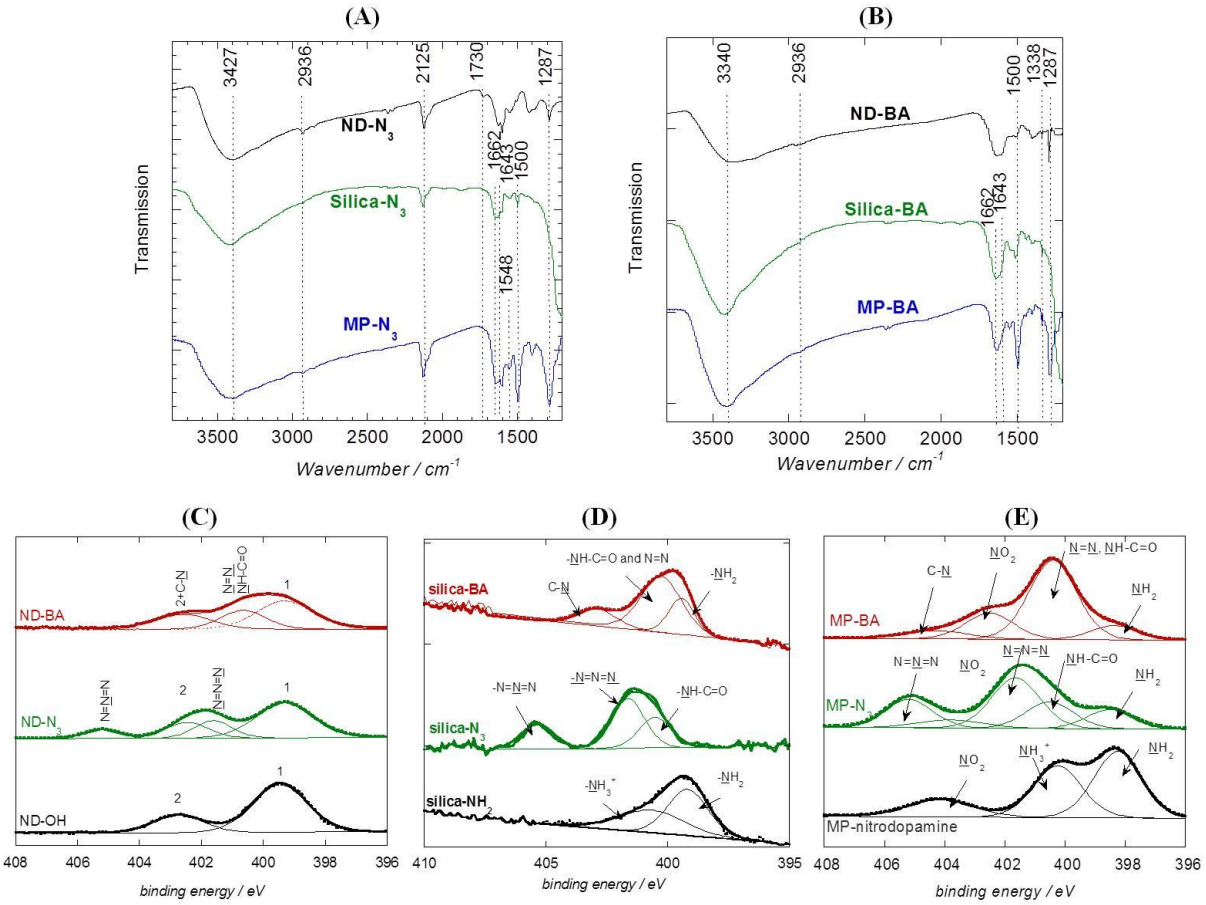

Figure 3.3. Transmission FT-IR spectra of azide terminated nanoparticles (A) and boronic acid-modified nanoparticles (B); NDs (black), Silica-NP (green) and MPs (blue). N1s high resolution XPS spectra of NDs (C), Silica-NP (D) and MP (E); where starting nanomaterials, azide terminated and boronic acid modified particles are represented in black, green and red color respectively.

In the case of Silica-N_3, the bands 1661 cm^{-1} and 1643 cm^{-1} (**Figure 3.3A**) corresponding to amides II and I respectively, are clearly observe in the spectrum of Silica-N_3

particles. The absorption corresponding to C-O related bands is overlapped with the strong stretching vibration of the Si-O-Si groups of silica occurring in the spectral range of 1000-1400 cm^{-1}, with a maximal absorption at ≈1089 cm^{-1} [23], so it is not observed in the spectrum. Likewise, FT-IR spectrum of MP-N_3 reveals the presence of the 2-nitodopamine anchor with prominent bands corresponding to C-O and C=C vibrations at 1287 and 1500 cm^{-1} respectively, as well as an intense band at 1548 cm^{-1} attributable to asymmetric NO_2 group vibrations.

In addition to FT-IR, XPS was also performed to further characterize and verify the modifications. To noticeably examine the success of each modification steps, it was worthwhile to follow the change in the N1s peak because in each modification steps different kind of nitrogen are introduced. The high-resolution N1s XPS spectra of ND-N_3 particles (**Figure 3.3C**) reveals clearly the presence of the azido function by the signals at 405.2 (Ar-N=$\underline{N}^+$=N^-) and 401.6 eV (Ar $\underline{N}$=N^+=$\underline{N}^-$) in a ratio of 1:2, as theoretically expected. Additional bands corresponding to azide groups are observed at 399.3 and 402.4 eV with a ratio of 3:1 but these are also characteristic of NH_2 functional groups (399.3 eV) present on the surface of the ND particles and are also found in other nitrogen containing functionalities such as C-N, N-O (402.4 eV) which can be generated from trinitrotoluene during the detonation process. Comparable XPS spectra were generated for Silica-NPs. The N1s XPS spectrum of silica-NH_2 features bands at 398.2 and 400.2 eV ascribable to -$\underline{N}H_2$ and -$\underline{N}H_3^+$ groups. The N1s high resolution XPS spectrum of the Silica-N_3 (**Figure 3.3D)** exhibits peaks at 405.3 (Ar-N=$\underline{N}^+$=N^-), 401.5 eV (Ar-$\underline{N}$=N^+=$\underline{N}^-$) and 400.6 eV (-NH-C=O linkage) with a ratio of 1:2:1, in accordance with the chemical composition of the surface. Having in hand the required NP precursors featuring surface-linked azido groups we were in a position to fabricate the targeted boronic acid analogs. The high-resolution N1s XPS spectra of MPs are somewhat more complex (**Figure 3.3E**). The spectrum of nitrodopamine-modified particles (MP-NH_2) shows bands at 404.2 (-$\underline{N}O_2$), 398.2 (-$\underline{N}H_2$) and 400.2 eV (-$\underline{N}H_3^+$). The ratio of NH_2/NO_2 is 2.2 and thus much higher than the theoretically expected one of 1/1. It is however known that NO_2 groups are not stable under XPS conditions (due to ultra-high vacuum conditions, X-ray excitation and interaction with secondary electrons or with electrons from the flood gun) and can thus be converting into NH_2 groups [24]. Upon surface-functionalization with 4-azidobenzoic acid moieties, the corresponding XPS spectra of these MP-N_3 shows bands at 405.1 eV (Ar-N=$\underline{N}^+$=N^-) and 401.6 eV (Ar-$\underline{N}$=N^+=$\underline{N}^-$), which are attributable to azido groups. A peak present at 400.5 eV (-NH-C=O linkage) is present in the N1s high-resolution XPS

spectra, as are bands at 403.9 and 398.5 eV. The latter are attributed to $\underline{N}H_2$ groups (formed from $\underline{N}O_2$) as well as residual NH_2 groups whose presence indicates inefficient coupling with 4-azidobenzoic acid.

The propargyl functionalized analog, 4-[(1-oxo-4-pentyn-1-yl) amino]phenylboronic acid or boronic acid derivative (**1**) was selected as the "click" partner and easily obtained *via* a modified literature procedure [25] from 4-amino phenylboronic acid chloride and 4-pentynoic acid and is illustrated in **Figure 3.4**.

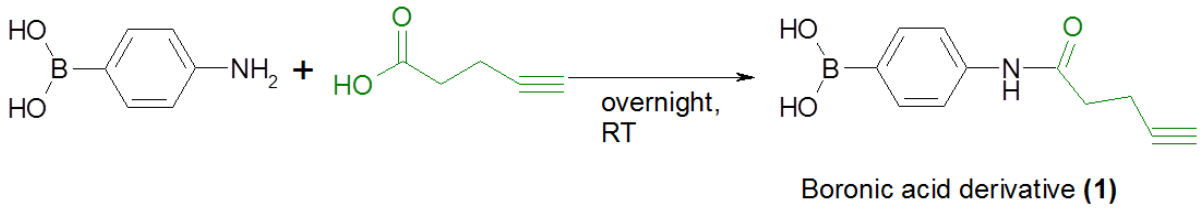

Figure 3.4. Chemical synthesis of boronic acid derivative **(1)** that has been used to create nanoparticles with multivalent boronic acid moieties.

When the propargyl analog (**1**) was subjected to "standard" click-coupling strategy with each of the NP-N_3 in turn, the expected phenylboronic acid-clicked NPs (ND-BA, Silica-BA and MP-BA) were formed smoothly and efficiently because of the chemoselectivity of the 'click reaction'. The successful attachment of boronic acid moieties to NPs is accompanied by simultaneous introduction of surface triazole groups and consequently can be monitored by the disappearance of bands expected for the $\nu_{as}(N_3)$ stretching mode at 2123 cm^1 in the FT-IR spectra of each of the particles **(Figure 3.3B)**. The presence of surface boronic acid functions is further evidenced by the stretching mode band of B-O at 1338 cm^{-1} in the FT-IR spectra of both successfully clicked particles [17]. The efficient conversion of surface azide groups into the corresponding triazole functions was further supported by the observation of the absence of the characteristic azide band at 405.2 eV in the N1s XPS spectra of each NP conjugate (**Figure 3.3C, D, E**). The N1s signal of ND-BA and Silica-BA can be fitted to bands at 402.6 eV (-C-N-) and 400.4 eV (-N=N-, -NH-C=O) respectively, present in a ratio of 1:3.9 typical of a triazole function. An additional band at 399.2 eV (-NH_2) indicates presence of azide groups, perhaps resulting from partial hydrolysis surface azidobenzoic ester functions. In the case of MP-BA additional bands at 404.19 and 398.5 eV present in its XPS spectra are probably due to the presence of -$\underline{N}O_2$ and -$\underline{N}H_2$ functions on its surface (**Figure 3.3E**).

3.2. Physico-chemical characteristics of boronic acid modified nanoparticles

The binding affinity of the any boronic-acid modified NPs to a particular glycan would ultimately depend not only on the number of boronic acid residues available for binding sugars but on their ability to form cyclic di-esters with diol functions of sugars at physiological pH. The majority of boronic acid analogs are weak acids with a pK_a generally in the order of 8-9, when in its anionic form as is the case in alkaline solutions (facilitated by addition of the OH^- ions to the boron atom) [26]. Consequently the surface density of the anionic charges on a particle will be a function of the pH at which it is dispersed and its pK_a value can be determined simply by measuring the variation of its zeta potential as a function of pH as shown in **Figure 3.5**.

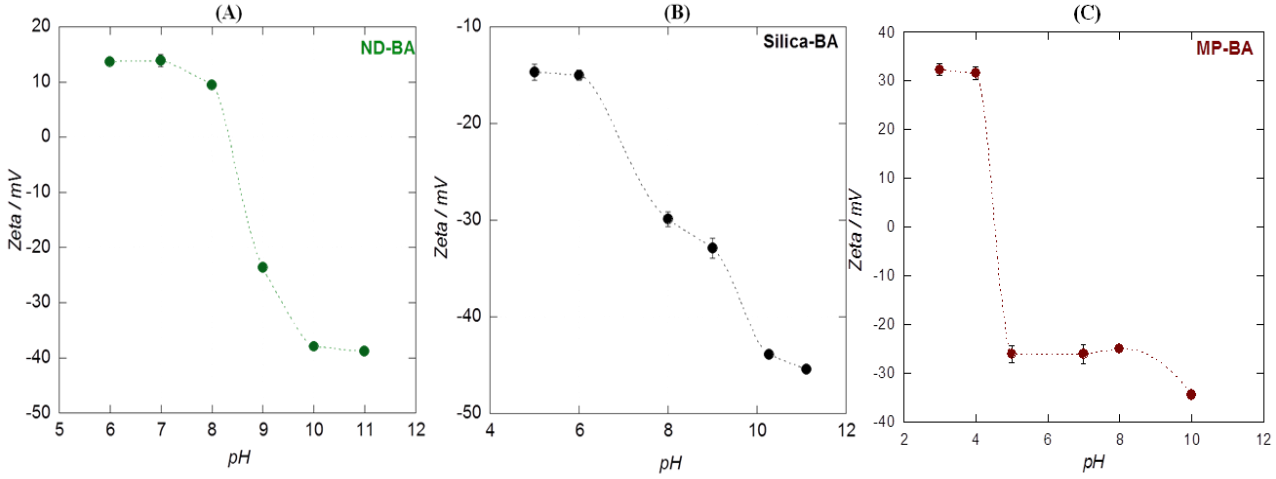

Figure 3.5. Determination of pKa value utilizing the variation of zeta potential with pH; ND-BA (**A**), Silica-BA (B) and MP-BA (C).

This method has facilitated to establish pK_a values of 8.0 for both ND-BA and Silica-BA's, respectively (summarized in **Table 3.1**) and 5.0 for MP-BA. The pK_a values observed for the ND-BA and Silica-BA are one pH unit lower than that expected for a phenylboronic acid without any substitutions on the aromatic ring. The latter compounds usually show values for pK_a's of 8.8 and therefore bind strongly to diols only at alkaline pH's [27]. Multivalent presentation of boronic acid unit [28] as well as dative bond formation with boron [8, 10, 11] and the addition of electron-withdrawing groups on the phenyl ring of the phenylboronic acid [27, 28] have all been found to decrease the pK_a and thus improve binding of diols at physiological pH's compared to that seen for unsubstituted phenylboronic acid. In the case of the ND-BA and Silica-BA, presence of multiple triazole functions and of residual

surface 'OH' groups are expected to favor intermolecular interaction of accessible nitrogen and oxygen functions with adjacent boronic acid groups and facilitate a decrease in the effective macroscopic pK_a's. However, the presence of multiple boronic acids would not be expected to wholly account for the unexpectedly low pK_a value observed for the MP-BA's. It might be presumed that this observation might be related to the presence in MP-BA particles of the electron-withdrawing nitro group in 2-nitrodopamine (incorporation of electron withdrawing groups onto phenylboronic acid derivatives is known to lower their pK_a [29]) as well as the observation that residual unreacted amine groups are present on its surface (boronic acids are known to be prone to dative bond formation with adjacent nitrogen or oxygen ligands resulting in lowering of their effective pK_a) [30, 31].

Table 3.1. Physico-chemical characteristics of the boronic acid-modified nanoparticles.

Particles	d_H/ nm	ζ-potential/ mV (pH 7.4)	BA µg/mg	BA on 60 µg/mL particles, µg/mL	pKa
ND-BA	83±2	15.7±0.6	65±2	3.9±0.3	8.0±0.2
Silica-BA	100±5	-17.7±0.15	64±5	3.6±0.3	8.0±0.2
MP-BA	93±7	-26.0±0.3	54±2	3.2±0.3	5.0±0.3

* d_H = hydrodynamic diameter

Quantification of "sugar-accessible" boronic acid grafted on the surface of each particle is essential as this would be believed to determine the glycan-binding efficiency of a particular NP. The determination of the amount of boronic acid ligands on the surface was performed by an indirect method [32]. In this experiment, mannose was chosen to indirectly quantify boronic acid moieties as glycan of envelope glycoprotein of HCV is enriched with mannose. Treatment of a given particle with mannose leads to its covalent binding to the NP-BA as a cyclic boronate ester and furnished the corresponding NP saturated with the maximal amount of "bound" sugar. Subsequently, thorough washing of these "sugar-saturated" NPs would remove all un-bound mannose. The concentration of particle-attached mannose was then determined using the well-established phenol-sulfuric acid colorimetric assay for the determination of carbohydrate concentration [33]. This method of quantifying the surface concentration of boronic acid moieties in fact allows for an estimation of those residues that are actually available for binding monosaccharides. Thus, in the assay the absorption difference between λ=570 nm (baseline) and λ=495 nm of an aliquot of a given mannose particle was measured with reference to a calibration curve. This gave sugar loadings of 65±2

µg /mg for ND-BA, 60±5 µg/mg for Silica-NP-BA and 54±2 for MP-BA, respectively (**Table 3.1**). Beside colorimetric assay, thermogravimetric analysis and solid state NMR can also be performed to quantify boronic acid moieties.

Once the surface characterization and physico-chemical determination was done, the nanoparticles were further preceded for the biological assays.

3.3. Effect of nanoparticles on Huh-7 cell viability

Various human cell lines are sensitive to trace of copper [34] and the azide-alkyne Huisgen cycloaddition reaction to graft BA-derivative (**1**) was catalysed by Cu (I). So, it was important to ensure complete removal of contaminant copper residues remaining after the reaction. This was conveniently achieved through three aqueous EDTA washing/centrifugation cycles into the post-"click" treatment of both particles prior being used in cell-based assays.

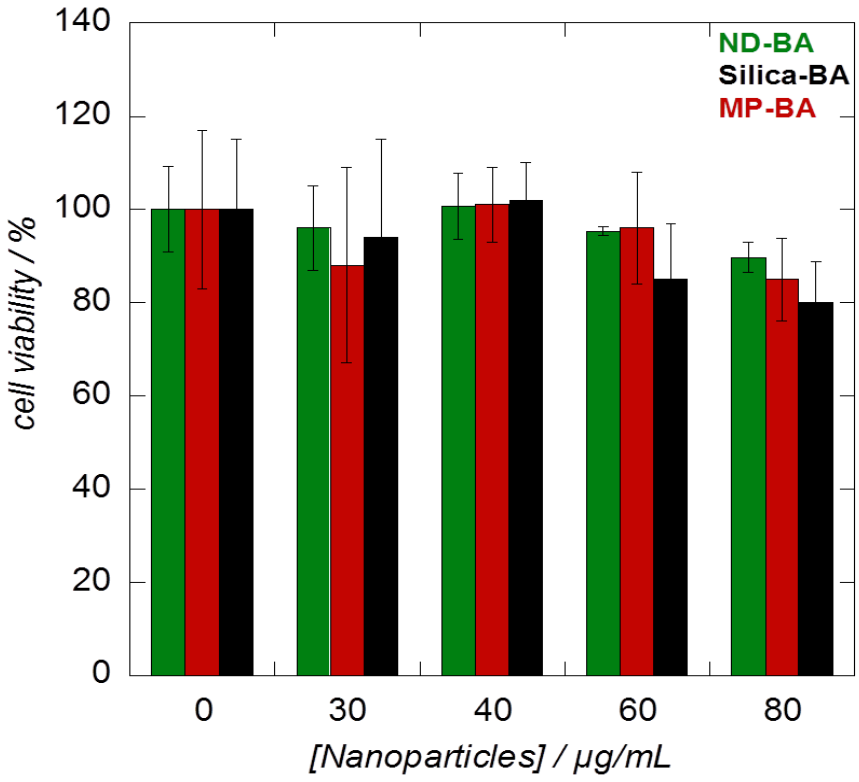

Figure 3.6. Huh-7 cell viability results after incubation of nanoparticles of increasing concentrations for 48 hours: ND-BA (green), Silica-BA (black) and MP-BA (red).

Furthermore, XPS analysis of these these "clicked" nanoparticles confirmed the absence of any copper traces. The efficiency of washing steps by EDTA for biological assays was recently demonstrated in the biofilm inhibition study carried out in presence of ND modified by "click" chemistry with mannose units [32].

The cell viability of each of the boronic acid-modified NPs was studied on the Huh-7 cell line after 48 h incubation, to be used in the subsequent HCV-entry inhibition experiments, were analysed by MTS assay on the Huh-7 cell line as described by the company (CellTiter 96 AQueous One Solution cell proliferation assay; Promega). At the highest concentration of ND-BA and MP-BA particles (80 µg/mL), no substantial reduction in the viability of Huh-7 cells was observed (**Figure 3.6**). The observed lack of cytotoxicity is in accordance with previous studies demonstrating the excellent biocompatibility of these NDs [35, 36]. Moreover, due to the fact that iron is present in human body (ferritin) as iron-containing nanoparticles are considered as biocompatible [37]. The Silica-BA particles however show a higher reduction in the viability of Huh-7 cells than the ND-BA's. It has been known from the previous studies that the toxicity of Silica-NPs is highly dependent on the physical, chemical and structural properties of a particular particle formulation [38-40]. Nevertheless, in the HCV inhibition experiments (see below, **Figure 3.7**), NP-BA particles are only exposed to Huh-7 target cells for a period of 2h (infection period) and, on this time frame, Silica-BA does not show any cytotoxicity effects on Huh 7 cells.

3.4. HCV entry inhibition assay by boronic acid-modified nanoparticles

After establishing safe concentration range of NPs that can be used in Huh-7 cell line, intended HCV inhibition assay has been preceded. For this assay, a protocol that measures the ability of cell culture-derived JFH1 virus (HCVcc) to infect hepatocytes was implemented to evaluate the potential of each boronic-acid modified NP as an inhibitor of viral entry. The modified JFH1 virus featuring mutations shown to increase the viral titers was used in experiments with HCV [41]. The various steps of the assay are simplified schematically in **Figure 3.7**.

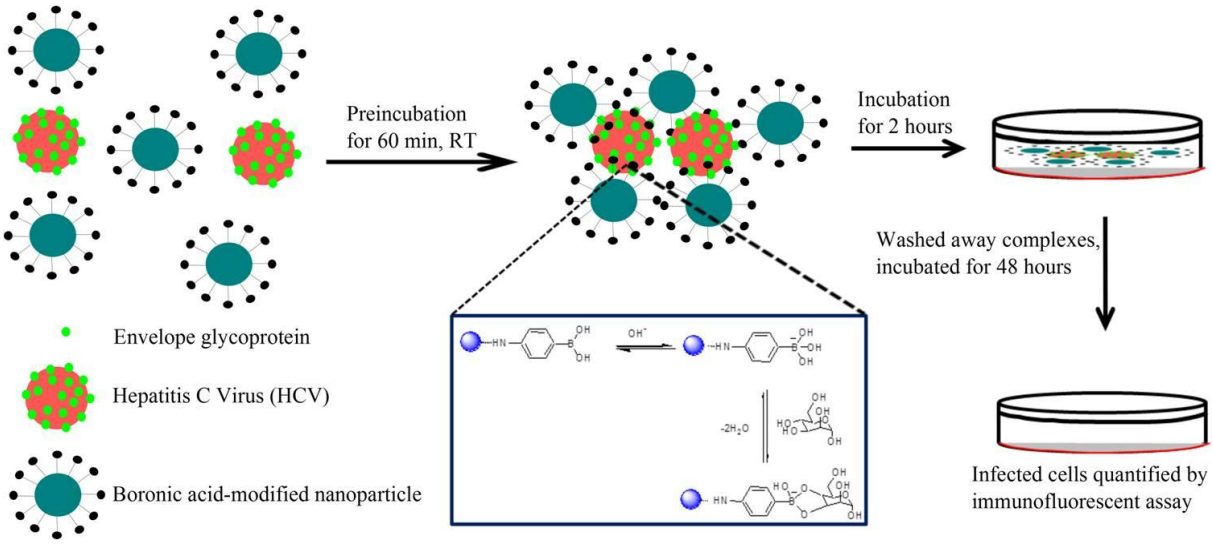

Figure 3.7. Schematic depicton of perfomed HCV entry inhibition assay reflecting each steps.

As shown in **Figure 3.7**, HCVcc was pre-incubated with serially increasing concentrations of a given particle before infecting the Huh-7 target cells. This pre-incubation is a time period allowed to form the diol complex in between the boronic acid and glycans present in the envelope of HCVcc. After an hour of pre-incubation of HCVcc with nanoaparticles, the Huh-7 target cells are infected by this complex. Upon incubation for 48 hours, the number of infected cells at each dilution was quantified by immunofluorescence using a monoclonal antibody (primary) recognizing HCV glycoprotein E1 (A4 epitope) and likewise secondary antibody carrying fluorophore (CY-3 tagged goat anti-mouse) that recognizes primary antibody [42]. **Figure 3.8A** shows typical fluorescence images of the Huh-7 target cells after being incubated with HCVcc for 48h, in the presence of various nanostructures including those modified with boronic-acid moieties. Nuclei are stained with 4'-6-diamidino-2-phenylindole (DAPI) identified as blue stain and the red colored cells are recognized as infected. It has been clearly observed the low level of infection in case of BA-modified particles than compare to unmodified and negative control. This level of infection was quantified by the help of ImageJ software. Percentage of infection for all the dilutions was relative value as compared to the negative control i.e. MQ water.

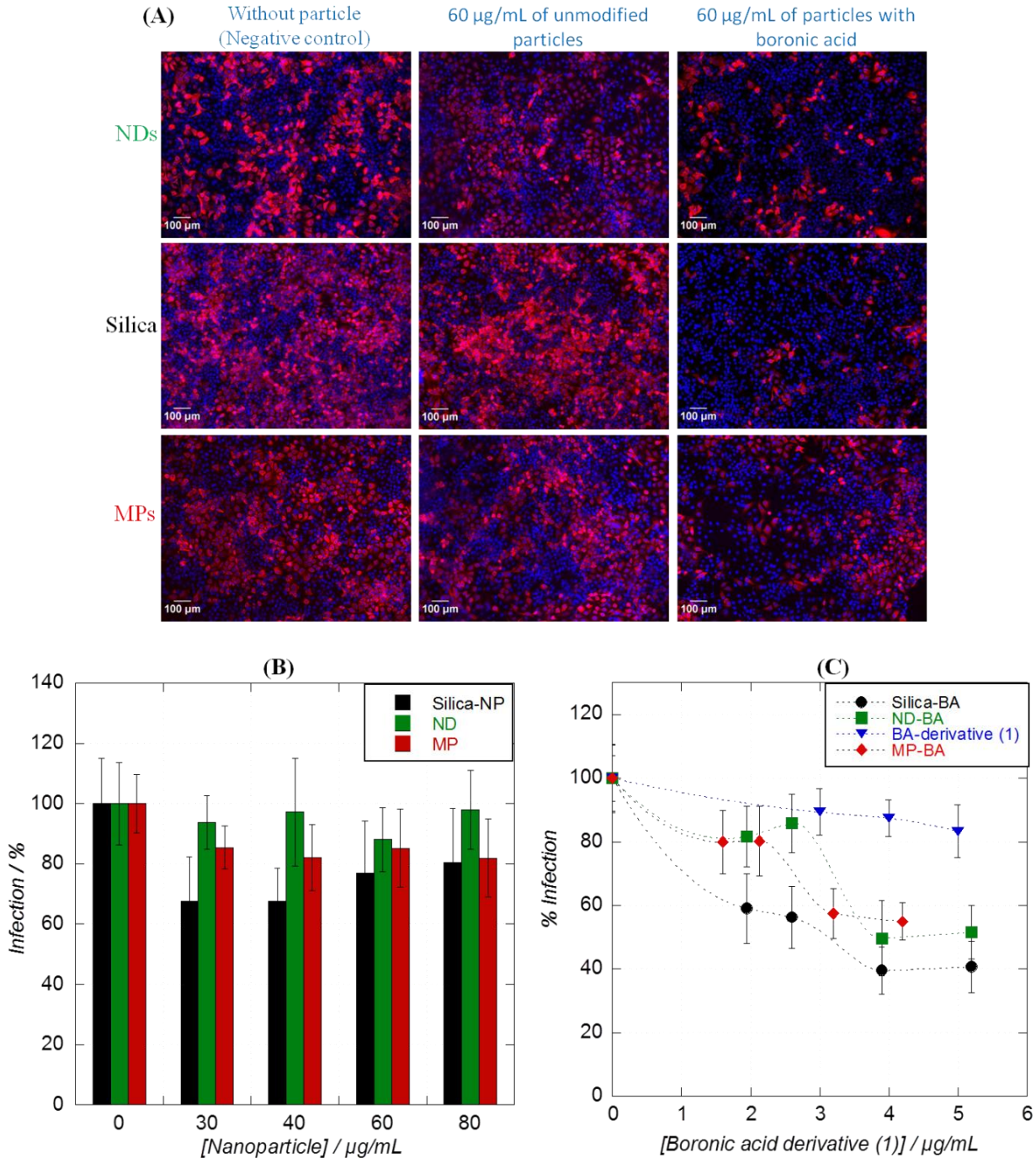

Figure 3.8. Fluorescent images (10x) of the Huh-7 target cells after incubation with HCVcc for 48 hours where infection of cells was carried out in three conditions of pre-incubation i.e. without any particles, with unmodified nanoparticles and with BA-modified nanoparticles. Red color and blue color correspond to infected cells and nucleus respectively (A); HCVcc infection inhibition effect of unmodified ND (green), Silica-NP (black) and MP (red) (B); Comparison of HCVcc infection inhibition effect of BA-derivative (1) modified NPs and BA-

derivative (**1**) alone to highlight the advantage of multivalency of boronic acid in nanostructures (C).

The quantified results of infection are displayed in **Figure 3.8B and C.** In **Figure 3.8B**, relative infection level was assembled where Silica-NP has shown to decrease level of infection than compared to NDs and MPs which are inactive in all the tested dilutions. Likewise in **Figure 3.8C**, viral infection results of BA-derivative (**1**) and nanoparticles modified with BA-derivative (**1**) were compared. It is exactly clear that the BA-derivative (**1**) alone has no significant inhibition on viral infection even in the highest tested concentration and the inhibition effect of BA-modified nanoparticles on viral infection is due to the presence of multiple copies of boronic acid moieties on the surface of nanostructures. In this assay, the ND-BA particles showed viral inhibition of up to 58±10 % (**Figure 3.8C**) for particle concentrations of 60 µg/mL, corresponding to 3.9 µg/mL of available boronic acid units (**Table 3.1**). The best results were obtained for Silica-BA particles which partly might have arrived from the activeness of unmodified Silica-NP on the inhibition assay. However, inhibition effect associated with MP-BA was observed to be the least as compared to other two tested nanoparticles. This could be related to the lower loading of BA-moieties and aggregation of particles at equivalent higher concentration of BA-moieties. The use of higher concentrations of any of the NP-BA's did not lead to any enhancement of their antiviral effects (data not shown). We consider this to be linked to formation of NP-derived precipitates at these elevated concentrations during the assay.

3.5. Competitive binding experiment with mannose:

Since it is assumed that the inhibition of viral assay by the BA-modified particles are due to the diol complex formation between boronic acid moieties and glycan present on the evelope glycoprotein of virus [11], an additional experiment was performed where the boronic acid moieties present on the BA-modified nanodiamond were saturated with mannose prior to their pre-incubation with the HCVcc particles. The mannose covered ND-BA does not show any inhibitiory effect (**Figure 3.9**). This experiment confirmed that masking of the mannose-binding function of ND-BA's result in the loss of antiviral activity and further that the antiviral activity was dependent on boronic cyclic di-ester-formation between the particle-appended boronic acid moieties and glycoproteins present on HCV envelope.

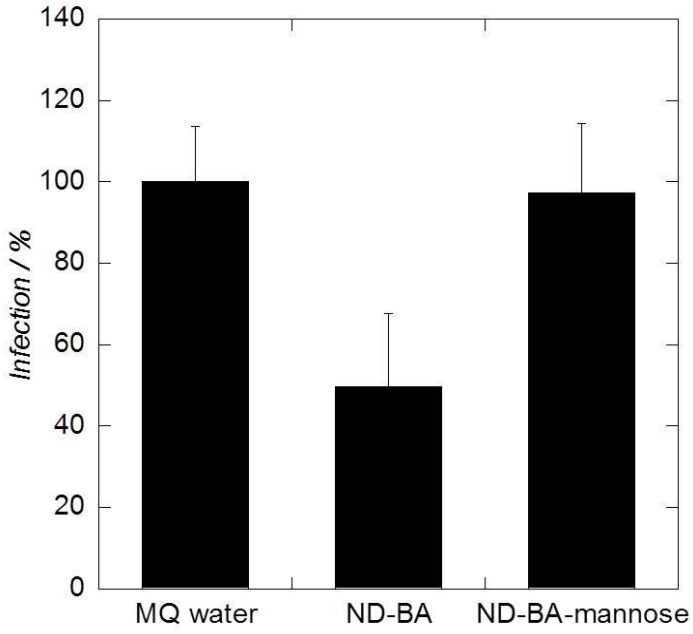

Figure 3.9. Effect of mannose blocking of boronic acid moieties on ND-BA on the viral entry inhibition activity.

In this study, ND-BA was chosen over Silica-BA due to the fact that unmodified Silica-NP has shown some inhibitory effect compare to ND and minimum artifacts is required in this experiment to compare and verify the effect of masking boronic acid moieties in inhibition assay.

3.6. Role of triazole ring in inhibition assay

As boronic acid acts as a Lewis acid, it has been demonstrated in numerous studies that triazole ring connected to phenylboronic acid can maintain a dative N-B bond, making the molecule able to bind sachharides under physiological pH efficiently [27, 28, 43]. Introduction of multiple triazole ring in ND-BA are expected to increase the interaction between nitrogen with adjacent boronic acid groups to favor lower pKa value leaving boronic acid moieties more acidic. More the boronic acid is acidic in the physiological pH, more will increase the binding affinity with sachharides [44].

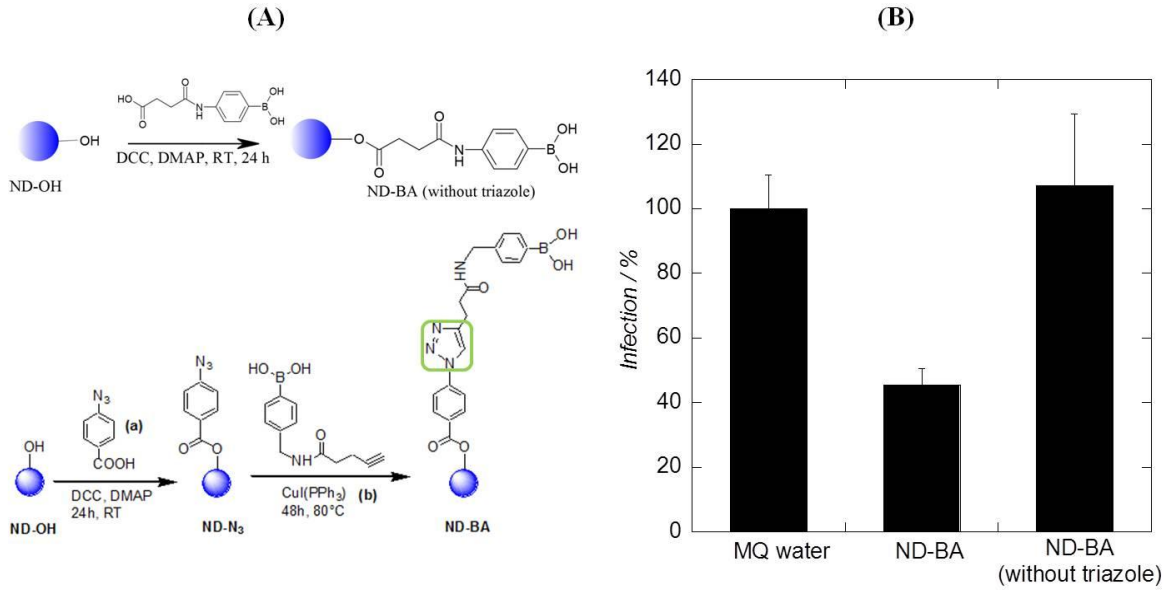

Figure 3.10. Role of trizole ring on the inhibition effect of viral infection. Scheme for the preparation of ND grafted with boronic acid without triazole ring, ND-BA (without triazole) and formation of ND-BA as described before (**A**). Comparison of HCVcc inhibition assay shown by ND-BA and ND-BA (without triazole) at 60 µg/mL concentration of particles (**B**).

To study the role of triazole ring, *N*-(4-Phenylboronic)succinamic acid was directly grafted into the hydroxyl group of commercial nanodiamond by using DCC and a catalytic amount of 4-dimethylaminopyridine to form ND-BA (without triazole ring) which serve as a control (**Figure 2.10A)**. An identical inhibition assay was performed as described before to compare the inhibition activity of ND-BA (without triazole) with ND-BA. From the result (**Figure 2.10B**) it indicates that ND-BA (without triazole) has no inhibition effect on the HCVcc infection. This study shows the importance of having triazole ring on binding affinity with glycans which might be the principle reason for ND-BA (without triazole) being inactive. This finding is also supported by the pKa of ND-BA (without triazole) which was determined by the same protocol as ND-BA (with triazole) and was found to be 9. This value is higher than pKa of ND-BA (with triazole).

3.7. Conclusion

A comparative study of the efficacy of three different nanoparticles modified by boronic acid moieties as synthetic viral entry inhibitors was performed. All boronic acid-modified nanoparticles exhibit viral entry inhibition activity against HCV, in *in vitro* studies

and the inhibition activity has been validated by blocking the HCV entry into the target Huh-7 cells. In compare to ND-BA, Silica-BA has shown the best inhibition of HCV entry; however the least biocompatibility of this particle cannot be overshadowed. Blocking HCV entry was dependent on the boronic cyclic di-ester-formation in between the boronic acid-grafted on nanoparticles and the glycan present envelope glycoprotein of HCV, which is the key factor for the adherence of viral particles to the targeted cell. This finding was further verified by masking the boronic acid moieties on nanoparticles by mannose and in this case there was no any inhibitory activity shown by the mannose covered ND-BA. Moreover in this study, the activity of the boronic acid-modified nanoparticles has been clearly demonstrated due to the fact that multiple copies of boronic acid moieties are present on their surfaces. The advantage of using these nanomaterials over the well established anti-viral lectins like cyanovirin-N and griffithsin is the facile way of fabrication, their low cost compared to lectin and use of "click" strategy described here to fabricate the nanomaterials by introducing the 1, 2, 3 triazole ring that has been proved to be essential for the viral inhibition effect. While the reduction of HCV infection of these 1st generation boronic-acid derived NPs is still modest (around 40%), the results nevertheless provide strong evidence that such entities might be further improved and developed as a viral entry inhibition strategy of HCV. Furthermore, in principle, the infectivity of any other pathogens that feature cell wall glycoproteins that are essential for their life cycle might also be reduced using similar NP-based boronolectins. That the newly developed borono-lectins described here reveal a lower cellular toxicity than alternative nanomaterials, sets the stage for the further exploration of NP-based pseudo-lectins as alternatives to their natural lectin counterparts. The study also supports that NP-derived borono-lectins should be further developed and pursued as a potential therapeutic strategy for blocking viral entry of HCV.

Though this study is an excellent first example of the NPs derived viral entry inhibitor that serve as "proof-of-concept", the lower level of inhibition activity cannot be ignored. This lower activity could be due to the less boronic acid moieties available. As shown in the result (**Figure 3.8C**) the increased concentration of nanoparticles does not decrease the level of infection. It has been noticed that the inorganic nanomaterials used in this study have stability issues in higher concentrations. They are more likely to aggregate and sediment faster with time. This could be another reason of unimproved infection level in higher concentration. In addition to stability issue, it has been figure out that the size of these nanomaterials which is around 100 nm might be another limiting factor. Due to these reasons and to develop better

inhibitory nanosystem which can overcome these limiting factors of nanodiamond and silica nanoparticles, we decided to use a well-established an organic nanomaterial i.e. lipid nanocapsule (LNC). The next chapter is about the use of LNC to improvise the boronic acid-based HCV entry inhibitior along with the detail study of mechanism.

3.8. References

1. Helle, F., et al., *Cyanovirin-N inhibits hepatitis C virus entry by binding to envelope protein glycans.* J Biol Chem, 2006. **281**(35): p. 25177-83.
2. Tan, S.L., et al., *Hepatitis C therapeutics: current status and emerging strategies.* Nat Rev Drug Discov, 2002. **1**(11): p. 867-81.
3. Ploss, A. and J. Dubuisson, *New advances in the molecular biology of hepatitis C virus infection: towards the identification of new treatment targets.* Gut, 2012. **61 Suppl 1**: p. i25-35.
4. Meuleman, P., et al., *Griffithsin has antiviral activity against hepatitis C virus.* Antimicrob Agents Chemother, 2011. **55**(11): p. 5159-67.
5. Takebe, Y., et al., *Antiviral lectins from red and blue-green algae show potent in vitro and in vivo activity against hepatitis C virus.* PLoS One, 2013. **8**(5): p. e64449.
6. Balzarini, J., *Targeting the glycans of glycoproteins: a novel paradigm for antiviral therapy.* Nat Rev Microbiol, 2007. **5**(8): p. 583-97.
7. Balzarini, J., *Targeting the glycans of gp120: a novel approach aimed at the Achilles heel of HIV.* Lancet Infect Dis, 2005. **5**(11): p. 726-31.
8. Trippier, P.C., J. Balzarini, and C. McGuigan, *Phenylboronic-acid-based carbohydrate binders as antiviral therapeutics: bisphenylboronic acids.* Antivir Chem Chemother, 2011. **21**(3): p. 129-42.
9. Trippier, P.C., C. McGuigan, and J. Balzarini, *Phenylboronic-acid-based carbohydrate binders as antiviral therapeutics: monophenylboronic acids.* Antivir Chem Chemother, 2010. **20**(6): p. 249-57.
10. Jay, J.I., et al., *Modulation of Viscoelasticity and HIV Transport as a Function of pH in a Reversibly Crosslinked Hydrogel.* Adv Funct Mater, 2009. **19**(18): p. 2969-2977.
11. Mahalingam, A., et al., *Activity and safety of synthetic lectins based on benzoboroxole-functionalized polymers for inhibition of HIV entry.* Mol Pharm, 2011. **8**(6): p. 2465-75.
12. Priestley, E.S., et al., *P1 Phenethyl peptide boronic acid inhibitors of HCV NS3 protease.* Bioorg Med Chem Lett, 2002. **12**(21): p. 3199-202.
13. Boloor, A., et al., *Synthesis and antiviral activity of HCV NS3/4A peptidomimetic boronic acid inhibitors.* Bioorg Med Chem Lett, 2009. **19**(19): p. 5708-11.
14. Xu, Y., et al., *Highly specific enrichment of glycopeptides using boronic acid-functionalized mesoporous silica.* Anal Chem, 2009. **81**(1): p. 503-8.
15. Xu, G., et al., *Boronic acid-functionalized detonation nanodiamond for specific enrichment of glycopeptides in glycoproteome analysis.* Analyst, 2013. **138**(6): p. 1876-85.
16. Zhang, X., et al., *Boronic acid modified magnetic nanoparticles for enrichment of glycoproteins via azide and alkyne click chemistry.* Journal of Materials Chemistry, 2012. **22**(32): p. 16520.
17. Lin, Z.-A., et al., *Synthesis of magnetic nanoparticles with immobilized aminophenylboronic acid for selective capture of glycoproteins.* Journal of Materials Chemistry, 2011. **21**(2): p. 518.

18. Lin, Z., et al., *One-pot synthesis of phenylboronic acid-functionalized core-shell magnetic nanoparticles for selective enrichment of glycoproteins.* RSC Advances, 2012. **2**(12): p. 5062.
19. Amstad, E., et al., *Ultrastable iron oxide nanoparticle colloidal suspensions using dispersants with catechol-derived anchor groups.* Nano Lett, 2009. **9**(12): p. 4042-8.
20. Amstad, E., Gehring, A. U., Fischer, H., Nagaiyanallur, V. V., and G. Hahner, Textor, M., Reimhult E., *Influence of Electronegative Substituents on the Binding Affinity of Catechol-Derived Anchors to Fe3O4 Nanoparticles.* J. Phys. Chem. C, 2011. **115**: p. 683–691.
21. Amstad, E., M. Textor, and E. Reimhult, *Stabilization and functionalization of iron oxide nanoparticles for biomedical applications.* Nanoscale, 2011. **3**(7): p. 2819-43.
22. Yeap, W.S., S. Chen, and K.P. Loh, *Detonation nanodiamond: an organic platform for the suzuki coupling of organic molecules.* Langmuir, 2009. **25**(1): p. 185-91.
23. Zhang, L., et al., *Boronic acid functionalized core-satellite composite nanoparticles for advanced enrichment of glycopeptides and glycoproteins.* Chemistry, 2009. **15**(39): p. 10158-66.
24. Iqbal, P., Critchley, K., Attwood, D., Tunnicliffe, D., Evans, S. D.,S. D. Preece, S. D. , *Chemical Manipulation by X-rays of Functionalized Thiolate Self Assembled Monolayers on Au.* Langmuir, 2008. **24**: p. 13969-13976.
25. Kanayama, N.K., H, *Interfacial Recognition of Sugars by Boronic Acid-Carrying Self Assembled Monolayer*. Langmuir, 2000. **16**: p. 577-583.
26. Takahshi, S.A., J.-I. , *Phenylboronic Acid Monolayer Modified Electrodes Sensitive to Sugars.* Langmuir, 2005. **21**: p. 5102-5107.
27. Yan, J., et al., *The relationship among pKa, pH, and binding constants in the interactions between boronic acids and diols—it is not as simple as it appears.* Tetrahedron, 2004. **60**(49): p. 11205-11209.
28. Kaur, G., et al., *Substituent effect on anthracene-based bisboronic acid glucose sensors.* Tetrahedron, 2006. **62**(11): p. 2583-2589.
29. Matsumoto, A., et al., *A totally synthetic glucose responsive gel operating in physiological aqueous conditions.* Chem Commun (Camb), 2010. **46**(13): p. 2203-5.
30. Wulff, G., *Selective binding to polymers via covalent bonds-the construction of chiral cavities as specific receptor-sites.* Pure Appl. Chem., 1982. **54**: p. 2093-2102.
31. Wulff, G., M. Lauer, and H. Bohnke, Angew. Chem. Int. Ed., 1984. **23**(9): p. 741-742.
32. Barras, A., et al., *Glycan-functionalized diamond nanoparticles as potent E. coli anti-adhesives.* Nanoscale, 2013. **5**(6): p. 2307-16.
33. Wang, X., O. Ramstrom, and M. Yan, *A photochemically initiated chemistry for coupling underivatized carbohydrates to gold nanoparticles.* J Mater Chem, 2009. **19**(47): p. 8944-8949.
34. Tardito, S., et al., *Copper binding agents acting as copper ionophores lead to caspase inhibition and paraptotic cell death in human cancer cells.* J Am Chem Soc, 2011. **133**(16): p. 6235-42.
35. Schrand, A.M., et al., *Are diamond nanoparticles cytotoxic?* J Phys Chem B, 2007. **111**(1): p. 2-7.
36. Marcon, L., et al., *Cellular and in vivo toxicity of functionalized nanodiamond in Xenopus embryos.* Journal of Materials Chemistry, 2010. **20**(37): p. 8064.
37. Markides, H., M. Rotherham, and A.J. El Haj, *Biocompatibility and Toxicity of Magnetic Nanoparticles in Regenerative Medicine.* Journal of Nanomaterials, 2012. **2012**: p. 1-11.

38. Bauer, A.T., et al., *Cytotoxicity of silica nanoparticles through exocytosis of von Willebrand factor and necrotic cell death in primary human endothelial cells.* Biomaterials, 2011. **32**(33): p. 8385-93.
39. McCarthy, J., et al., *Mechanisms of toxicity of amorphous silica nanoparticles on human lung submucosal cells in vitro: protective effects of fisetin.* Chem Res Toxicol, 2012. **25**(10): p. 2227-35.
40. Yu, T., A. Malugin, and H. Ghandehari, *Impact of silica nanoparticle design on cellular toxicity and hemolytic activity.* ACS Nano, 2011. **5**(7): p. 5717-28.
41. Delgrange, D., et al., *Robust production of infectious viral particles in Huh-7 cells by introducing mutations in hepatitis C virus structural proteins.* J Gen Virol, 2007. **88**(Pt 9): p. 2495-503.
42. Dubuisson, J., et al., *Formation and intracellular localization of hepatitis C virus envelope glycoprotein complexes expressed by recombinant vaccinia and Sindbis viruses.* J Virol, 1994. **68**(10): p. 6147-60.
43. Uddin, K.M.A.Y., L. J. , *Fluorogenic Affinity Gels Constructed from Clickable Boronic Acids.* J. Appl. Polym. Sci. , 2013. **128**: p. 1527-1533.
44. Yang, W., X. Gao, and B. Wang, *Boronic acid compounds as potential pharmaceutical agents.* Med Res Rev, 2003. **23**(3): p. 346-68.

CHAPTER 4

Boronic acid-modified lipid nanocapsules as a novel class of highly efficient hepatitis C viral inhibitors

Particle's agglomeration at higher concentration was the major problem with the boronic-acid modified nanostructures used in the previous chapter, This was believed to be one of the underlying reasons why the level of HCV inhibition could not be improved even by increasing the concentration of the bornic-acid modified nanostructures beyond 60 µg/mL. To overcome the limitations of the inorganic nanomaterials used in the previous chapter and to improve the efficacy of nanosystem on inhibition of hepatitis C virus infection, alternative nanostructures were looked for. One viable alternative investigated were lipid nanocapsules (LNC) (**Figure 4.1)**. The nanometric scale of lipid nanocapsules (LNCs) along with their biomimetic properties makes these nanostructures of high interest for nanomedical developments and appears to be a useful and efficient therapeutic option [1].

LNCs are prepared from low-toxicity materials such as triglycerides and PEGylated surfactants by a solvent-free process to obtain particles of less than 100 nm in diameter with good stability and monodispersity. These LNCs provide considerable drug encapsulation capacity with sustained-release functions at the site of action. Moreover, the semi-rigid shell of LNCs allows their modification by post-insertion of amphiphilic molecules and allows the further attachment of targeting ligands into LNCs [2, 3]. The synthesis of amphiphilic polysaccharides could be achieved through the formation of an oxime linkage between an amphiphilic hydroxylamine derivative and the reductive end of a 40 kDa dextran. The formation of the amphiphilic ligand as well as the formulation of the nanocapsules is generally performed under aqueous conditions without organic solvents, which is considered as an important feature when biological or pharmaceutical applications are engaged. Moreover, this chemoselective reaction allows controlling the lipidation site and the number of lipids introduced on the ligand molecule [2].

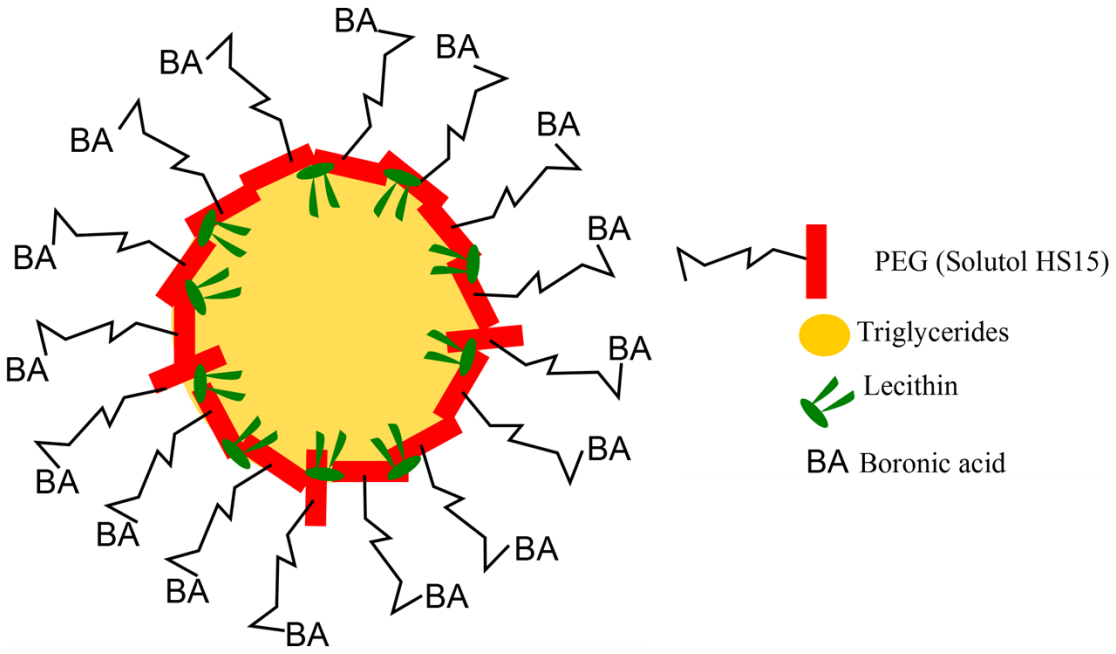

Figure 4.1. Schematic representation of boronic acid modified lipid nanocapsule for HCV infection inhibition.

This method constitutes thus an attractive potential for decorating lipid nanocapsules with functional ligands with the aim of active cell and disease targeting. The main objective of this chapter is to validate this concept for HCV infection inhibition. An amphiphilic boronic acid was synthesized and post-inserted into the LNC's surface to prepare boronic acid decorated LNCs (BA-LNCs) used in an identical HCV inhibition assay as carried out for inorganic nanomaterials in Chapter 3.

4.1. Synthesis of the amphiphilic boronic acid compound (ABA)

The amphiphilic boronic acid (ABA) compound was synthesized in two steps using commercial nonionic detergent Brij-58P, which consists of a C16 alkyl chain bearing an average of 20 ethylene glycol units (PEG), as starting material. The first step was to introduce carboxylic acid function by coupling free hydroxyl groups at the chain end of Brij-58P which was accomplished by succinic anhydride (**Figure 4.2A**). Then, DCC amide formation chemistry was utilized to link 4-aminophenylboronic in presence of triethylamine (TEA) and dichloromethane. The reaction was carried out at room temperature for 24 h to form the

corresponding ABA compound. After washing steps, the final product was purified on silica gel column to give the BA derivative in a yield of 81%.

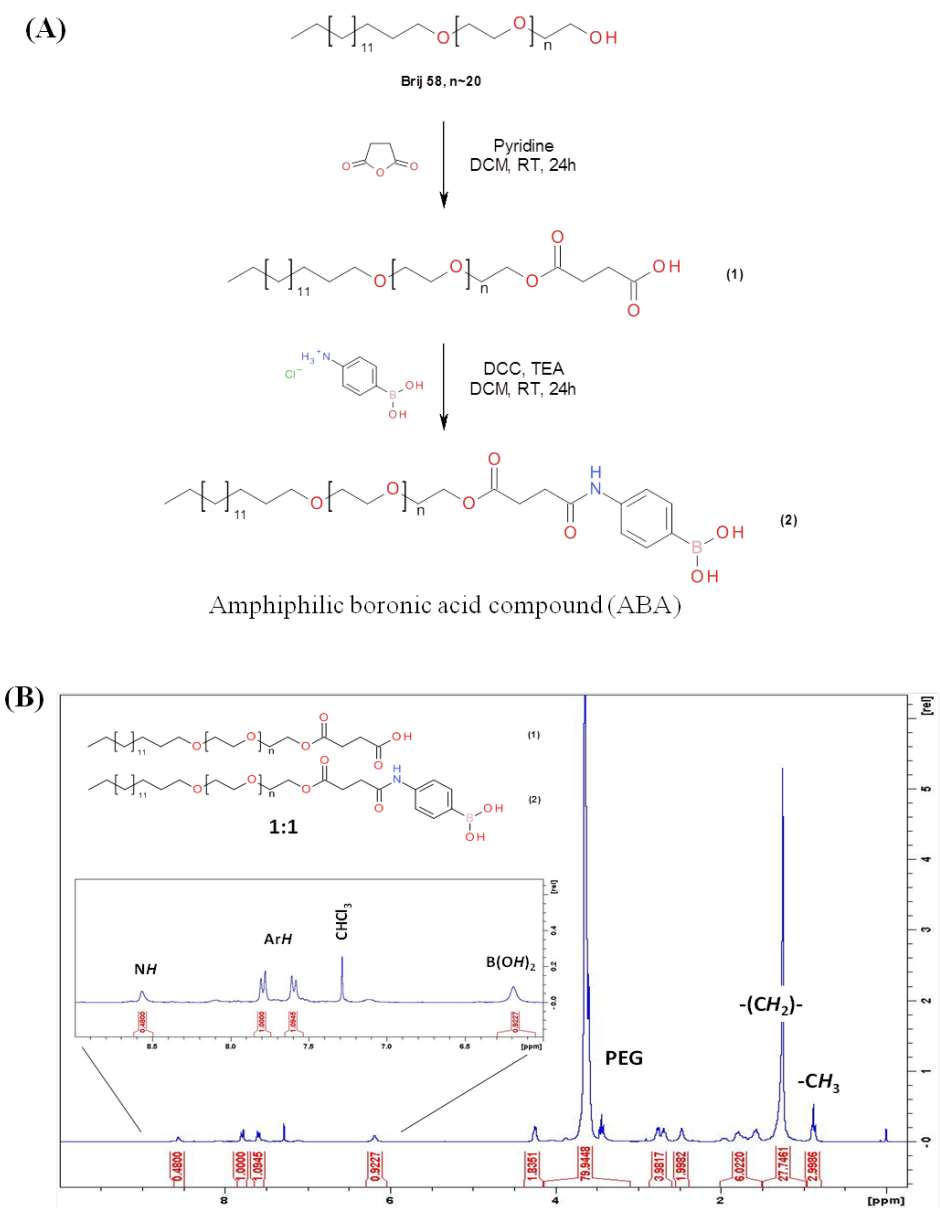

Figure 4.2. (A) Synthetic route to amphiphilic boronic acid (ABA) and (B) ^{1}H NMR analysis of ABA compound**.**

The appearance of a doublet at 7.80 ppm and 7.59 ppm in ^{1}H NMR analysis of ABA compound confirms the presence of the aromatic proton of the aminophenylboronic acid moieties (**Figure 4.2B**). Another singlet peak at 8.56 ppm in NMR analysis verifies the existence of the amide link between the 4-aminophenylboronic acid and the carboxylic acid

compound **(1)**. Moreover, taking one aromatic proton of the BA moieties (2 x 2 H for the 4-aminophenylboronic acid) as integration reference, the $–CH_3$ of Brij-58P at 0.88 ppm integrates for roughly 3 H. It is thus concluded that the ABA represents 50% of BA moieties at the chain end of Brij-58P.

4.2. Post-insertion of the ABA compound onto lipid nanocapsules (LNCs)

After successful synthesis and characterization of ABA, the next step was to incorporate the synthesized ABA compound onto the surface of lipid nanocapsule using a post-insertion technique (**Figure 4.3**). The formulation of lipid nanocapsules (LNCs) was based on a phase inversion process according to the patent filed by Heurtault et al. [4]. This thermal manipulation allow the preparation of very small LNCs, consisting of an oily liquid triglyceride core surrounded by a hydrophilic surfactant, which exposes a medium PEG chain containing an average of 15 ethyleneglycol units (**Figure 4.1**). In the present study, blank LNCs were achieved by mixing labrafac, solutol and phospholipon at optimized concentrations using the phase inversion-based process.

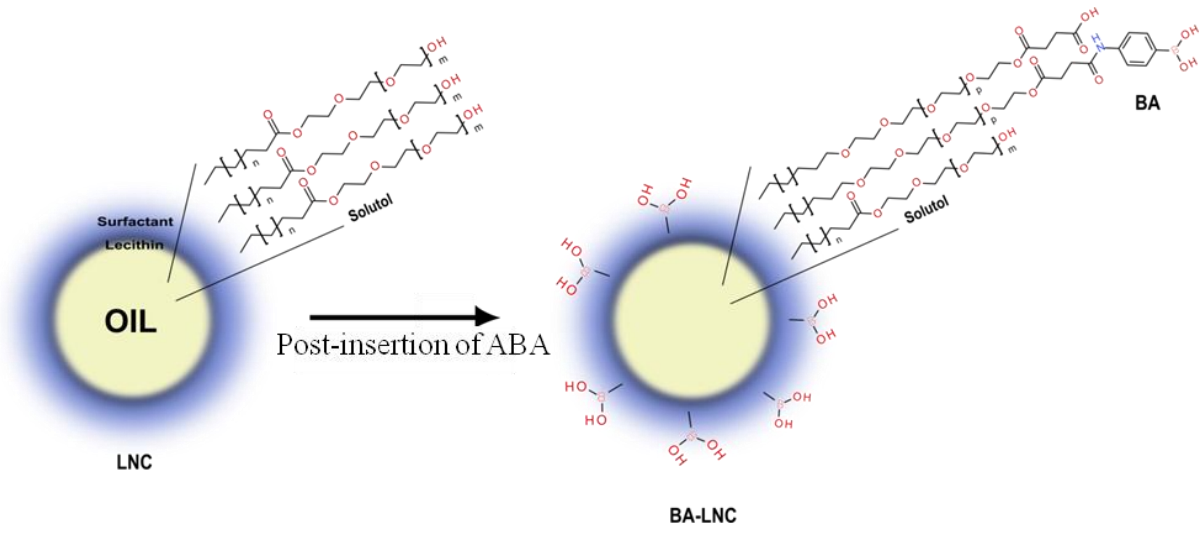

Figure 4.3. Schematic representation of the formulation of boronic acid-modified lipid nanocapsules (BA-LNCs).

Briefly, the oil phase was mixed with the appropriate amounts of Solutol, Phospholipon 90G, NaCl and distilled water, and heated under magnetic stirring up to 85°C. The mixture was subjected to 3 temperature cycles from 70 to 90°C under magnetic stirring.

Then, it was cooled to 78°C, 3.3 mL of distilled cold water (0°C) were added, and the suspension was further stirred at room temperature for another 10 min before further use. The composition of the formulation is summarized in **Table 4.1**. The percentage composition is just the mass percentage of the components for the lipid nanocapsules (a total initial mass of 1.26 g). LNCs were purified from supernatant using disposable PD-10 desalting columns (Sephadex® G-25 for gel filtration as stationary phase, Amersham Biosciences). A column was stabilized with 25 mL of distilled water. Then 2 mL of a suspension of LNCs were deposited on the column, 0.5 mL of water were added to complete the dead volume of the column, then 4 mL of distilled water eluted and the LNCs were collected in this eluent.

The suspension was then dialyzed (pore size: 6000-8000 Da) against deionized water overnight. The solution was freeze-dried and weighed in order to estimate the mass concentration. This process offers a good control over the nanocapsules' size (31.6 ± 0.4 nm) with narrow size distributions (PI<0.1) (**Table 4.2**). Due to Solutol HS-15, which exposes PEG chains, zeta potential of LNCs was -10.0 ± 0.3 mV. This value is similar to the zeta potential of other pegylated vectors such as liposomes [5] and identical to the previously reported in the literature [6].

Table 4.1. Composition of the components for the lipid nanocapsules preparation for a total initial mass of 1.26 g.

	Labrafac (%)	Solutol (%)	Phospholipon 90G (%)	NaCl (%)	Water (%)
LNC	20.0	32.4	3.0	1.7	42.9

Transfer of amphiphilic PEG from micellar phase to pre-formed liposomes was first demonstrated by Uster *et al*. in order to increase *in vivo* circulation time of these carriers [7]. Similarly, BA-LNCs were obtained by classical post-insertion method on preformed LNCs [2, 3] by incubating LNCs solution (4 mg mL^{-1}) with 2 mg mL^{-1} of ABA compound (**Figure 4.3**). The quantity of phenylboronic acid moieties incorporated into LNCs was established using UV/vis spectroscopic data (**Figure 4.4**). The amphiphilic boronic acid compound **(2)** displays an absorption band at 259 nm, in accordance with the absorption of the phenylboronic acid moiety (**Figure 4.4A**). As observed from **Figure 4.4B**, the absorption intensity scales linearly with the concentration of ligand (**2**) from 12.5 to 100 μg mL^{-1}. The concentration of BA moieties in the suspension was found to be 0.83 ± 0.06 mg/mL (0.62 ± 0.04 mM). Thus the

concentration of incorporated BA is estimated as 0.42± 0.06 mg/mL, which corresponds to 16.6% of mass concentration. The success of the post-insertion process was in addition confirmed by the presence of 3.9 at % of B1s in XPS analysis. The B1s high resolution XPs spectrum shows a band at 191.1 eV corresponding to -C-B$(OH)_2$ bond (**Figure 4.4C**) as expected for the BA-LNCs. The mean diameter of the BA-LNCs is 38.8 ± 0.3 nm, slightly larger than the mean diameter of blank LNCs (**Table 4.2**). The low size distribution (PDI = 0.225 ± 0.004) was also retained (**Table 4.2**). The zeta potential of BA-LNCs remained negative at -17.6 ± 0.8mV.

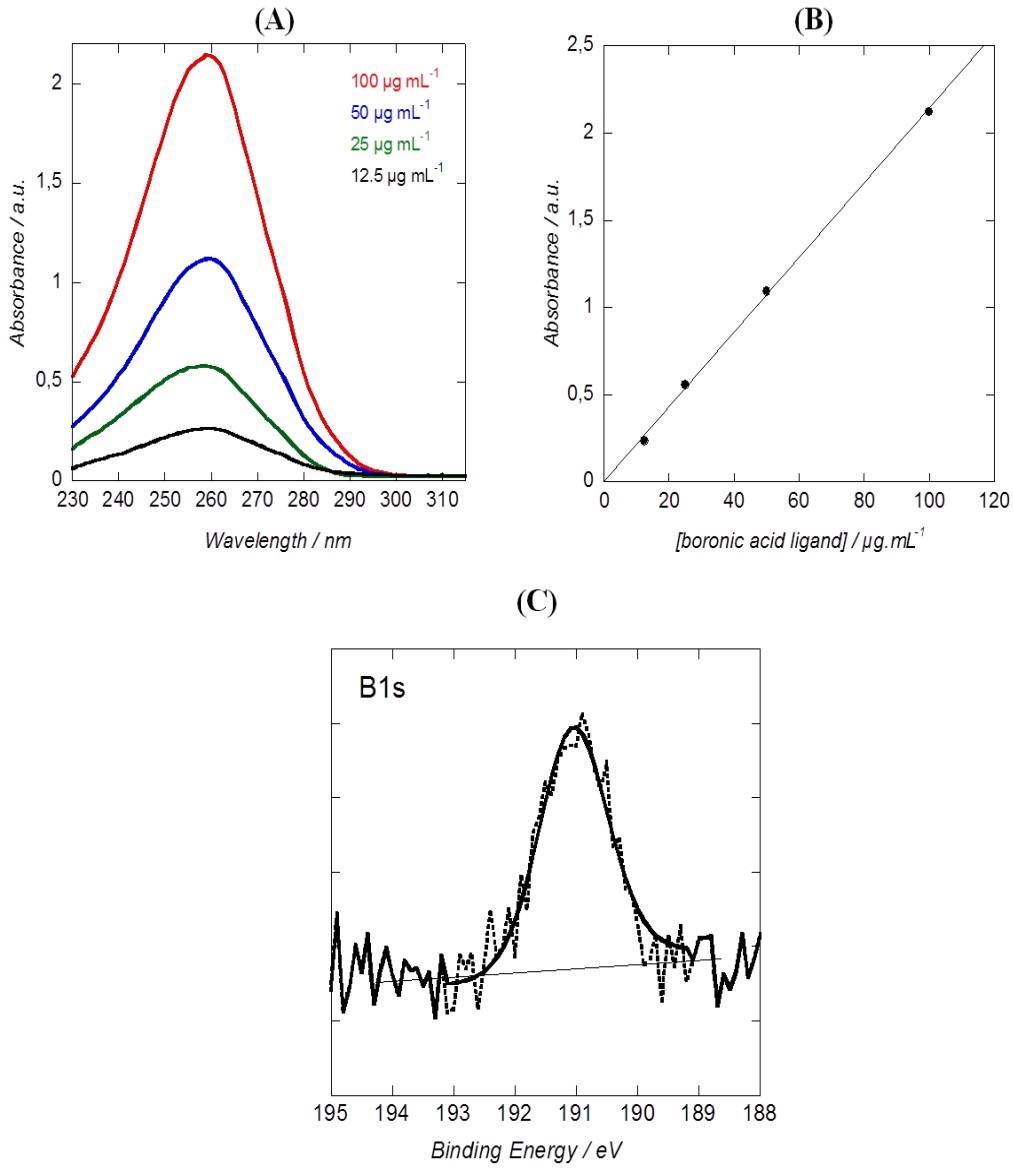

Figure 4.4. (A) UV/Vis spectra of ABA compound in dichloromethane; (B) Calibration curve of ABA compound in dichloromethane: ($A_{259} – A_{310}$) = f [boronic acid ligand].

Table 4.2. Physicochemical characterizations of the BA-LNC.

	Size / nm	PDI	Zeta potential / mV
ABA-compound	205.5 ± 10.9	0.328 ± 0.022	-27.7 ± 4.2
Blank LNC	31.6 ± 0.4	0.065 ± 0.014	-10.0 ± 0.3
BA-LNCs	38.8 ± 0.3	0.225 ± 0.004	-17.6 ± 0.8

In the present study, blank LNCs with a nominal size of 25 nm, were achieved by mixing labrafac, solutol and phospholipon at optimized concentrations using the phase inversion-based process as described in supporting information. This process offers a good control over the nanocapsules' size (31.6 ± 0.4 nm) with narrow size distributions (PI<0.1) (**Table 4.2**). Due to Solutol HS-15, which exposes PEG chains, zeta potential of LNCs was -10.0 ± 0.3 mV. This value is similar to the zeta potential of other pegylated vectors such as liposomes [5] and identical to the previously reported literature [6].

4.3. Effect of BA-LNCs on Huh-7 cell viability

The cell viability of blank LNCs, BA-LNCs and the amphiphilic boronic acid compound were analyzed on the Huh-7 cell line using 3-(4,5-dimethylthiazol-2-yl)-5-(3-carboxymethoxyphenyl)-2-(4-sulfophenyl)-2H-tetrazolium (MTS) MTS is a well-known colorimetry assay to determine number of viable cells in proliferation, cytoxicity or chemosensitivity. MTS is tetrazolium compound on which an electron coupling reagent, phenazine ethosulfate (PES) has been added prior use to enhance stability of MTS solution. Mitochondrial reductase of the viable cells reduces the tetrazolium ring, which is initially yellow into fromazen (dark red). Thus formed formazan product has an absorption maximum at 490-500 nm in phosphate-buffered saline. Huh-7 cells were incubated with the three samples at increasing concentrations for 2 h (to be used in the virus entry inhibition assay). Thereafter, the nanocapsules were washed away and the MTS assay was carried out after 48 h of incubation with fresh medium.

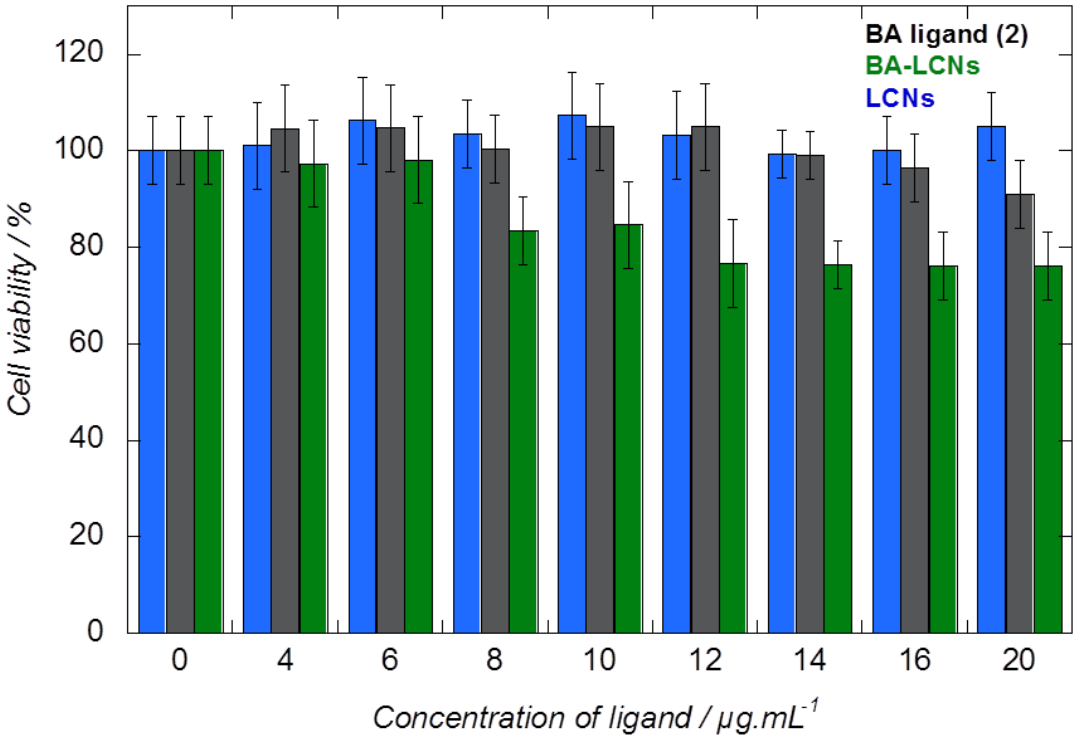

Figure 4.5. In vitro cytotoxicity of LNC, ABA ligand and BA-LNCs on the Huh 7 cell culture after 2 h of incubation with cells. LNC25 at different concentrations.

The blank LNCs did not show any cytotoxicity even at the highest analyzed concentration (100 µg mL^{-1}, data not shown) for 2 h incubation (**Figure 4.5**). The ABA ligand is non-toxic up to a 20 µM concentration of BA moieties. For BA-LNCs, a slight decrease in cell viability was observed for concentrations higher than 8 µM of BA moieties (**Figure 4.5**). However no further decrease was observed at higher concentrations even up to the highest concentration examined in this assay.

4.4. Virus entry inhibition assay

Modified JFH1 cell cultured virus (HCVcc) was used in this assay to evaluate the potential of BA-LNCs as HCV entry inhibitor. The experimental system and protocol followed is similar to the protocol used in **Chapter 3** with inorganic nanomaterials. The increasing concentrations of BA-LNCs and BA ligand were first incubated with HCVcc, 1h later, these HCVcc-BA-LNCs and HCVcc-BA ligand complexes were used to infect the Huh-7 cells. After 2 h of infection, the complexes were removed and replaced by fresh medium

and infection was scored by using immunofluorescent assay after 48 h. A dose-dependent reduction in HCVcc infection was observed in the presence of BA-LNCs, with a 50 % inhibitory concentration (IC_{50}) of 5.8 µM concentration of BA moieties (**Figure 4.6**).

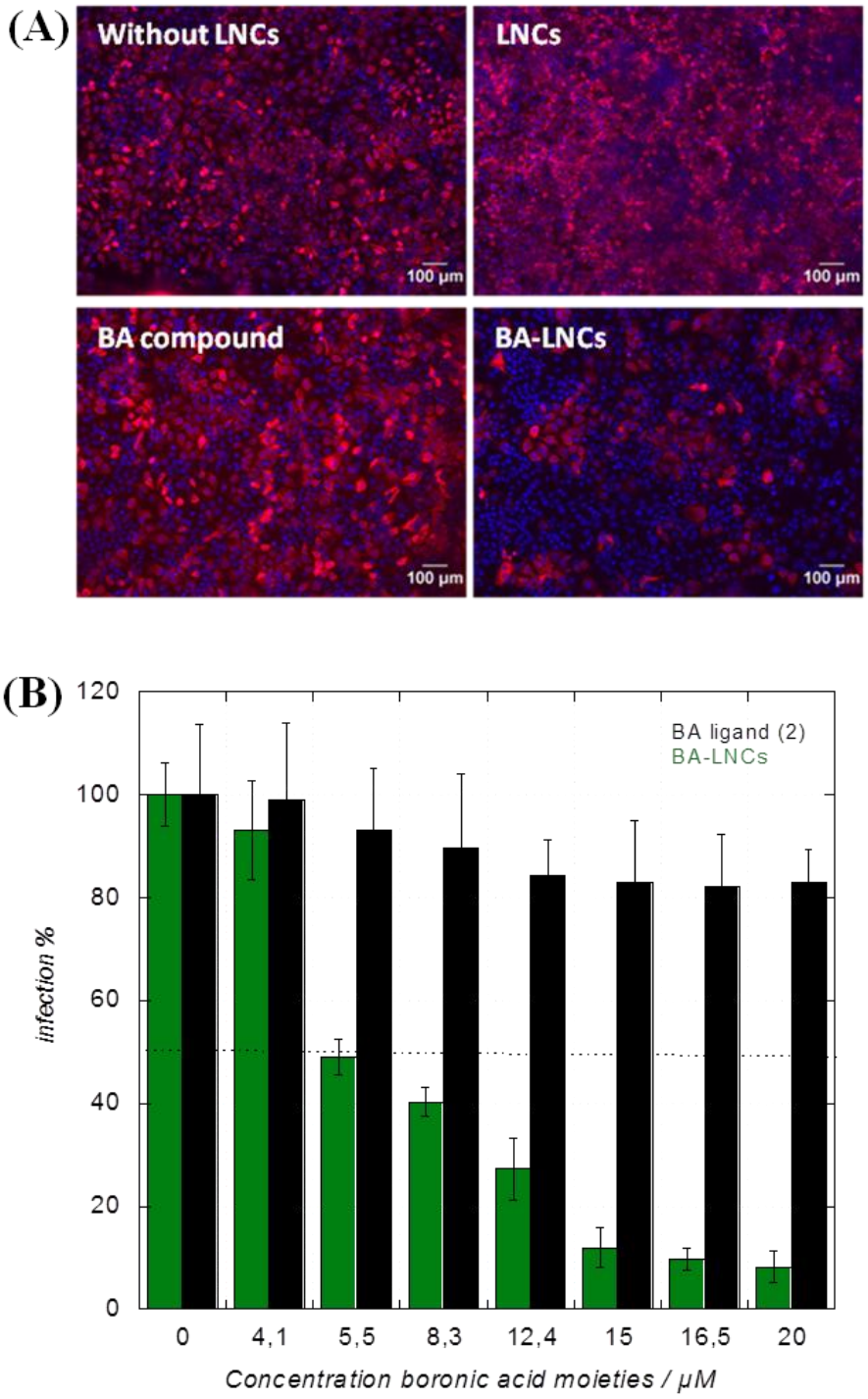

Figure 4.6. HCV infection inhibition assay on the Huh 7 targeted cell.; (A) Effect of BA ligand alone and BA-LNCs at different concentrations in the infection activity; (B)

Fluorescent image (10×) of the Huh 7 target cells after incubation with modified JFH1 virus for 48h, incubation in the presence of the blank LNCs (80 µg/mL), ABA compound (concentration of boronic acid moieties = 15 µM) and BA-LNCs (concentration of boronic acid moieties = 12.4 µM), along with absence of any nanocapsules (red color and blue color correspond to infected cells and nucleus, respectively).

In contrast, the equivalent concentrations of monovalent BA compound did not show any significant effect on the inhibition of HCVcc, even at the highest concentration tested. This result strongly supports the concept of multivalency of boronic acid moieties to be able to establish strong cis-diol complex with glycans of envelope glycoproteins.

4.5. Mode of action of the inhibitory effect of BA-LNCs

To determine whether BA-LNCs specifically act on the early stage of entry of virus, lipid nanocapsules decorated with ABA at concentration of BA moieties of 12.4 µM were added at different time points before, during and after infection of Huh-7 cells with HCVcc.

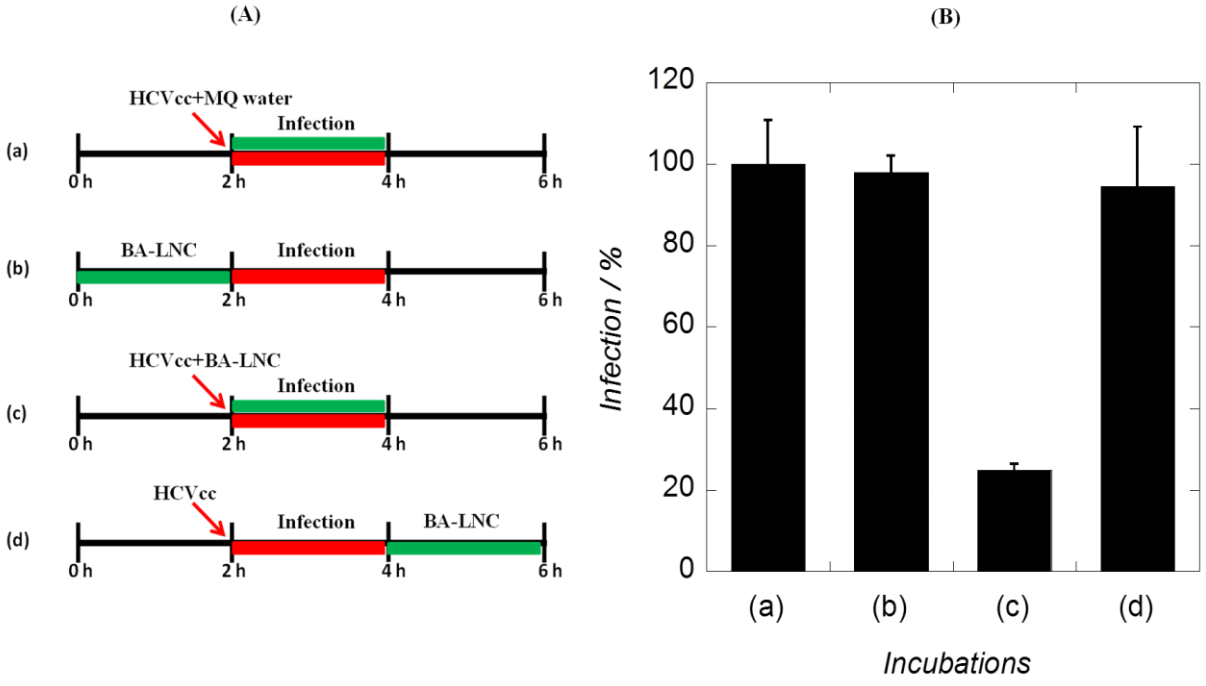

Figure 4.7. Pre-, co- and post-incubation of BA-LNCs and HCV infection on the Huh 7 cell culture. (A) Schematic representation of different incubations; (B) Effect of BA-LNCs (concentration of boronic acid moieties = 12.4 µM) in the infection activity.

The results (**Figure 4.7B**) clearly shows that the pre-incubation of virus with nanocapsules before infection remarkably inhibits viral infection in cell culture, whereas the addition of nanocapsules 2 h post-infection, after the virus is washed off, has no effect. This suggests that BA-LNCs is specifically acting on the early phase of virus entry. This is also supported by the result where nanocapsules were incubated with Huh-7 for 2 h before infection. No inhibition was observed in this case. In contrast to some studies where lectin-based antiviral drug like griffithsin and cyanovirin N-bind with glycan structures present on the surface of epithelial cells [8], BA moieties organized onto nanocapsules have a direct interaction with viral particles.

4.5.1. Competitive binding experiment with mannose/Man-9

BA-LNCs is supposed to interact with terminal mannose moieties present on N-linked high mannose oligosaccharides, here we tried to interfere the inhibitory effect of BA-LNCs by covering the active boronic acid group for an hour either with single mannose (Mann) unit or N-linked high mannose oligosaccharides mannonanose-di-(*N*-acetyl-D-glucosamine) (Man-9) (**Figure 4.8**) to observe whether mannose and/or Man-9 pretreatment could reverse the inhibitory effect of BA-LNCs.

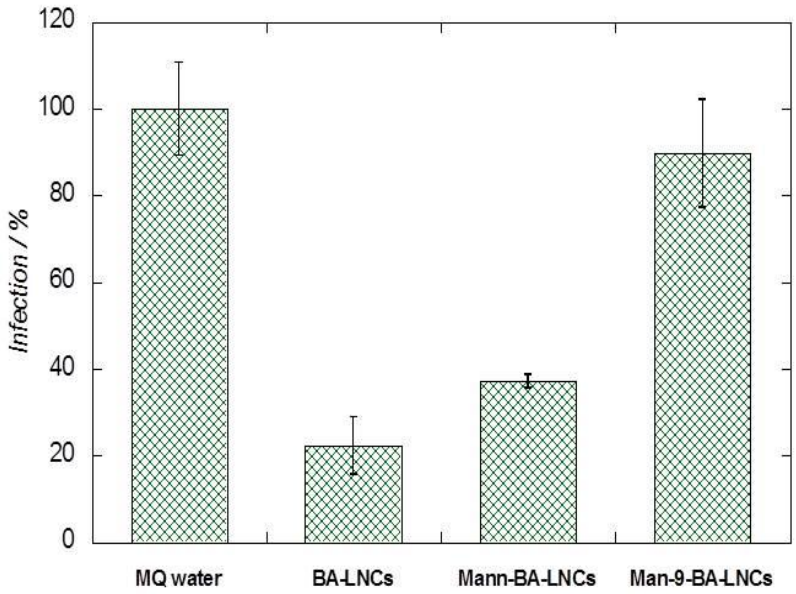

Figure 4.8. Competitive assays and selectivity. Effect of mannose blocking BA functions on BA-LNCs on the viral entry inhibition activity: negative control (MQ water), BA-LNCs at concentration of 12.4 µM of boronic acid moieties and BA-LNCs (at similar concentration of boronic acid moieties) covered with with mannose (57.78 µM) and Man-9 (5.4 µM).

The result indicates that Man-9 efficiently compete with BA-LNC binding to HCV, whereas mannose itself was a poor competitor. These data support the hypothesis that the inhibitory effect of BA-LNCs is due to the active BA moieties that can recognize the N-linked high mannose glycan present on envelope glycoprotein of HCVcc. Indeed, we have demonstrated previously that boronic acid modified inorganic nanostructures when saturated with mannose prior to infection of Huh-7 cells with HCVcc lose their antiviral activity [9].

4.5.2. HCV Pseudotyped Particles (HCVpp)

To establish that the effect of BA-LNCs is on the HCV entry step additional proof was obtained using the infectious HCV pseudo-virus (HCVpp) system [10]. HCVpps are retroviral cores carrying HCV glycoproteins in their envelope. In this context, only the early steps of the viral life cycle, i.e. virus interaction with receptors, uptake and fusion, are HCV specific, whereas all later steps are dependent on the retroviral nucleocapsid elements. Luciferase expressed from the retroviral genome can be measured and is used to determine HCVpp entry efficiency. Moreover, to determine the conservation of the antiviral effect of BA-LNCs on different HCV isolates, HCV envelope glycoproteins from different genotypes were used (**Figure 4.9**). These pseudoparticles are defective for reinfection since they do not contain the genetic information to express envelope glycoproteins in their genome. As they only contain the envelope glycoproteins of HCV, these pseudoparticles have been widely used as a surrogate model to study HCV entry [11]. The level of virus entry is therefore determined by measuring the luciferase activity. As a control, retroviral particles pseudotyped with vesicular stomatitis virus glycoprotein G (VSVg) instead of HCV envelope glycoproteins were used. In this study, BA-LNCs at a BA concentration of 8.3 µM inhibited HCVpp infection of the different genotypes tested, which is likely due to the high level of glycosylation of HCV envelope glycoprotein (**Figure 4.9**). In the same assay, BA-LNCs at the similar BA moieties concentration did not have any significant inhibitory effect on entry of pseudoparticles containing the envelope glycoprotein G of VSV.

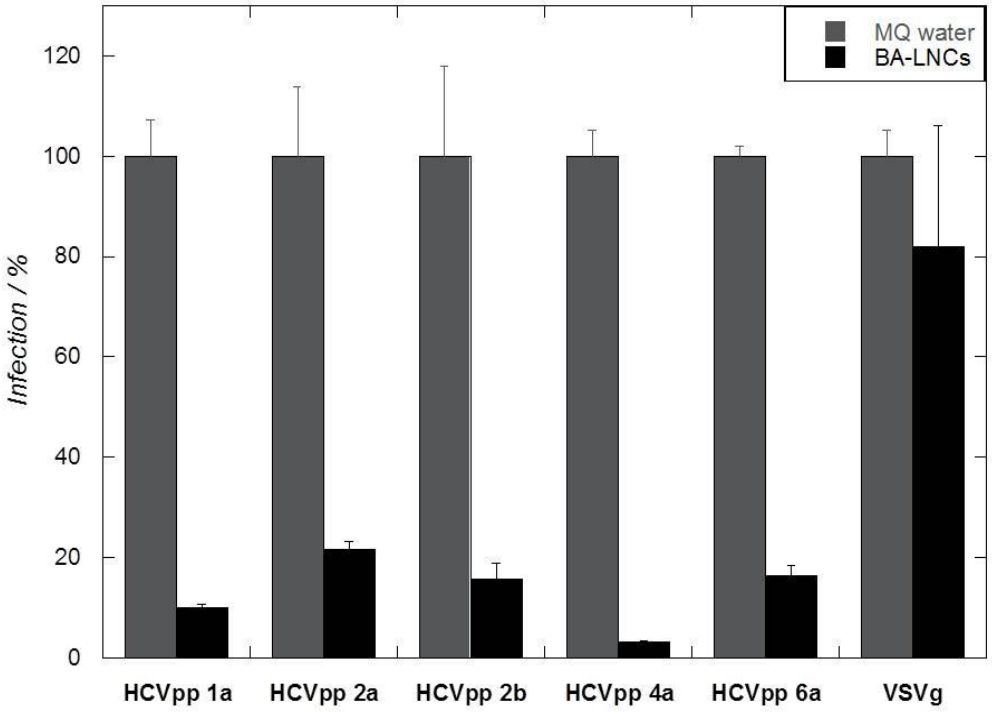

Figure 4.9. Selectivity of BA-LNCs at concentration of 8.3 µM of boronic acid moieties on the entry of different HCVpp genotyped over pseudotyped (control) virus particle with envelope protein of VSV.

This might be due to the presence of only two *N*-linked glycans of a complex type, which might not be recognized by BA-LNC as also observed when HCVpp are pre-incubated with griffithsin lectin [12]. This is an important finding for itself, as one of the major difficulties in HCV vaccine preparation lies on the fact that there exist variable genotypes and particularly its envelope glycoprotein. This reality encourages for the search of more-conserved features of the virus as an attractive targets for the development of antiviral therapeutics. Envelope glycoproteins are highly glycosylated at well defined locations in specific variants [13] and the fact, that these glycans play an essential role in HCV entry [14] motivates investigations of several cost effective and efficient therapeutic systems.

4.6. Conclusion

The development of boronic acid modified LNCs seems to be a promising and efficient manner to inhibit HCV entry and might replace the pre-existing natural lectins. The

synthesis of ABA ligand and preparation of multiple copies of BA moieties on the lipid nanocapsule was accomplished successfully. This study has demonstrated that these BA-LNCs inhibit HCVcc as well as HCVpp entry regardless of the genotype. The major difficulty in the vaccine preparation against HCV lies on the fact that there exist variable genotypes and particularly its envelope glycoprotein. This verity encourages for the search of more-conserved features of the virus as an attractive targets for the development of antiviral therapeutics. Envelope glycoproteins are highly glycosylated at well defined location in specific variants [13] and the fact, that these glycans play an essential role in HCV entry [15], motivates investigations of several cost effective and efficient therapeutic systems. Therefore, from this study, we introduce a novel nanocarrier system that carries multiple copies of oligomannose specific boronic acid moieties as an effective anti-HCV entry agent. It is well-known that boronic acid has high affinity for sugars and can easily make diol complex with glycans, but the effectiveness of binding depends not only the concentration but the most importantly on the multivalency, which was demonstrated on the previous chapter with inorganic nanomaterials anti-HCV studies [9]. This 'proof-of-concept' is further validated by this study of BA-LNCs against HCV entry. In this work, we have shown that BA-LNCs, a biocompatible nanomaterial, having multiple copies on the surface of LNC can efficiently prevent HCV infection in micromolar range (IC_{50} = 5.4 µM of boronic acid moieties) where as monomer ABA ligand did not show any significant inhibition even at the highest analyzed concentration (20 µM). When the active boronic acid moieties were blocked by Man-9 and mannose, we observe no any prevention and reduction in activity respectively on infection. This strongly supports the hypothesis that BA-LNCs acts by forming cyclic di-ester-formation between the particle-appended boronic acid moieties and glycans present on HCV envelope protein. Moreover, the BA-LNCs inactiveness in 'pre' and 'post' –incubations of infection further suggest that the BA-LNCs exhibit the inhibition property by specifically blocking the entry of HCV into the target cell. This finding was further supported by using HCV pseudo-particle (HCVpp) where it is clearly shown the inhibition of different genotypes, which is probably due to the high degree of glycosylation of evelope glycoprotein of all genotypes. Therefore, this study has brought up the most promising stable and efficient nanocarrier that can be further studied in *in vivo* and apply as a potential therapeutic strategy for blocking viral entry.

4.7. References

1. Huynh, N.T., et al., *Lipid nanocapsules: a new platform for nanomedicine.* Int J Pharm, 2009. **379**(2): p. 201-9.
2. Richard, A., et al., *Minimal chemical modification of reductive end of dextran to produce an amphiphilic polysaccharide able to incorporate onto lipid nanocapsules.* Bioconjug Chem, 2008. **19**(7): p. 1491-5.
3. Hirsjarvi, S., et al., *Layer-by-layer surface modification of lipid nanocapsules.* Eur J Pharm Biopharm, 2010. **76**(2): p. 200-7.
4. Heurtault, B., et al., *A novel phase inversion-based process for the preparation of lipid nanocarriers.* Pharm Res, 2002. **19**(6): p. 875-80.
5. Yang, T., et al., *Preparation and evaluation of paclitaxel-loaded PEGylated immunoliposome.* J Control Release, 2007. **120**(3): p. 169-77.
6. Perrier, T., et al., *Post-insertion into Lipid NanoCapsules (LNCs): From experimental aspects to mechanisms.* Int J Pharm, 2010. **396**(1-2): p. 204-9.
7. Uster, P.S., et al., *Insertion of poly(ethylene glycol) derivatized phospholipid into pre-formed liposomes results in prolonged in vivo circulation time.* FEBS Lett, 1996. **386**(2-3): p. 243-6.
8. Kouokam, J.C., et al., *Investigation of griffithsin's interactions with human cells confirms its outstanding safety and efficacy profile as a microbicide candidate.* PLoS One, 2011. **6**(8): p. e22635.
9. Khanal, M., et al., *Phenylboronic-acid-modified nanoparticles: potential antiviral therapeutics.* ACS Appl Mater Interfaces, 2013. **5**(23): p. 12488-98.
10. Bartosch, B.D., J.; Cosset, F. L., *Infectious hepatitis C pseudo-viruses containing functional E1E2 envelope protein complexes.* J. Exp. Med., 2003. **197**: p. 633-642.
11. Lavie, M., A. Goffard, and J. Dubuisson, *Assembly of a functional HCV glycoprotein heterodimer.* Curr Issues Mol Biol, 2007. **9**(2): p. 71-86.
12. Meuleman, P., et al., *Griffithsin has antiviral activity against hepatitis C virus.* Antimicrob Agents Chemother, 2011. **55**(11): p. 5159-67.
13. Goffard, A. and J. Dubuisson, *Glycosylation of hepatitis C virus envelope proteins.* Biochimie, 2003. **85**(3-4): p. 295-301.
14. Helle, F., et al., *The neutralizing activity of anti-hepatitis C virus antibodies is modulated by specific glycans on the E2 envelope protein.* J Virol, 2007. **81**(15): p. 8101-11.
15. Helle, F., et al., *Role of N-linked glycans in the functions of hepatitis C virus envelope proteins incorporated into infectious virions.* J Virol, 2010. **84**(22): p. 11905-15.

CHAPTER 5

Nanodiamond as a nanovehicle for gene delivery

5.1. Gene delivery

Human cancer is one of the biggest human threats that results from a variety of genetic mutations, which alter cellular proliferation, angiogenesis, metastasis, and tumor immunogenicity [1]. Many malignancies remain resistant to the traditional treatment despite of rapid advancement in understanding of underlying molecular mechanism of cancers [2, 3]. However, gene therapy is gaining massive interest as cancer treatment [4, 5] due to its significant potential for treatment of inherited and acquired life threatening diseases caused by genetic deficiencies and abnormalities.

Gene delivery is a technique to introduce new genetic materials to hosts and has become an important experimental tool to study gene function and protein expression. It aids to establish various disease models, to acquire DNA-based immunization, and therefore to explore potential therapeutic applications to various acquired or inherited diseases. Besides treatment of genetic diseases, gene transfer is also used to produce large quantities of secreted proteins for direct therapeutic application or vaccines production. However, it is not an easy task to transfer gene to cell nucleus since it is well known that naked DNA molecules do not enter cells efficiently because of their large size, negatively charged phosphate groups and susceptibility to nuclease mediated degradation. Thus various strategies have been developed for gene delivery [6, 7]. The ideal gene delivery system should have high transfection efficiency and low cytotoxicity. Therefore, the primary challenge lies on the development of convenient methods to develop carriers (commonly called vectors) and physical methods that facilitate gene transfer to targeted cells without degradation of the delivered gene. An example is demonstrated in **Figure 5.1** which is designed and implemented by Deng and co-workers. Silencer RNA (siRNAs)/polycations have been fitted as a sandwich between a layer of doxorubicin and an outer layer with stealth along with molecular tumor targeting agents.

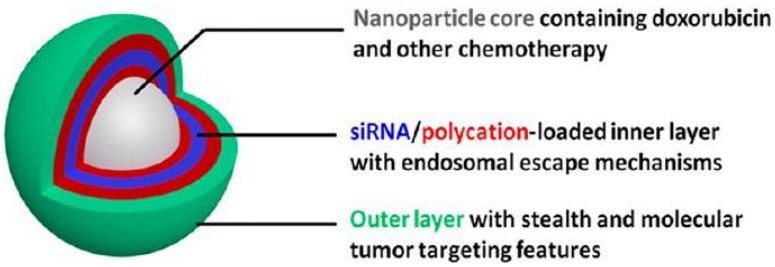

Figure 5.1. Schematic representation of combination drug delivery system based on layer by layer nanoparticles.In this multilayered nanoparticles, genetic materials are nicely condensed and protected from degradation by the nuclease [8].

Currently, gene transfection systems contain three major groups: viral (transduction), physical (direct micro injection) and chemical methods. Commonly used vectors for gene transfer are recombinant viruses such as retrovirus, lentivirus, adenovirus, adeno-associated virus, and herpes simplex virus [9]. Efficient gene transfer by viruses is possible through their favorable cell uptake and intracellular trafficking machineries. However, viral gene transfer systems have several intrinsic drawbacks including difficulty in production, limited opportunity for repeated administrations due to acute inflammatory response, and delayed cellular immune responses. Insertional mutagenesis is also a potential issue for some viral vectors that integrate foreign DNA into the genome. The nonviral gene delivery methods including physical and chemical methods, on the other hand, use physical forces or synthetic or natural compounds to deliver a piece of DNA into a cell. The materials used are generally less toxic and immunogenic than the viral counterparts. Other practical advantages of nonviral approaches include ease of production and the potential for repeat administration. Nonviral methods are generally viewed as less efficacious than the viral methods [10]. Biolistics, jet injection and electroporation are commonly as physical methods for gene transfer [11, 12]. These methods propose the direct penetration of genetic materials into the cytosol and are effective for single and multiple target cells at an intended location and carry less risk of the transfection reagent dispersion. However, several drawbacks of this system includes the difficulty for genes to get transported to the nucleus because of enzymatic digestion of naked DNA or RNA resulting low transfection efficiency and thus limits its application. Moreover, they cause cell damage and exhibit the difficulty in large-scale manipulation [13]. Therefore, to overcome the drawbacks of viral and physical methods, a variety of chemical transfection systems like cationic polymer, lipids, dendrimers etc have been introduced since late 1960s

[14, 15]. Recently, a variety of synthetic transfection reagents are indeed commercialized for *in vitro* cellular transfection and they are summarized in **Table 5.1**.

Table 5.1. Commercially available transfection reagents [16].

Transfection reagent	Product origin	Based material
FuGENE HD	Roche, Switzerland	non-liposomal lipid
jetPEI	Polyplus-transfection, USA	linear PEI
Lipofectamine 2000	Invitrogen, USA	cationic lipid
SuperFect	Qiagen, USA	activated-dendrimer

The reason behind the popularity of these nanomaterials-based gene delivery system is that they can interact with genetic materials to condense them into the nanosized-complexes making them easy to pass through the cell membrane and protect those genetic materials from degradation [16].

Since in this thesis, we have developed a nanodiamond-based gene delivery system; the recent researches on nanodiamonds for gene delivery will be discussed in this chapter.

5.2. Extra and Intracellular barriers for gene transfer

The overall efficiency of gene transfer has been limited by the various anatomical and cellular barriers as demonstrated in **Figure 5.2**. Anatomical barriers include epithelial, endothelial cell linings and the extracellular matrix surrounding the cells that prevent direct access of macromolecules to the target cells. Genetic material loaded colloidal particles administered through blood circulation are often cleared by the professional phagocytes such as Kuffer cells in liver and residential macrophages in the spleen. Moreover, various nucleases existing in blood and extracellular matrix can also rapidly degrade free and unprotected nucleic acids following the administration [10]. The most critical step for an efficient transfection is considered to be the plasma membrane crossing. Genetic materials cannot pass through cell membrane unless their entry is facilitated by creating transient holes by physical meanings [13] or through utilizing the various cellular uptake mechanisms such as endocytosis, pinocytosis or phagocytosis [17].

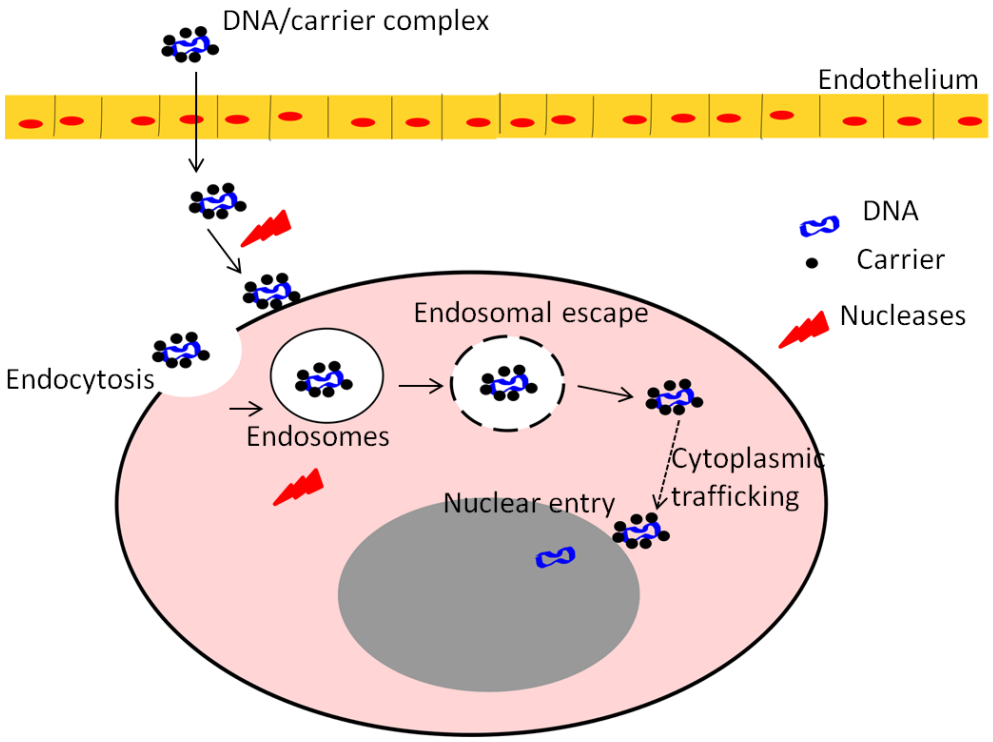

Figure 5.2. Schematic representation of limiting factors that are faced by nanovehicle for gene delivery.

Upon the nanovehicle/genetic material complexes being taken up by via endocytosis, these complexes are often captured within endosomes and usually transform into the digestive lysozomes unless some escape mechanisms are used to interrupt this maturation process. Two escape mechanisms are well known. The first involves the use of membrane active or fusogenic molecules such as fusion peptides [18] or lipid components with acid-sensitive bond and large hydrophobic portion of the molecules to rupture the endosome membrane [19]. The other mechanism acts on building up osmostic pressure within the endosomal compartment that eventually triggers the swelling or burst of the endosomal vesicles [20]. Generally, amine compounds such as cationic polymer like polyethylenimine (PEI) absorb protons and slow down the acidification process which is important for the endosome-lysozome transition [21]. After releasing from endosomes, the complexes must travel through cytoplasmic space filled with viscous protein solution towards the nucleus where transcription takes place. The nuclear membrane is another important barrier for the entry of genetic materials. This double- membrane envelope is interrupted by large protein structures generally referred as nuclear pore complexes (NPC) having pore size of around 9 nm, which regulates the transportation of molecules and macromolecules through nuclear membrane. It allows the free diffusion of molecules and ions of small to medium sizes such as proteins of

upto 40-60 kDa, or nucleic acid of upto 300 base pair [22]. Mostly, the cationic lipids dissociate from genetic material through lipid mixing and exchange during cytoplasm entry with lipids of the host cell whereas complexes formed with cationic polymer like PEI remain stable even after the endosomal escape. The complexes with polymer disintegrates later in nucleus [23].

Green fluorescence protein (GFP) encoded plasmid DNA (pDNA) or luciferase encoded pDNA are commonly used experimental model to investigate the cellular transfection efficiency. In this thesis, we have worked on GFP gene as a reporter of expression.

5.3. Nanoparticles for cellular transfection

To be an ideal carrier system, nanoparticles can be considered as a good candidate since they have the nanometric size possessing large surface areas and ability to bind a large number of surface functional groups. In addition they offer controllable size and surface properties along with absorption and release of the genetic materials [24]. Cationic polymeric and lipidic nanoparticles are commonly used for transfection and exhibit relatively higher cellular transfection efficiency (**Table 5.1**). Besides organic, inorganic nanomaterials are gaining attention recently due to the fact that they can offer multifunctional applications like targeted gene delivery along with bio-imaging. The surface of these particles can be coated to facilitate DNA binding and simultaneously the targeting agent can be introduced onto the surface for target gene delivery. Taking advantage of small particle size, they usually bypass most of the physiological and cellular barriers and produce gene expression [25]. In addition, these inorganic nanomaterials exhibit no or less cellular toxicity and are inert to immune responses when coated with polyethylene glycol. Moreover, magnetic nanoparticles can also provide magnetic field responsiveness in a magnetic field guided targeted delivery [26]. Rapid progress in the *in vivo* applications of inorganic nanoparticles has recently picked up considerable speed for gene delivery too. Nevertheless, extensive studies are still required to assess the effect of their types, sizes, shapes on transfection efficiency.

Though plenty of work on NDs-based nanomedicine has been successfully carried out, NDs mediated approaches particularly towards gene therapy has been rarely reported. In the long competitive list of nanomaterials for transfection, NDs, being an inert and biocompatible material, have started to gain researcher's attention. The key factors for developing NDs as an

effective nanovehicle for gene delivery lie on improvement of stability in physiological solution and possibility to introduce fluorescent dye which could further help to follow the fate of the NDs-delivery system. The details on the NDs-based gene delivery system are presented below.

5.4. Nanodiamonds (NDs)-based gene delivery system

Generally, nanodiamonds are considered to be highly up-taken [27] via clathrin-mediated endocytosis pathway [28], but also depends on the surface charge and size of NDs, and exhibit several superior qualities such as good biocompatibility than compare to other carbon-based nanomaterials [29], easy functionalizations [30] and are commercially available at relatively low cost. Therefore, rapid advancement in the ND-based drug and gene delivery has been currently observed [31-34]. Generally, the pDNAs or RNAs are condensed by NDs *via* the electrostatic force generated in between positively charged surface of NDs and the negative charges from the genetic materials (**Figure 5.3A**). Positively charged NDs are created either by covalent grafting for example small molecules like (3-aminopropyl)-triethoxysilane (APTMS) or non-covalent adsorption of amine terminated polymer like PEI [31, 35, 36]. **Figure 5.3B** summarizes the strategies that have been used till now for the gene transfer. In all of the cases pGFP reporter plasmid was used to follow the transfection. Zhang et al has reported a novel cationic NDs-polymer brush which was synthesized by 2-bromoisobutyrate-modified ND surface-initiated atomic transfer radical polymerization of 2-(dimethylamino)ethyl methacrylate (DMAEMA) [36]. This study has shown that the ND-brushes were capable not only of condensing pDNA into stable nanoparticles, protecting DNA from enzyme degradation, but also were efficient enough to deliver plasmids into COS-7 cells as compared to PEI25k (PEI 25 kDalton)/pDNA complex with much lower cytotoxicity.

Likewise, in another study performed by Ho and coworkers, a structure that combined nanodiamond and polyethylenimine 800 Da (PEI800) has been designed, and successfully transfected cells with both plasmid [31] and siRNA [37]. However, the transfection efficiency of their vectors when delivering plasmid DNA is 2-3 folds lower than that of PEI25K. In this study, NDs were coated with amino groups from PEI and ND-PEI800 may possess the properties of proton sponge which may later help to rupture and escape the complexes from endosomes into the cytoplasm. The decreased cell viability cannot be ignored too. In another study carried out by Martin and co-workers, Fenton treated NDs have been covalently

functionalized with fluorescent dye to track NDs entry into the HeLa cells and in addition the ability of NDs to cross the cell membrane was exploited to assist the intracellular delivery of pDNA [32].

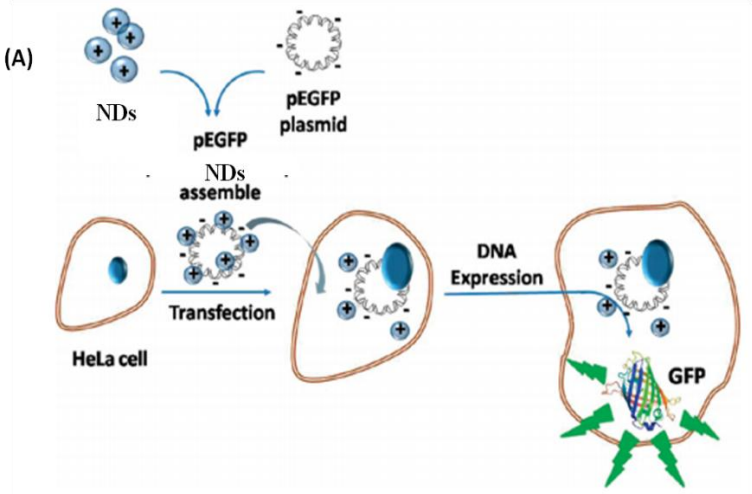

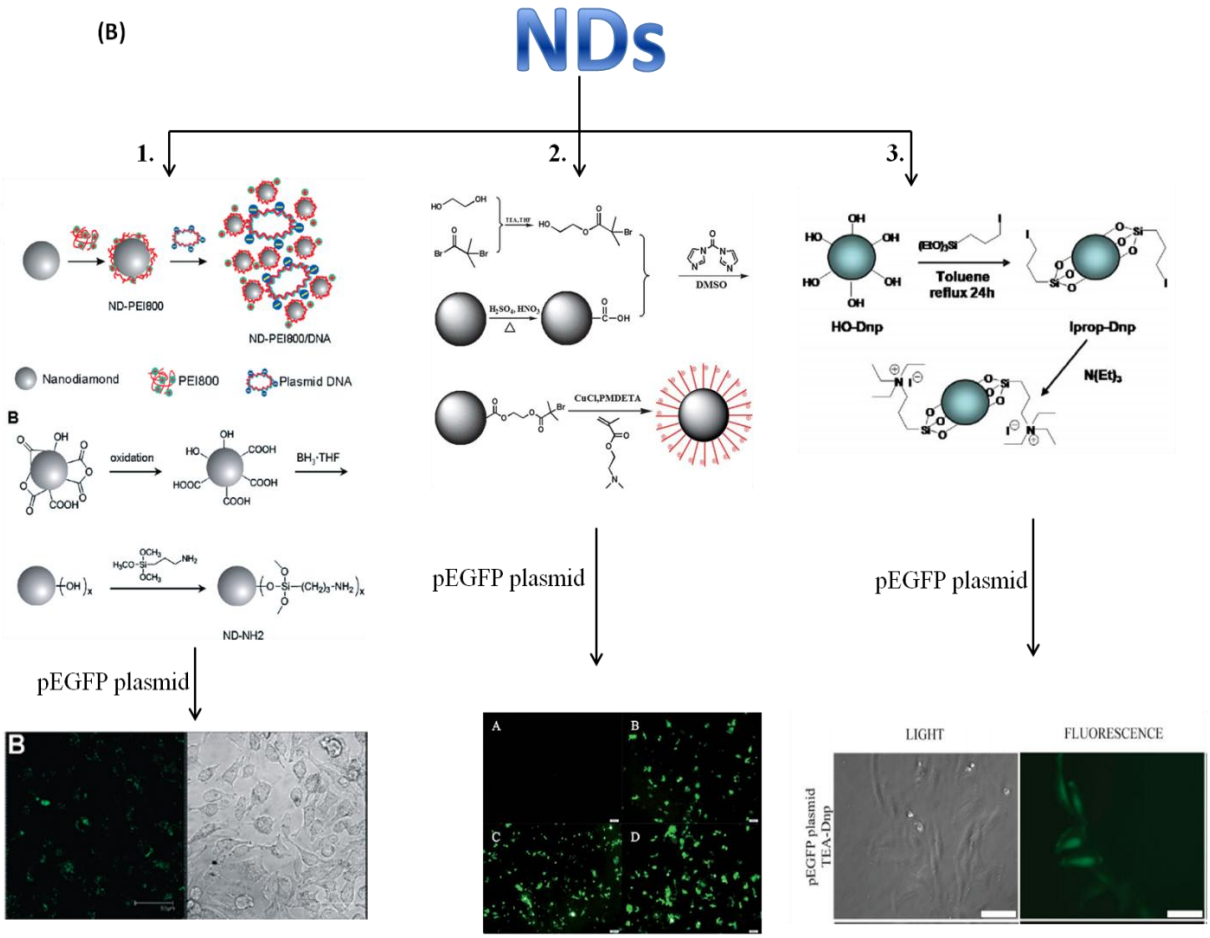

Figure 5.3. Schematic representation of the transfection experiment using pEGFP and cationic NDs (A) [32], Different strategies for surface modification of NDs to make them cationic for grafting pDNA; (1) physical adsorption of PEI and silanization of NDs to create amine terminated NDs [31], (2) NDs modified with cationic polymer brush [36] and (3) triethylammonium modified NDs are capable of gene delivery [32]. All the confocal images have shown the expression of GFP

The positively charged groups available on the PEI coated NDs can bind negatively charged DNA binding through electrostatic interactions and facilitates cellular uptake [38, 39]. Conversely, the high positive charge density of PEI makes the particles moderately toxic [40], limiting its use as a gene delivery vector *in vivo*. Thus, it is essential to improve the cell viability and transfection level simultaneously.

5.5. Multifunctional nanodiamonds for gene delivery

All of the existing and future applications of NDs in biology and biomedicine including gene delivery critically depend on the formation of stable aqueous NDs suspensions. As NDs have the tendency to aggregate and thus to precipitate under physiological conditions, appropriate surface modification is required to form stable hydrosols of NDs. The introduction of polyethylene glycol (PEG) units onto the NDs surface has shown to make the nanoparticles surface not only hydrophilic and thus highly water dispersible but also decreased protein opsonization and subsequent phagocytosis by the mononuclear phagocytic system [41, 42]. Moreover, stable NDs colloidal solution could increase the cellular uptake and is believed to improve the cell viability which could be the advantage for effective gene delivery.

Direct grafting of the functional ligand is always preferable where multistep reactions can be skipped. Barras and co-workers have recently reported ‘one step’ functionalization of hydroxylated NDs by using dopamine derivatives containing terminal azide functional group (**Figure 5.4A**) [43]. This work has also demonstrated that post functionalization is possible on dopamine derivative grafted NDs. At the same time, our group has used this approach for the construction of multifunctional magnetic particles (MPs) (**Figure 5.4B**) [44].

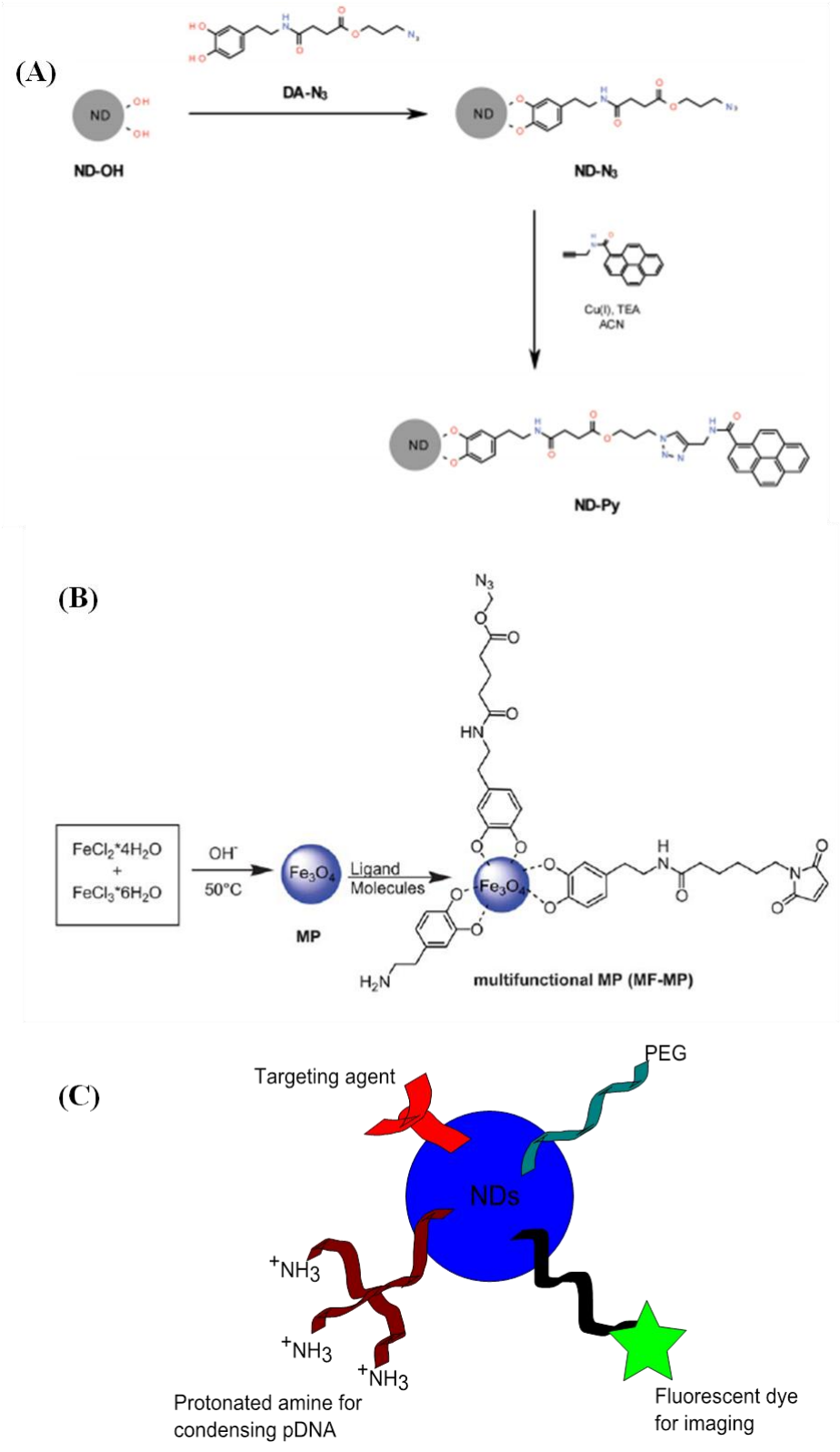

Figure 5.4. Direct functionalization of NDs using azide terminated dopamine derivative followed by 'click' reaction (A) [43], Dopamine derivatives-derived multifunctional MPs (B)

[44] and Schematic representation of novel NDs surface functionalization strategy to improve the stability and transfection efficiency (C) which could be achieved through dopamine derivatives.

In this thesis, the concept of the formation of multifunctional particles using different dopamine ligands will be utilized for NDs. In a proof of principle, amine terminated ligands will be 'clicked' to such nanostructures and used as gene nanocarrier for cellular transfection. This could be achieved by designing the multifunctional NDs as demonstrated in **Figure 5.4C**.

5.6. References

1. Gupta, A., et al., *Radiotherapy supports protective tumor-specific immunity.* Oncoimmunology, 2012. **1**(9): p. 1610-1611.
2. Chang, H.J., et al., *Hypofractionated radiotherapy for primary or secondary oligometastatic lung cancer using Tomotherapy.* Radiat Oncol, 2012. **7**: p. 222.
3. Henson, K.E., et al., *Radiation-related mortality from heart disease and lung cancer more than 20 years after radiotherapy for breast cancer.* Br J Cancer, 2013. **108**(1): p. 179-82.
4. Gill, S. and M. Kalos, *T cell-based gene therapy of cancer.* Transl Res, 2013. **161**(4): p. 365-79.
5. Song, H., et al., *Suppression of hepatocarcinoma model in vitro and in vivo by ECRG2 delivery using adenoviral vector.* Cancer Gene Ther, 2012. **19**(12): p. 875-9.
6. Mannell, H., et al., *Site directed vascular gene delivery in vivo by ultrasonic destruction of magnetic nanoparticle coated microbubbles.* Nanomedicine, 2012. **8**(8): p. 1309-18.
7. Iwashita, S., et al., *Polyamidoamine dendron-bearing lipid assemblies: their morphologies and gene transfection ability.* J Biomater Appl, 2012. **27**(4): p. 445-56.
8. Deng, Z.J., et al., *Layer-by-layer nanoparticles for systemic codelivery of an anticancer drug and siRNA for potential triple-negative breast cancer treatment.* ACS Nano, 2013. **7**(11): p. 9571-84.
9. Walther, W. and U. Stein, *Viral vectors for gene transfer: a review of their use in the treatment of human diseases.* Drugs, 2000. **60**(2): p. 249-71.
10. Al-Dosari, M.S. and X. Gao, *Nonviral gene delivery: principle, limitations, and recent progress.* AAPS J, 2009. **11**(4): p. 671-81.
11. Sirsi, S.R. and M.A. Borden, *Advances in ultrasound mediated gene therapy using microbubble contrast agents.* Theranostics, 2012. **2**(12): p. 1208-22.
12. Orio, J., et al., *Electric field orientation for gene delivery using high-voltage and low-voltage pulses.* J Membr Biol, 2012. **245**(10): p. 661-6.
13. Villemejane, J. and L.M. Mir, *Physical methods of nucleic acid transfer: general concepts and applications.* Br J Pharmacol, 2009. **157**(2): p. 207-19.
14. Vu, L., et al., *Generation of a focused poly(amino ether) library: polymer-mediated transgene delivery and gold-nanorod based theranostic systems.* Theranostics, 2012. **2**(12): p. 1160-73.

15. Khosravi-Darani, K., et al., *Calcium based non-viral gene delivery: an overview of methodology and applications.* Acta Med Iran, 2010. **48**(3): p. 133-41.
16. Jin, L., et al., *Current progress in gene delivery technology based on chemical methods and nano-carriers.* Theranostics, 2014. **4**(3): p. 240-55.
17. Medina-Kauwe, L.K., J. Xie, and S. Hamm-Alvarez, *Intracellular trafficking of nonviral vectors.* Gene Ther, 2005. **12**(24): p. 1734-51.
18. Li, W., F. Nicol, and F.C. Szoka, Jr., *GALA: a designed synthetic pH-responsive amphipathic peptide with applications in drug and gene delivery.* Adv Drug Deliv Rev, 2004. **56**(7): p. 967-85.
19. Xu, Y. and F.C. Szoka, Jr., *Mechanism of DNA release from cationic liposome/DNA complexes used in cell transfection.* Biochemistry, 1996. **35**(18): p. 5616-23.
20. Akinc, A., et al., *Exploring polyethylenimine-mediated DNA transfection and the proton sponge hypothesis.* J Gene Med, 2005. **7**(5): p. 657-63.
21. Sonawane, N.D., F.C. Szoka, Jr., and A.S. Verkman, *Chloride accumulation and swelling in endosomes enhances DNA transfer by polyamine-DNA polyplexes.* J Biol Chem, 2003. **278**(45): p. 44826-31.
22. Bastos, R., N. Pante, and B. Burke, *Nuclear pore complex proteins.* Int Rev Cytol, 1995. **162B**: p. 257-302.
23. Chen, H.H., et al., *Quantitative comparison of intracellular unpacking kinetics of polyplexes by a model constructed from quantum dot-FRET.* Mol Ther, 2008. **16**(2): p. 324-32.
24. Nitta, S.K. and K. Numata, *Biopolymer-based nanoparticles for drug/gene delivery and tissue engineering.* Int J Mol Sci, 2013. **14**(1): p. 1629-54.
25. Cai, X., S. Conley, and M. Naash, *Nanoparticle applications in ocular gene therapy.* Vision Res, 2008. **48**(3): p. 319-24.
26. Peng, X.H., et al., *Targeted magnetic iron oxide nanoparticles for tumor imaging and therapy.* Int J Nanomedicine, 2008. **3**(3): p. 311-21.
27. Zhu, Y., et al., *The biocompatibility of nanodiamonds and their application in drug delivery systems.* Theranostics, 2012. **2**(3): p. 302-12.
28. Liu, K.K., et al., *Endocytic carboxylated nanodiamond for the labeling and tracking of cell division and differentiation in cancer and stem cells.* Biomaterials, 2009. **30**(26): p. 4249-59.
29. Schrand, A.M., et al., *Are diamond nanoparticles cytotoxic?* J Phys Chem B, 2007. **111**(1): p. 2-7.
30. Vaijayanthimala, V. and H.C. Chang, *Functionalized fluorescent nanodiamonds for biomedical applications.* Nanomedicine (Lond), 2009. **4**(1): p. 47-55.
31. Zhang, X.Q., et al., *Polymer-functionalized nanodiamond platforms as vehicles for gene delivery.* ACS Nano, 2009. **3**(9): p. 2609-16.
32. Martin, R., et al., *Fenton-treated functionalized diamond nanoparticles as gene delivery system.* ACS Nano, 2010. **4**(1): p. 65-74.
33. Liu, K.K., et al., *Covalent linkage of nanodiamond-paclitaxel for drug delivery and cancer therapy.* Nanotechnology, 2010. **21**(31): p. 315106.
34. Guan, B., F. Zou, and J. Zhi, *Nanodiamond as the pH-responsive vehicle for an anticancer drug.* Small, 2010. **6**(14): p. 1514-9.
35. Alhaddad, A., et al., *Nanodiamond as a vector for siRNA delivery to Ewing sarcoma cells.* Small, 2011. **7**(21): p. 3087-95.
36. Yang, K., et al., *In vivo pharmacokinetics, long-term biodistribution, and toxicology of PEGylated graphene in mice.* ACS Nano, 2011. **5**(1): p. 516-22.

37. M. Chen, X.Q.Z., H. B. Man, R. Lam, E. K. Chow, D. Ho,, *Nanodiamond Vectors Functionalized with Polyethylenimine for siRNA Delivery.* J. Phys. Chem. Lett., 2010. **1**: p. 3167–3171.
38. Haensler, J. and F.C. Szoka, Jr., *Polyamidoamine cascade polymers mediate efficient transfection of cells in culture.* Bioconjug Chem, 1993. **4**(5): p. 372-9.
39. Pack, D.W., et al., *Design and development of polymers for gene delivery.* Nat Rev Drug Discov, 2005. **4**(7): p. 581-93.
40. Stekar, J.N., G.; Kutscher, B.; Engel, J.; Hilgard, P., *Synthesis, Antitumor Activity, and Tolerability of Phospholipids Containing Nitrogen Homologues.* Angewandte Chemie International Edition in English, 1995. **34**(2): p. 238-240.
41. Takimoto, T., et al., *Preparation of Fluorescent Diamond Nanoparticles Stably Dispersed under a Physiological Environment through Multistep Organic Transformations.* Chemistry of Materials, 2010. **22**(11): p. 3462-3471.
42. Zhang, X., et al., *PolyPEGylated nanodiamond for intracellular delivery of a chemotherapeutic drug.* Polymer Chemistry, 2012. **3**(10): p. 2716.
43. Barras, A., et al., *Direct functionalization of nanodiamond particles using dopamine derivatives.* Langmuir, 2011. **27**(20): p. 12451-7.
44. Mazur, M., et al., *Iron oxide magnetic nanoparticles with versatile surface functions based on dopamine anchors.* Nanoscale, 2013. **5**(7): p. 2692-702.

CHAPTER 6

Orthogonal surface modification strategy of nanodiamonds using dopamine anchors for gene delivery

Nanodiamonds (NDs) have currently been investigated extensively for the biomedical applications due to their excellent physicochemical properties, biocompatibility and inexpensive large scale synthesis [1, 2]. Moreover, a wide variety of studies examining the behavior of NDs in *in vitro* and *in vivo* have concluded that the particles are highly biocompatible and are less toxic in comparison to other carbon-based nanomaterials like carbon nanotubes, fullerenes, etc [3-7]. As such, nanodiamonds have been assessed for their ability to delivery drugs [8-10], genes [11-14] and to interfere with hepatitis C virus infection [15], and *E.coli* film formation [16]. However, the successful application of NDs in biology and biomedicine critically depend on the formation of stable aqueous nanodiamond colloidal suspensions [17]. As NDs have the tendency to aggregate [17] and thus to precipitate under physiological conditions [18], appropriate surface modification is required to form stable hydrosols of NDs. The introduction of polyethylene glycol (PEG) units onto the NDs surface has shown to make the nanoparticles surface not only hydrophilic and thus highly water dispersible but decreased in addition protein opsonization and subsequent phagocytosis by the mononuclear phagocytic system [18, 19].

To overcome the stability issue of NDs, in this work we have shown an easy and versatile surface functionalization strategy allowing introduction of different funtional ligands onto NDs with the aim of rendering the particles water dispersible over a wide concentration range and time frame while at the same time enabling ligands to be chemically linked to the particles surface. The orthogonal surface modification strategy is based on the use of different dopamine anchors (**Figure 6.2**), one bearing PEG units (dop-PEG), the other an azide function (dop-N_3). Dopamine is known to have strong interactions with different metal oxides [20-23], graphene [24, 25] and NDs [26]. The interest in using dopamine as moiety is the ease of its functional groups like azide and others can be introduced *via* amine functional group of dopamine. This also limits its self-polymerization process forming polydopamine at weak alkaline pH.

However, for most biological applications stable colloidal solution is not enough. Therapeutics/diagnostics vectors or target ligands need to be in addition available on the surface of NDs. We thus investigated if different dopamine ligands can be integrated onto the surface of NDs simultaneously (**Figure 6.3A**). In a proof of principle that post-synthetic modification can be performed on these multifunctional NDs, "click" chemistry between the azide group on the particles and an alkynyl-terminated aminated ligands was performed. The potential of these particles for use as carriers for genetic materials is in addition investigated.

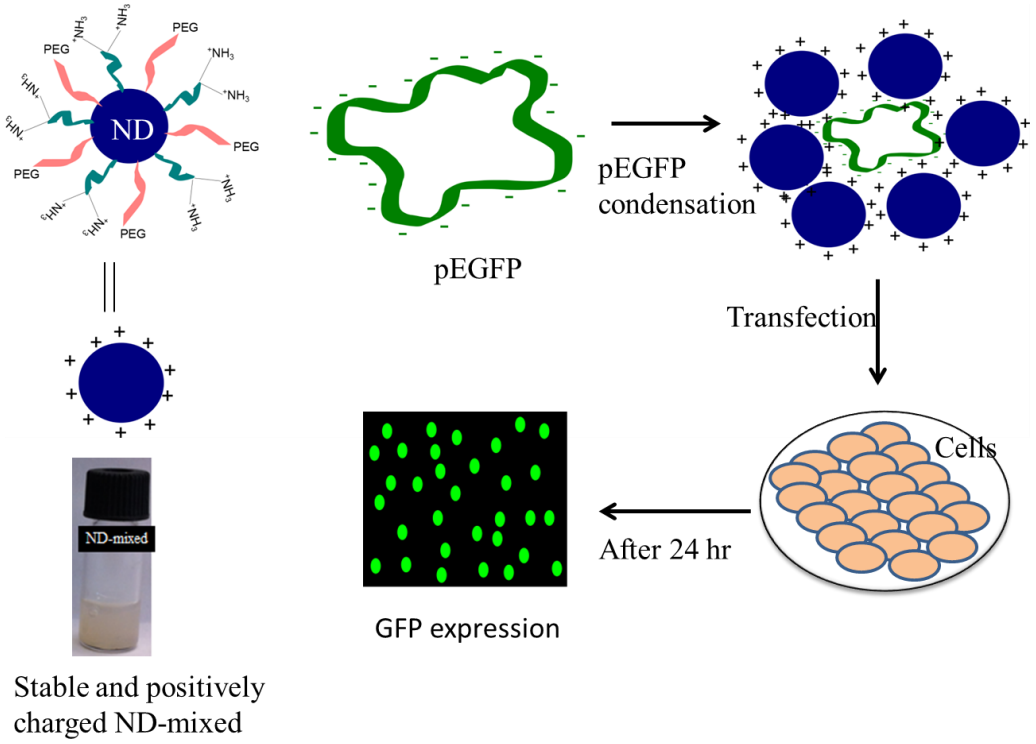

Figure 6.1. Schematic depiction of gene delivery using nanostructures.

The integration of positively charged amine groups can be beneficial for the integration of plamid DNA (**Figure 6.1**) Generally, wide varieties of amine terminated NPs have been studied as gene carrier [12, 27] due to the fact that the protonated amine groups can condense genetic material gently and also these amine groups can play role for the endosomal escape by absorbing protons which further slow down the acidification process important for the endosome-lysozome transition [28]. **Figure 6.1** has highlighted the general concept of this work. Here, first the formation and stability of dopamine-derived multifunctional NDs will be discussed which will be followed by the cellular transfection ability of thus formed NDs. As a

control, we have used 3-aminopropyltrimethoxysilane (APTMS) and dopamine modified NDs.

6.1. Anchoring of different dopamine ligands onto NDs

The dopamine ligands prepared to be grafted onto hydroxylated nanodiamonds are shown in **Figure 6.2**. Azide modified dopamine (dop-N_3) was formed through reaction of azido-heptyl succinimic acid with the amide groups of dopamine through the formation of an amide bond. Polyethyelne glycol modified dopamine (dop-PEG) was synthesized in a multiple steps reaction from 2-[2-(2-chloroethoxy)ethoxy]ethanol.

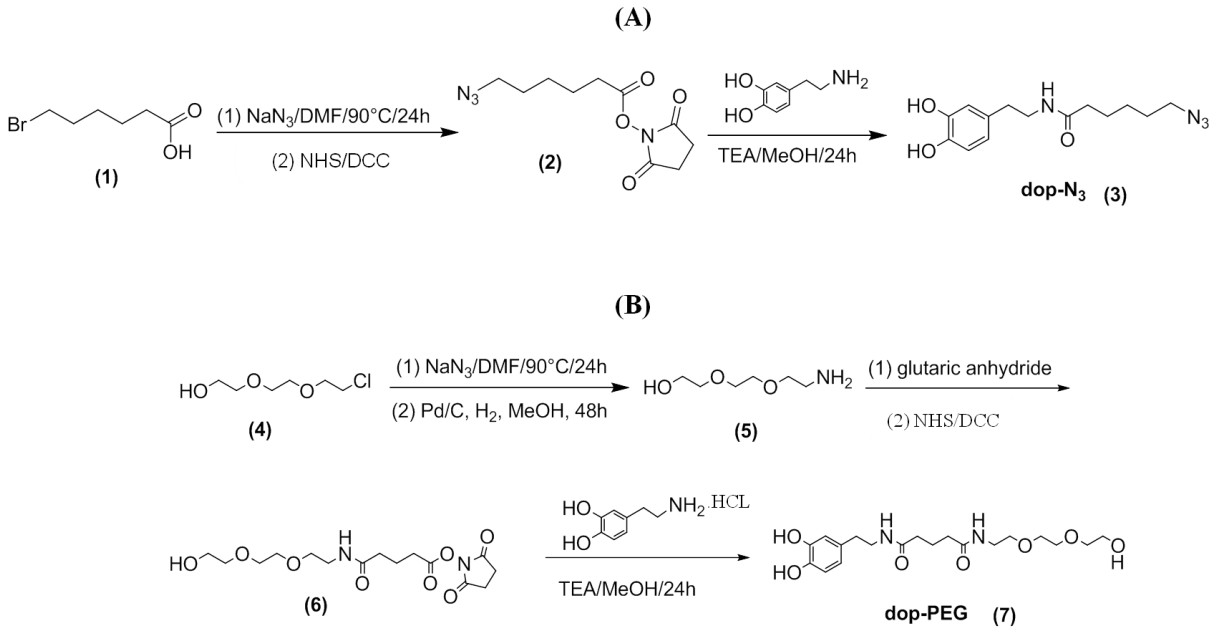

Figure 6.2. Synthetic route to (A) azide-modified dopamine (dop-N_3) and (B) polyethylene glycol-modified dopamine (dop-PEG).

These dopamine ligands were used for the modification of hydroxylated nanodiamonds (ND-OH). Sonication of a suspension of ND-OH particles in dry acetonitrile with solutions of dop-N_3 or dop-PEG or a mixture of dop-N_3 and dop-PEG (1/1) at room temperature for several hours resulted in dopamine modified particles (**Figure 6.2A**). The physcio-chemical characteristics of the different particles are listed in **Table 6.1**.

Table 6.1. Physcio-chemical properties of dopamine modified NDs

Sample	[a]d_H nm	PI[b]	Zeta potential mV	C1s	O1s	N1s
ND-OH	79 ± 13	0.246±0.002	35 ± 1.6	88.4	10.1	1.5
ND-dop-PEG	106 ±12	0.246±0.004	36 ± 0.9	84.5	11.2	4.3
ND-dop-N_3	150 ± 7	0.324±0.003	28 ± 0.5	84.4	8.3	7.3
ND-dop-PEG+N_3	120 ± 19	0.358±0.012	30 ± 0.1	84.5	9.7	5.8

[a]Hydrodynamic diameter, [b] Polydispersity index

The successful integration of the dopamine ligands onto NDs can be evaluated from the increase in the atomic percentage of the N1s component as determined by XPS. The ND-OH particles show some nitrogen presence of 1.5 at % most likely generated during the detonation process where trinitrotoluene is used. The nitrogen component can be deconvoluated into bands a 399.2 and 402.75 eV assigned to C-N and N-O linkages (**Figue 6.3B**).

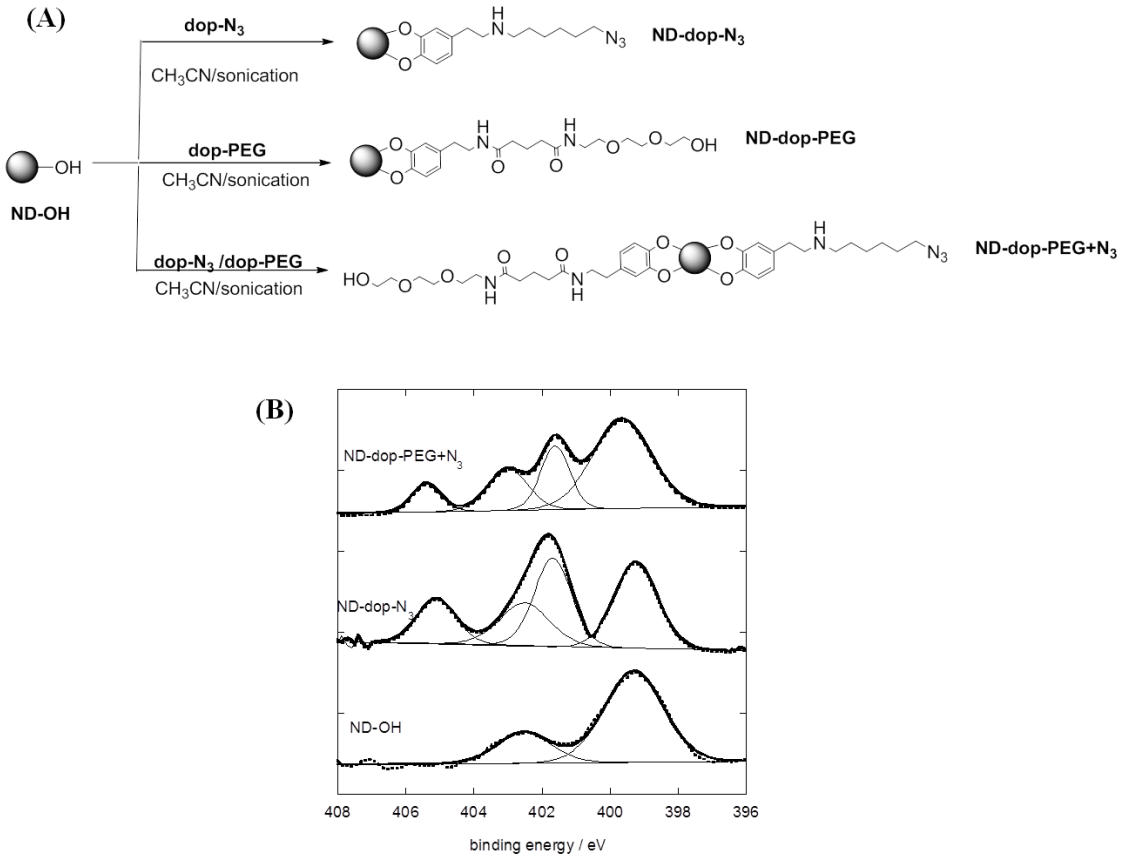

Figure 6.3. (A) Dopamine modified nanodiamonds using dop-N3 and dop-PEG as ligands, (B) N1s high resolution XPS Characterization of ND-OH and ND-dop-N_3

Integration of dop-N_3 onto the particles results in an increase of the atomic percentage of N1s to 7.3 at%. The presence of the N_3 band could be in addition conformed by XPS analysis. **Figure 6.3B** displays characteristic bands for the -N_3 group at 405.2 (-N=$\underline{N}^+$=N^-) and 401.9 eV (-$\underline{N}$=N^+=$\underline{N}^-$) together with the band at 402.7 and 399.2 for N-O and C-N from the diamond itself. However, the stability of ND-dop-N_3 in aqueous solution over time is limited as seen in **Figure 6.4**. The particle sized increased from the initial 150 nm to around 600 nm in the short time span of 3h (**Figure 6.4B**). This limits the particles for further use in biological assays.

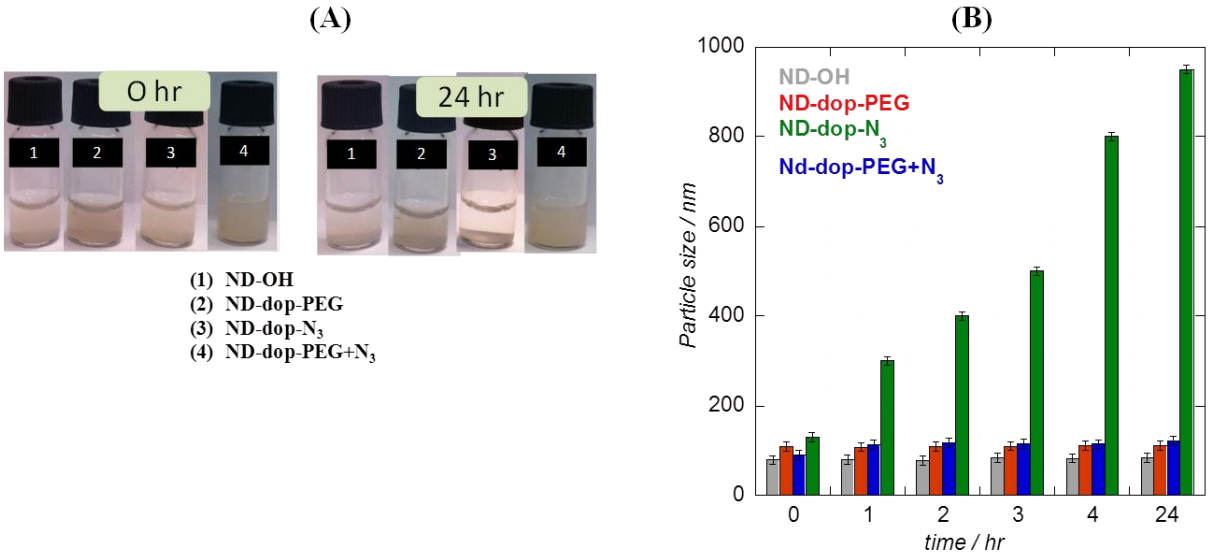

Figure 6.4. (A) Photographs of different NDs solutions over time, (B) Stability of the formed nanostructures over time in aqueous medium.

Polyethylene glycol (PEG) is indeed a class of hydrophilic polymers with excellent water solubility and biocompatibility widely used to render nanostructures water dispersable [19]. The conjugation of pegylated dopamine linker (dop-PEG) onto the diamond particles is expected to render dispersion in aqueous medium and to reduce the uptake of the nanoparticles by the mononuclear phagocytic system [12]. As expected, integration of dop-PEG onto ND (**Figure 6.3A**) improves the stability of ND in water. As can be observed in **Figure 6.4,** the size of ND-dop-PEG remained unchanged over a day. The enhanced dispersity and stability of ND-dop-PEG is likely due to the hydrophilic PEG chains anchored to the ND surface. Most biomedical applications rely however not only on highly dispersable particles, but need the integration of specific targets and vectors onto its surface. In a proof of

principle experiment the water soluble and functional NDs can be obtained using different dopamine ligands, NDs were modified simultaneously with dop-PEG and dop-N_3 by mixing NDs with a 1/1 ratio of the respective dopamine ligand (**Figure 6.3A**). The stability of the resulting ND-dop-PEP+N_3 particles is comparable to those of ND-dop-PEG alone (**Figure 6.4**). The integration of the azid function onto the PEGylated NDs was validated by the presence of the peak at 405.2 (-N=$\underline{N}^+$=N$^-$) and 401.9 eV (-$\underline{N}$=N$^+$=$\underline{N}^-$) (**Figure 6.3B**). The atomic percentage of N1s on the particles was lower than on only dop-N_3 modified NDs but higher than on ND-dop-PEG, pointing clearly towards an integration of both dopamine ligands onto the NDs surface (**Table 6.2**).

6.2. Subsequent post-fuctionalization of ND-dop-PEG+N_3 particles

For a particulier application, surface-modification steps on the nanoparticles are normally required. Therefore, to be functional for different biomedical applications, the ND-dop-PEG+N_3 particles need to sustain a further reaction. In a proof of principle that the azide functions can be used in 'click' chemistry related reactions, a propargly-terminated branched amide structures was interacted with the particles (**Figure 6.5A**). The success of the 'click' reaction was evidenced by the drastic increase in the atomic percentage of the N1s component (**Table 6.2**). The success of the 'click' reaction is further followed by FT-IR.

Table 6.2. Physcio-chemical properties of aminated NDs.

Sample	[a]d_H nm	PI[a]	Zeta potential mV	C1s	O1s	N1s
ND-dop-PEG+$(NH_2)_2$	130 ± 19	0.357±0.012	39 ± 0.1	75.5	9.2	15.3
ND-NH_2	137 ± 7	0.357 ± 0.02	23 ± 1.1	87.4	10.3	2.3
ND-dopamine	130±2	0.2±0.09	39±1.32	87.5	10.5	2.0
ND-sil-NH_2	190 ±17	0.402±0.019	37 ±1.1	87.2	10.3	2.5

[a]Hydrodynamic diameter, [b] Polydispersity index

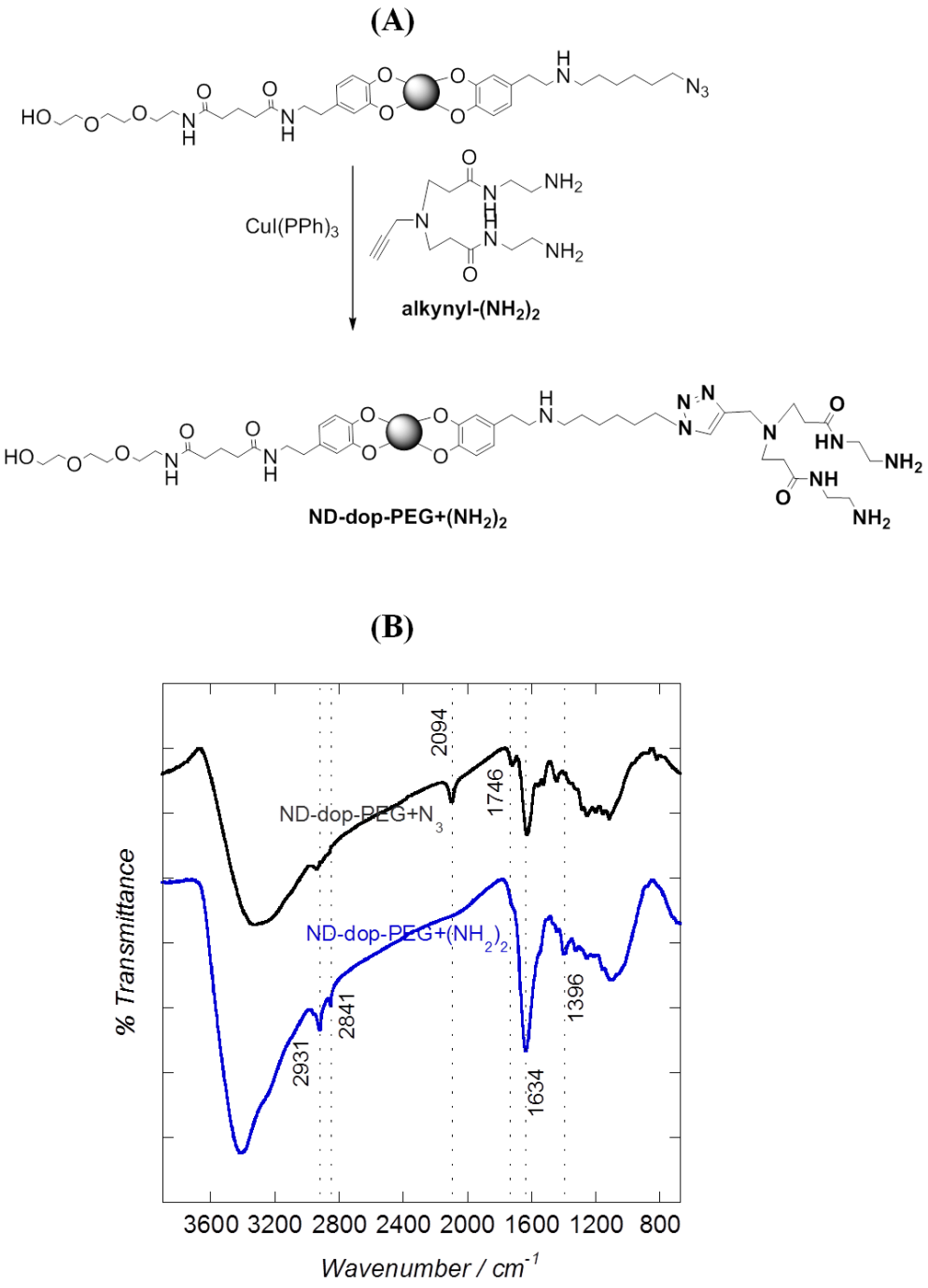

Figure 6.5. (A) Post functionalization of ND-dop-PEG+N_3. Alkynyl-terminated amine ligand was 'clicked' utilizing 'click' chemistry and (B) FT IR of ND-dop-PEG+N_3 (a) before (black) and after 'click' reaction (blue)

An identical band at 2094 cm^{-1} corresponds to the $\nu_{as(N3)}$ which is observed in ND-dop-PEG+N_3 and is the prove that azide group is integrated on NDs (**Figure 6.5B**). A board band at 3447 cm^{-1} assigned to the stretching mode of unreacted surface hydroxyl group or could be

more because of adsorbed water molecules. Presence of band at 1746 cm^{-1} which corresponds to C=O in azide terminated NDs confirms the formation of an ester linkage. After integrating alkynyl-$(NH_2)_2$, on ND-dop-PEG/N_3, the disappearance of the azide band at 2094 cm^{-1} was observed that confirms the success of the 'click' reaction on the dopamine-derivatives modified NDs (**Figure 6.5B**). However, the FT-IR is dominated by two peaks at 3421 and 1634 cm^{-1}. The broad band between 3000 and 3600 cm^{-1} can be assigned to the vibration of surface amino groups or/and adsorbed water molecules, while the peak at 1625 cm^{-1} is most likely due to a superposition of N-H scissoring mode and OH deformation mode of adsorbed water. Similar vibration modes were reported for amine-terminated ND particles prepared from hydroxyl-terminated ND particles functionalized with 3 aminopropyltrimethoxysilane [11]. The amount of nitrogen integrated is much higher than on commercial available ND-NH_2 (**Table 6.2**). The stability of the "clicked" probe remains unchanged (**Figure 6.4B**) making such particles interesting vectors for gene delivery.

6.3. ND-dop-PEG-$(NH_2)_2$ based DNA delivery

Encouraged by the previous results showing that fairly stable highly aminated diamond nanoparticles can be formed, we investigated the usefulness of such structures for the delivery of genes. The current reported strategies on the use of NDs as gene vectors are based on the coating of NDs with polyethyleneimine (PEI), a polycationic polymer considered as one of the most effective vectors among the synthetic polycations [11-13]. The positively charged groups available on the PEI coated NDs can bind negatively charged DNA binding through electrostatic interactions and facilitates cellular uptake [29, 30]. Conversely, the high positive charge density of PEI makes the particles moderately toxic [31], limiting currently its use as a gene delivery vector *in vivo*. One way to overcome the undesirable side effects of PEI is to take advantage of the the ND-dop-PEG-$(NH_2)_2$ particles discusses previously. For comparison, commercial available aminated diamonds (ND-NH_2) and ND-OH modified in a silanization reaction with 3-aminopropyltrimethoxysilane (ND-sil-NH_2) were used (**Figure 6.6**). The corresponding physico-chemical properties of these vectors are listed in **Table 6.2**.

6.3.1. Loading of plasmid DNA (pDNA) onto nanodiamonds

An important step for any NPs-based gene delivery is the proper condensation of pDNA to the cationic nanoparticles. Before DNA binding, all of the 4 investigated NDs (**Figure 6.6A**) show positive surface potentials at neutral pH (**Figure 6.6B** and **Table 6.2**), with ND-dop-PEG+$(NH_2)_2$ being highly positively charged. Positively charged NDs are able to form complexes with (pDNA) *via* electrostatic interaction, and this interaction exhibits a typical weight ratio-dependent relationship.

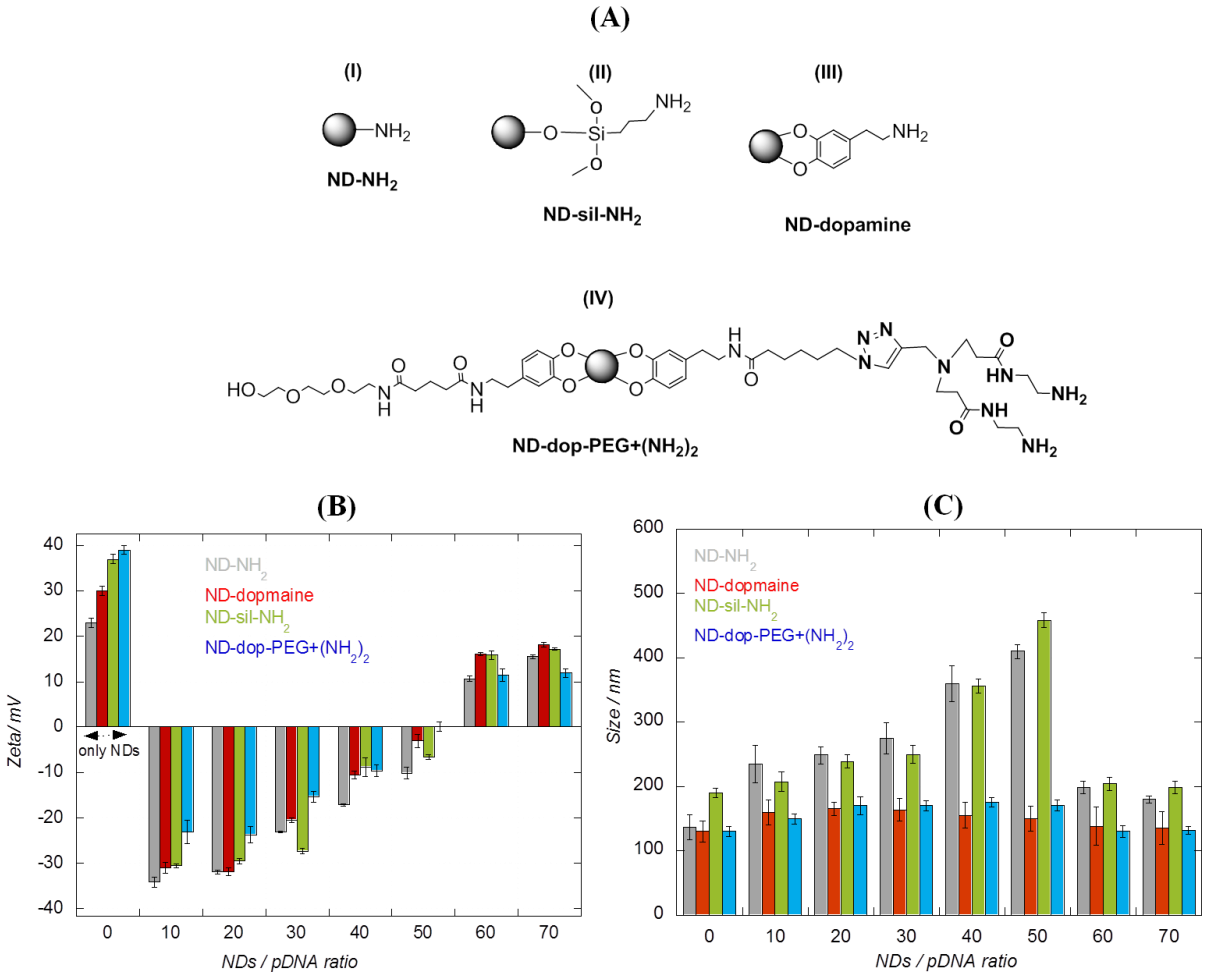

Figure 6.6 (A) Structures of NDs used in gene delivery experiements, (B) Zeta potential and (C) size measurements of NDs/pDNA complexes in aqueous solutions (1 mL); 1 µg of pDNA was incubated with increasing amounts of NDs in water for 30 min at room temperature.

As shown in the result aggregation occurred at a weight ratio of 10-60 for all modified NDs and commercial ND-NH_2 (**Figure 6.6B**), which is likely due to the fact that protonated

amine grafted NDs have nearly neutral surfaces at weight ratio close to 60 (**Figure 6.5A**). As weight ratio increased, the particle sizes of all NDs complexes decreased to a plateau of about 120-200 nm. As expected, the net surface charge of modified NDs increased from negative to positive as the weight ratio increased, and their ζ-potentials reached to constant charge of about 11-15 mV at or above weight ratio 60. All NDs had shown an equal interaction with pDNA. After pDNA binding, the occurrence of severe aggregation was delayed to weight ratio around 40, and particle sizes reached to a constant value of about 120-200 nm up to weight ratios as high as 70. positively charged NDs/pDNA complexes could facilitate their endocytosis since a positive surface charge is essential not only for DNA binding *via* electrostatic interactions, but also for the cellular uptake [32]. Thus, an appropriate weight ratio for the efficient transfection could be around 60 or higher. Since, the size and surface charge are almost similar between 60 and 70; we have chosen to work with weight ratio of 60:1 (NDs/pDNA).

The binding efficiency of the different NDs with pDNA was further confirmed with agarose gel retardation assay (**Figure 6.7**) for the weight ratio of 60:1, before performing transfection experiment.

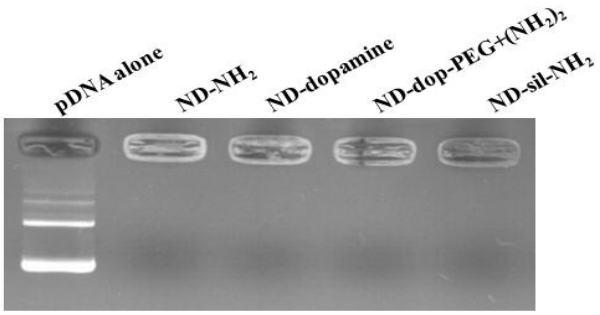

Figure 6.7. Agarose gel electrophoresis; gel retardation assay of NDs/pDNA complexes at weight ratio of 60:1. pDNA (0.5 µg) alone without any NDs was taken as negative control.

Complete retardation of 0.5 µg of pDNA was observed at the weight ratio of 60:1, suggesting that pDNA was bound tightly and completely with all studied amine-terminated NDs for a weight ratio of 60. The results indicated a nearly complete neutralization of the negative charge of pDNA and further validate the result of zeta potential of all NDs that the ratio 60:1 can condense all pDNA.

6.3.2. Effect of amine-terminated NDs on cell viability

Effect of nanovehicles on cell viability can affect the transfection efficiency. Due to the high cationic density and membrane destabilization, it is well-known that high molecular weight (MW) polyethylenimine (PEIs) show high toxicity [33] whereas low MW PEIs are almost non-toxic to cells [34] Therefore, it is of primary importance for designing cationic NDs that enhance the transfection efficiency, while reducing the cytotoxicity. In this study, the cytotoxicity of NDs/pDNA complexes was studied on Human Embryonic Kidney (HEK) cells.

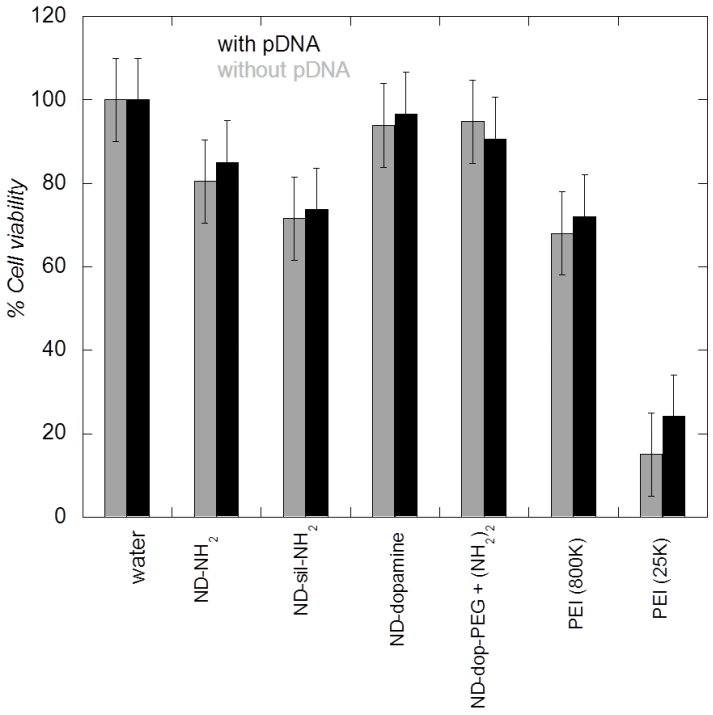

Figure 6.8. Result of HEK cell viability assay of NDs/pDNA (with and without pDNA) complexes at ratio of 60:1. Cells were incubated with NDs (without or with pDNA) for 4 hours and then the complexes were washed off and replaced with complete cell culture medium and the MTT assay was performed after 24 hours.

The *in vitro* cytotoxicity of the different ND carriers was evaluated on Human embryonic kidney (HEK) 293 cells and compared to polyethyleneimine (PEI25kDa and PEI 800 kDa). All ND/DNA complexes exhibit good biocompatibility (**Figure 6.8**). With a weight ratio of 60, which corresponds to 60 µg/mL NDs no significant cytotoxicity was observed for the dopamine modified nanostructures, while about 80 % and 70 % of cells survived when incubated with ND-NH_2 and ND-sil-NH_2 which could arise from the aggregation tendency of

these particles and this might further affect on the transfection efficiency despite their ability to condense pDNA. This is comparable to complexes of polyethyleneimine (PEI 800 kDa) with pDNA (weight ratio 30, zeta potential 35 mV). However, less than 30% of cells were viable when incubated with lower molecular weighted PEI25kDa (weight ratio 10, zeta potential 33 mV). Similar finding were reported by Zhang et al [11]. It is worthwhile to note that presence of pDNA has helped to improve the cell viability in some cases though differences are not significant.

6.3.3. Cellular transfection

Transfection studies were performed using the reporter gene (green fluorescent protein pDNA, pEGFP-N1 pDNA). NDs/ pDNA complexes were prepared by mixing a constant amount (1 µg) of plasmid DNA with 60 µg of various modified NDs. The level of transfection of these complexes and free pDNA was examined on HEK cell lines. After incubation of HEK cells with NDs/pDNA complexes at weight ratios of 60:1 for 4 h, the expression of green fluorescent proteins (GFPs) of transfected cells was observed by confocal microscopy (**Figure 6.9**).

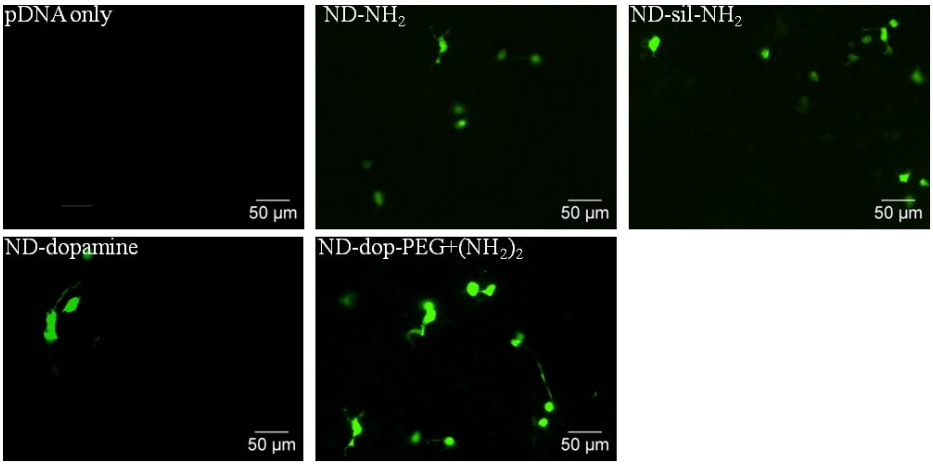

Figure 6.9. Confocal images (20x) of the *in vitro* transfected cells using NDs/pDNA and pDNA alone. Images were captured after 24 hour of transfection.

Confocal images have confirmed that in the presence of amine-terminated NDs, cellular transfection is possible though numbers of transfected cells are not high in none of the cases as expected. However, it is clear from the images that the level of transfection is found to be higher in the multifunctional pegylated NDs (ND-dop-PEG+$(NH_2)_2$) than compared to

other tested NDs. The stability due to the PEG could facilitate the endocytosis and furthermore, more numbers of amine groups compare to other tested NDs (**Table 6.**2) might have played role for the endosomal escape because of better buffering capacity. However, this has to be verified in future. The low transfection level in case of ND-NH_2 and ND-sil-NH_2 might be due to the fact that either they tend to aggregate resulting bigger particles which could have problem for endocytosis or due to their toxicity observed (**Figure 6.8**) in the tested weight ratio than compare to other particles. The level of transfection is also affected by the nuclease enzyme, thus protection of pDNA from deoxyribonuclease is also important. An additional experiment is still required to prove the protection of pDNA from nuclease.

Though it is clear that NDs used in this work are capable of transfection, the quantification of transfected cells (flow cytometry) is required to have the clear picture of the level of transfection.

6.4. Conclusion

We have successfully developed the new facile way for the preparation of stable multifunctional NDs to overcome the aggregation problem that has been faced by researchers working on detonated nanodiamonds. The method is based on the orthogonal surface modification strategy of NDs using various dopamine-derived anchors. This dopamine-derived method opens up different possibilities to graft desirable bioconjugates for various applications. The superior stability of ND-dop-PEG+$(NH_2)_2$ is believed to be because of PEG. The amine terminated NDs were further investigated for their cellular transfection ability. The confocal images have shown the GFP expressed cells proving that this stable ND-dop-PEG+$(NH_2)_2$ are better for cellular transfection than compared to other tested NDs. However, detail studies are required to track the endocytosis, protection from nuclease and quantification of transfected cells.

6.5. References

1. Krueger, A., *New carbon materials: biological applications of functionalized nanodiamond materials.* Chemistry, 2008. **14**(5): p. 1382-90.
2. Mochalin, V.N., et al., *The properties and applications of nanodiamonds.* Nat Nanotechnol, 2012. **7**(1): p. 11-23.

3. Marcon, L., Riquet, F., Vicogne, D., Szunerits, S., Bodart, J-F., Boukherroub R., *Cellular and in vivo toxicity of functionalized nanodiamond in Xenopus embryos.* J. Mat. Chem. , 2010. **20**: p. 8064-8069.
4. Yu, S.J., et al., *Bright fluorescent nanodiamonds: no photobleaching and low cytotoxicity.* J Am Chem Soc, 2005. **127**(50): p. 17604-5.
5. Huang, H., et al., *Active nanodiamond hydrogels for chemotherapeutic delivery.* Nano Lett, 2007. **7**(11): p. 3305-14.
6. Schrand, A.M., et al., *Are diamond nanoparticles cytotoxic?* J Phys Chem B, 2007. **111**(1): p. 2-7.
7. Zhu, Y., et al., *The biocompatibility of nanodiamonds and their application in drug delivery systems.* Theranostics, 2012. **2**(3): p. 302-12.
8. Chen, M., et al., *Nanodiamond-mediated delivery of water-insoluble therapeutics.* ACS Nano, 2009. **3**(7): p. 2016-22.
9. Shimkunas, R.A., et al., *Nanodiamond-insulin complexes as pH-dependent protein delivery vehicles.* Biomaterials, 2009. **30**(29): p. 5720-8.
10. Smith, A.H., et al., *Triggered release of therapeutic antibodies from nanodiamond complexes.* Nanoscale, 2011. **3**(7): p. 2844-8.
11. Zhang, X.Q., et al., *Polymer-functionalized nanodiamond platforms as vehicles for gene delivery.* ACS Nano, 2009. **3**(9): p. 2609-16.
12. Zhang, P., et al., *Cationic polymer brush grafted-nanodiamond via atom transfer radical polymerization for enhanced gene delivery and bioimaging.* Journal of Materials Chemistry, 2011. **21**(21): p. 7755.
13. Martin, R., et al., *Fenton-treated functionalized diamond nanoparticles as gene delivery system.* ACS Nano, 2010. **4**(1): p. 65-74.
14. Kaur, R., et al., *Lysine-functionalized nanodiamonds: synthesis, physiochemical characterization, and nucleic acid binding studies.* Int J Nanomedicine, 2012. **7**: p. 3851-66.
15. Khanal, M., et al., *Phenylboronic-acid-modified nanoparticles: potential antiviral therapeutics.* ACS Appl Mater Interfaces, 2013. **5**(23): p. 12488-98.
16. Barras, A., et al., *Glycan-functionalized diamond nanoparticles as potent E. coli anti-adhesives.* Nanoscale, 2013. **5**(6): p. 2307-16.
17. Pentecost, A., et al., *Deaggregation of nanodiamond powders using salt- and sugar-assisted milling.* ACS Appl Mater Interfaces, 2010. **2**(11): p. 3289-94.
18. Takimoto, T., et al., *Preparation of Fluorescent Diamond Nanoparticles Stably Dispersed under a Physiological Environment through Multistep Organic Transformations.* Chemistry of Materials, 2010. **22**(11): p. 3462-3471.
19. Zhang, X., et al., *PolyPEGylated nanodiamond for intracellular delivery of a chemotherapeutic drug.* Polymer Chemistry, 2012. **3**(10): p. 2716.
20. Lee, H., et al., *Mussel-inspired surface chemistry for multifunctional coatings.* Science, 2007. **318**(5849): p. 426-30.
21. Mazur, M., et al., *Iron oxide magnetic nanoparticles with versatile surface functions based on dopamine anchors.* Nanoscale, 2013. **5**(7): p. 2692-702.
22. Spadavecchia, J., et al., *Approach for plasmonic based DNA sensing: amplification of the wavelength shift and simultaneous detection of the plasmon modes of gold nanostructures.* Anal Chem, 2013. **85**(6): p. 3288-96.
23. Turcheniuk, K., et al., *Recent advances in surface chemistry strategies for the fabrication of functional iron oxide based magnetic nanoparticles.* Nanoscale, 2013. **5**(22): p. 10729-52.

24. Kaminska, I., et al., *Reduction and functionalization of graphene oxide sheets using biomimetic dopamine derivatives in one step.* ACS Appl Mater Interfaces, 2012. **4**(2): p. 1016-20.
25. Kaminska, I., et al., *Preparation of a responsive carbohydrate-coated biointerface based on graphene/azido-terminated tetrathiafulvalene nanohybrid material.* ACS Appl Mater Interfaces, 2012. **4**(10): p. 5386-93.
26. Barras, A., et al., *Direct functionalization of nanodiamond particles using dopamine derivatives.* Langmuir, 2011. **27**(20): p. 12451-7.
27. Skandrani, N., et al., *Lipid nanocapsules functionalized with polyethyleneimine for plasmid DNA and drug co-delivery and cell imaging.* Nanoscale, 2014. **6**(13): p. 7379-90.
28. Sonawane, N.D., F.C. Szoka, Jr., and A.S. Verkman, *Chloride accumulation and swelling in endosomes enhances DNA transfer by polyamine-DNA polyplexes.* J Biol Chem, 2003. **278**(45): p. 44826-31.
29. Haensler, J. and F.C. Szoka, Jr., *Polyamidoamine cascade polymers mediate efficient transfection of cells in culture.* Bioconjug Chem, 1993. **4**(5): p. 372-9.
30. Pack, D.W., et al., *Design and development of polymers for gene delivery.* Nat Rev Drug Discov, 2005. **4**(7): p. 581-93.
31. Stekar, J.N., G.; Kutscher, B.; Engel, J.; Hilgard, P., *Synthesis, Antitumor Activity, and Tolerability of Phospholipids Containing Nitrogen Homologues.* Angewandte Chemie International Edition in English, 1995. **34**(2): p. 238-240.
32. Godbey, W.T., K.K. Wu, and A.G. Mikos, *Tracking the intracellular path of poly(ethylenimine)/DNA complexes for gene delivery.* Proc Natl Acad Sci U S A, 1999. **96**(9): p. 5177-81.
33. Tao, Y., et al., *Polycations-functionalized water-soluble gold nanoclusters: a potential platform for simultaneous enhanced gene delivery and cell imaging.* Nanoscale, 2013. **5**(13): p. 6154-60.
34. Sawant, R.R., et al., *Polyethyleneimine-lipid conjugate-based pH-sensitive micellar carrier for gene delivery.* Biomaterials, 2012. **33**(15): p. 3942-51.

CHAPTER 7

Conclusion and Perspectives

The past decade has observed significant advancement in the field of nanobiotechnology. Large number of nanoparticles (NP)-based products have been enormously approved and used for both diagnostic and therapeutic purposes, and more are recently under clinical trials. Among the large numbers of NPs, functionalized NPs are gaining recognition due to the facts that they can be well fitted for the development of targeted and personalized nanomedicines.

For the surface functionalization of NPs, different strategies have been reported making such functionalized nanostructures suitable for grafting therapeutics or diagnostics. In this thesis, we have developed surface modification pathways that can be adopted for varies of nanostructures like nanodiamonds (NDs), silica NPs (Silica-NPs) and magnetic particles (MPs). Surface modification of lipid nanocapule (LNCs), an organic nanomaterial has also been exploited. As an application, we have grafted boronic acid derivative on surface of NDs, Silica-NPs and MPs. These BA-modified particles were shown their ability to inhibit the hepatitis C virus entry.

Since, the level of viral infection inhibition was not satisfactory with the first generation NPs due to the stability issues, LNCs modified with BA ligand were further investigated as potential HCV entry inhibitiors. This study has demonstrated that BA-LNCs inhibit HCVcc as well as HCVpp entry regardless of the genotypes. This verity encourages for the search of more-conserved features of the virus as an attractive targets for the development of antiviral therapeutics. In this work, we have shown that BA-LNCs, a biocompatible nanomaterial, having multiple copies on the surface of LNC can efficiently prevent HCV infection in micromolar range (IC_{50} = 5.4 µM of boronic acid moieties) where as the monomer ABA ligand did not show any significant inhibition even at the highest analyzed concentration (20 µM). Therefore, BA-LNCs could be the alternative for the pre-existing lectins that are considered to be expensive. This finding was further supported by using HCV pseudo-particle (HCVpp) where it is clearly shown the inhibition of different genotypes, which is probably due to the high degree of glycosylation of evelope glycoprotein

of all genotypes. Therefore, this study has brought up the most promising stable and efficient nanocarrier that can be further studied in *in vivo* and apply as a potential therapeutic strategy for blocking viral entry.

In this thesis, we have given special attention to nanodiamonds which are considered as a promising candidate for various biological applications because of its superior biocompatibility nature and an excellent surface chemistry. We have mainly focused on the surface modifications strategies and improvement of NDs stability since they tend to aggregate and form bigger particles which limit its applications. Dopamine derivative–based multifunctional NDs, inspiring from the previous work that has done by our group, have been developed and shown its usefulness for the formation of stable NDs dispersion. The method is based on the orthogonal surface modification strategy of NDs using various dopamine derived anchors. In a proof of principle that post-synthetic modification can be performed on these multifunctional NDs, "click" chemistry between the azide group on the particles and an alkynyl-terminated aminated ligands was performed. This dopamine-derived method opens up different possibilities to graft desirable bioconjugates for various applications. The impressive stability of this particle makes them promising candidates for the biological applications. Indeed, we used these NDs to investigate their cellular transfection ability. The confocal images have validated that the stable multifunctional NDs were better for cellular transfection as compared to other tested NDs. However, detail studies are required to track the endocytosis, protection from nuclease and quantification of transfected cells which could further help to improve the cellular transfection level of ND-based gene delivery system.

The perspectives of such nanostructures are wide. Applications to inhibit biofilm formation and to study sugar/lectin binding events or to inhibit other viral infections such as Human Immunodeficiency Virus (HIV) are and will be under considerations. The future of the interdisciplinary research that brings organic chemistry, nanotechnology and biology together is thus bright.

APPENDIX
EXPERIMENTAL PART

8.1. Materials

Ammonium hydroxide, iron (II) chloride tetrahydrate ($FeCl_2 \bullet 4H_2O$), iron (III) chloride hexahydrate ($FeCl_3 \bullet 6H_2O$), 4-(bromomethyl)-phenylboronic acid, 3-(bromomethyl)-phenylboronic acid, 4-aminophenylboronic acid hydrochloride, 4-pentynoic acid, *N*,*N*'-dicyclohexylcarbodiimide (DCC), 4-dimethylaminopyridine (DMAP), ethylenediaminetetraacetic acid (EDTA), triethylamine, copper iodide (CuI), anhydrous ethanol, dimethylformamide (DMF), 3-hydroxytyramine hydrochloride, sodium nitrite, sulfuric acid (H_2SO_4), sodium hydroxide (NaOH) anhydrous acetonitrile, 4-aminopropyltrimethoxysilane (APTMS) and silicon dioxide nanopowder (10-20 nm particle size, Nr. 637238, silica NP) were obtained from Sigma-Aldrich and used without any further purification. 4-azidobenzoic acid was purchased from TCI Europe, Belgium. Hydroxylated diamond particles (ND-OH particles) were obtained from the International Technology Centre, Raleigh, NC, USA. Lipid nanocapsules were made of Labrafac™ Lipophile WL 1349 (caprylic/capric triglyceride), Phospholipon® 90G (soybean lecithin at 97.1% of phosphatidylcholine), and Solutol® HS15 (a mixture of free polyethylene glycol 660 and polyethylene glycol 660 hydroxystearate) generously provided by Gattefosse S.A.S. (Saint-Priest, France), Phospholipid GmbH (Köln, Germany), and Laserson (Etampes, France), respectively.

8.2. Synthesis of organic compounds and nanoparticles

8.2.1. Copper iodide triphenylphospine ($CuI(PPh_3)$)

$CuI(PPh_3)$ was synthesized as described in the literature [1]. In short, a solution of triphenylphosphine (0.69 g, 2.63 mmol) in 10 mL of acetonitrile was added to a solution of CuI (0.50 g, 2.63 mmol) in the same solvent (50 mL). A complex started to precipitate after a few seconds. The mixture was stirred for 1 h then the precipitate was filtered, washed with acetonitrile and vacuum dried (yield 80%).

8.2.2. Boronic acid (BA)-derivative (1) 4-[(1-oxo-4-pentyn-1-yl)amino]phenylboronic acid

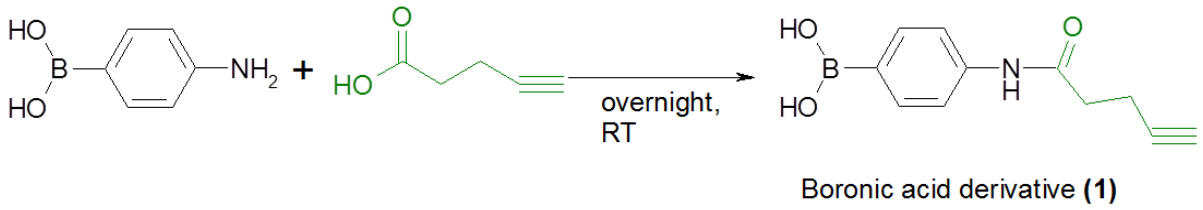

Figure 8.1. Chemical synthesis of BA-derivative **(1).**

BA-derivative (**1**) was synthesized according to the literature with some modifications [2]. 4-pentynoic acid (150 mg, 1.5 mmol) was dissolved in water (5 mL), and the pH of the solution was adjusted to 4.8 with a 0.1 N NaOH solution. 4-Aminophenylboronic acid hydrochloride (312 mg, 1.8 mmol) was dissolved in water (5 mL) in a round-bottom flask, and the pH value of the solution was adjusted to 4.8 using 0.1 N NaOH. EDC (345 mg, 1.8 mmol) was added, and the solution was stirred at 0 °C for 20 min. Then 4-pentynoic acid solution was slowly added to the reaction medium with a syringe, and the reaction mixture was incubated for 1 h in ice, and afterward overnight at room temperature. White precipitate appeared and was collected by filtration. The solid was washed with water (3 times) and finally oven dried at 50 °C for 24 h. The product was isolated as a white solid (260 mg, yield 67%). ^{1}H NMR (300 MHz, DMSO-d_6): δ 10.00 (s, 1H, O=CNH), 7.91 (s, 2H, B–OH), 7.71 (d, *J* = 8.1 Hz, 2H, Ar–H), 7.55 (d, *J* = 8.1 Hz, 2H, Ar–H), 2.81 (t, *J* = 2.5 Hz, 1H, HC≡CR), 2.6 – 2.4 (m, 4H, -CH_2–CH_2-)

8.2.3. 2-nitrodopamine

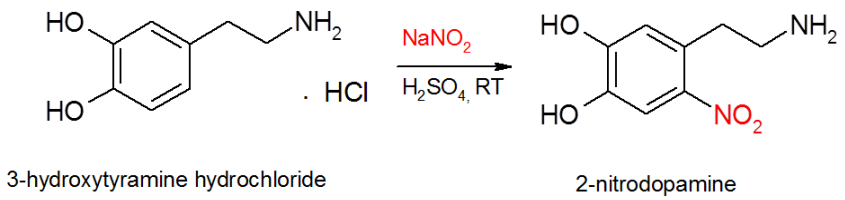

Figure 8.2. Chemical synthesis of 2-nitrodopamine

3-Hydroxytyramine hydrochloride (1.90 g, 10 mmol) and sodium nitrite (1.52 g, 22 mmol) were dissolved in water (25 mL) and cooled to 0 °C. Sulfuric acid (17.4 mmol in 10 mL of water) was added slowly to the mixture, and a yellow precipitate was formed. After stirring overnight at room temperature, the precipitate was filtered and recrystallized from water to give a product as a hemisulfate salt [3]. Yield 1.9 g (77%). ^{1}H NMR (300 MHz, DMSO-d_6): 7.47 (s, 1H, Ar-H), 6.85 (s, 1H, Ar-H), 3.10 (br s, 4H, -CH_2–CH_2-). The product was purified through a column with Dowex ion-exchange resin to get free amine as reddish solid.

8.2.4. Amphiphilic boronic acid (ABA)

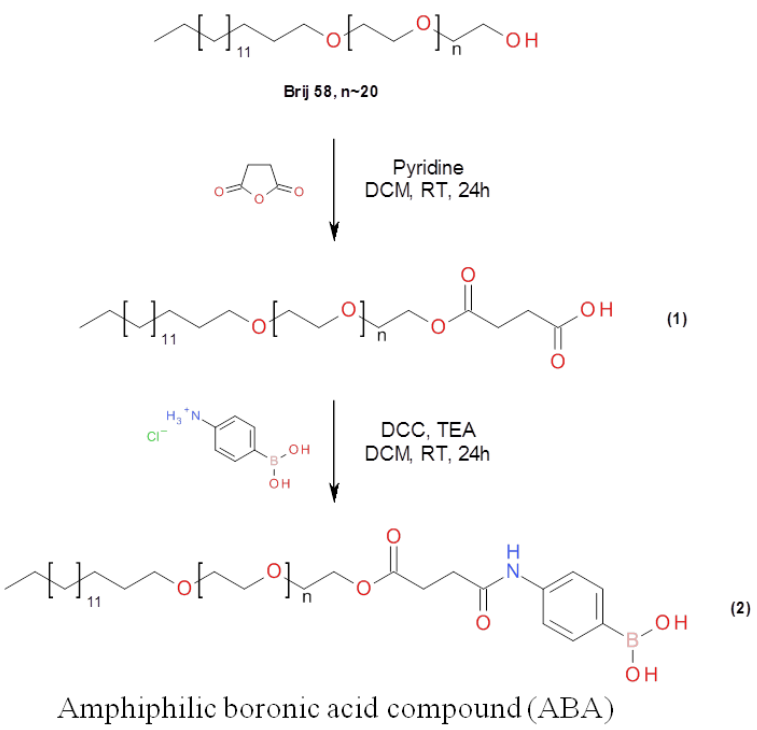

Figure 8.3. Chemical synthetic pathway of ABA.

For the synthesis of compound **(1)**: 2.2 g (2 mmol, 1 equiv) of Brij-58P, 1.2 g (12 mmol, 6 equiv) of succinic anhydride, and 950 µL (12 mmol, 6 equiv) of pyridine were dissolved in 40 mL of dry DCM. The reaction medium was stirred for 24 h and was concentrated under vacuum. The residue was precipitated in dry diethyl ether at 4 °C and then filtred. The resulting solid was collected, dissolved in DCM and again triturated twice with dry diethyl ether at 4 °C. The white solid filtred was dried under vacuum in the presence of

P_2O_5 overnight. 2 g of the acid derivative was collected. Yield: 83%. ^{1}H NMR, $CDCl_3$, ppm: 4.27 (t, 4.5 Hz, 2H); 3.65 (m, 82H); 3.44 (t, 6.9 Hz, 2H); 2.65 (m, 4H); 1.57 (quint, 6.9 Hz, 2H); 1.25 (s, 28H); 0.88 (t, 7.0 Hz, 3H). Compound **(2)**: 450 mg (0.37 mmol, 1 equiv) of compound **(1)** was dissolved in 20 mL of dry DCM with 115 mg (0.55 mmol, 1.5 equiv) of DCC, and 205 µL (1.50 mmol, 4 equiv) of TEA was added. Then, 96 mg (0.55 mmol, 1.5 equiv) of 4-aminophenylboronic acid hydrochloride dissolved in 10 mL of dry DCM was added. The reaction medium was stirred for 24 h and filtered. The organic phase was washed with water, dried with $MgSO_4$ and evaporated under reduced pressure. The crude product was purified on silica gel column (DCM/MeOH 95:5). The white solid was dried under vacuum in the presence of P_2O_5 overnight. 400 g of the boronic acid derivative was collected. Yield: 81% (ratio **(1)/(2)** 1:1 ^{1}H NMR, $CDCl_3$, ppm: 8.56 (s, 0.5H, N*H*); 7.80 (d, 8.1Hz, 1H, Ar*H*); 7.59 (d, 8.1Hz, 1H, Ar*H*); 6.19 (s, 1H); 4.25 (m, 2H); 3.64 (m, 80H); 3.44 (t, 6.7 Hz, 2H); 2.76 (m, 5.5 Hz, 2H); 2.69 (t, 5.5 Hz, 2H); 2.47 (s, 2H); 2-1.5 (m, 6H); 1.25 (s, 28H); 0.88 (t, 6.9 Hz, 3H).

8.2.5. 1-(6-{[2-(3,4-dihydroxyphenyl)ethyl]amino}-6-oxohexyl)triaza-1,2-dien-2-ium (4), (DOP-N_3)

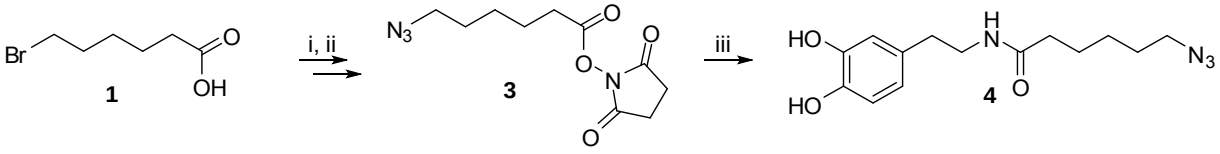

Figure 8.4. Synthetic pathway for the DOP-N_3 Reagents and conditions: (i) NaN_3, DMF, 90 °C, 24h, 85% (yield); (ii) NHS, DCC, RT, overnight, 95% (iii) dopamine hydrochloride, TEA, MeOH, RT, 24h, 68.4 % (yield).

*8.2.5.1.6-azidohexanoic **(2)***

To the bromohexanoic acid (4g, 0.02 mmol) in DMF sodium azide (2.77g, 0.04mmol) and the mixture was heated on the oil bath at 95 C and stirred overnight. Then it was evaporated under reduced presure, dilluted with water and extracted using DCM to give 2.8 g of yellow oil. ^{1}H NMR (300 MHz, $CDCl_3$) δ 3.38-3.27 (t, 2H), 2.46-2.39 (t, 2H), 1.75-1.67 (m, 4H), 1.51-1.44 (m, 2H). MS (ESI): m/z (%) = 182 $[M+Na]^+$.

*8.2.5.2. 6-azidohexanoic N-hydroxysuccinimide ester **(3)***

To the solution of 6-azidohexanoic acid (1.95 g, 0,01 mmol) in DCM

dicyclohexycarbodiimide (2,56 g, 0,01 mmol) and N-hydroxysuccinimide (1,43 g, 0.01 mmol) and this mixture was stirred overnight at room temperature. it was filtrated and the filtrate was evaporated under presure to give 2.8 g 99% (yield) of crude product. ^{1}H NMR (300 MHz, $CDCl_3$) δ 3.35-3.27 (t, 2H), 2.82 (s, 4H, succinimide), 2.65-2.58 (t, 2H), 1.82-1.76 (m, 2H), 1.65-1.60 (m, 2H), 1.54-1.49 (m, 2H). MS (ESI): m/z (%) = 255 $[M+Na]^+$.

8.2.5.3. 1-(6-{[2-(3,4-dihydroxyphenyl)ethyl]amino}-6-oxohexyl)triaza-1,2-dien-2-ium ***(4)***

Dopamine hydrochloride (162.5 mg, 0.86mmol) was mixed with TEA (0.155 ml, 1.12 mmol) in methanol. Then the NHS ester (**3**) (200 mg, 0.86mmol) was added and reaction mixture was stirred overnight at room temperature under argon. After removing solvent by evaporation, water was added. Later, compound (**4**) was extracted using DCM and washed by water. Organic layer was dried with $MgSO_4$ and evaporated under vacuum. Then the residue was purified by flash column chromatography using EtOAc:Hex=3:1 as eluent to give 150 mg 68.4 % (yield) of slightly yellow oil. ^{1}H NMR (300 MHz, DMSO) δ 8.66 (s, 2H), 7.79-7.76 (t, *J* = 10.9, 1H), 6.63-6.60 (d, *J* = 7.9, 1H), 6.55 (s, 1H), 6.43-6.39 (d, *J* = 10.1, 1H), 3.29-3.27 (d, *J* = 6.9, 2H), 3.19-3.12 (q, *J* = 20.5, 2H), 2.05-2.00 (t, *J* = 14.6, 2H), 1.56-1.43 (m, *J* = 36.2, 4H), 1.31-1.23 (d, *J* = 24.5, 2H). ^{13}C NMR (75 MHz, DMSO) δ 165.56 (s), 144.35 (s), 143.25 (s), 135.54 (d), 120.34 (s), 117.33 (s), 114.55 (s), 49.79 (s), 40.57 (s), 35.38 (s), 34.41 (s), 29.53 (s), 25.45 (s), 24.92 (s). MS (ESI): m/z (%) = 319 $[M+Na]^+$.

8.2.6. Polyethylene glycol terminated dopamine derivatives (dop-PEG) (10)

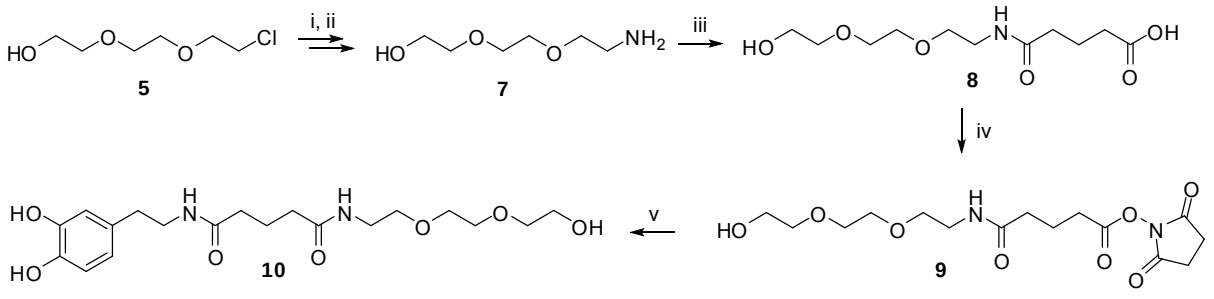

Figure. 8.5. Synthetic pathways for Dop-PEG. Reagents and conditions: (i) NaN_3, DMF, 90 ^{0}C, 24h, 90 % (yield); (ii) Pd/C, H_2, MeOH, R.T, 48h, 96 % (yield); (iii) glutaric anhydride, THF, R.T, 24h, 92 % (yield); (iv) NHS, DCC, R.T, overnight, 83.2 % (yield); (v) dopamine hydrochloride, TEA, MeOH, r.t, 24h .

8.2.6.1. 2-[2-(2-azidoethoxy)ethoxy]ethanol ***(6)***

To the solution of 2-[2-(2-chloroethoxy)ethoxy]ethanol (4.79 g, 0.031) in DMF sodium azide (2g, 0.046 mmol) was added and the reaction mixture was stirred at 90 C for 24h. The mixture was filtered of, evaporated under reduced pressure, diluted with DCM and washed with water, dried with $MgSO_4$ and evaporated to give 4.6 g 90 % (yield) of yellow oil. ^{1}H NMR (300 MHz, $CDCl_3$) δ 3.75-3.68 (broad, 2H) 3.67-3.63 (m, 6H), 3.59-3.57 (m, 2H), 3.39-3.36 (t, 2H). MS (ESI): m/z (%) = 184 $[M+Na]^+$.

8.2.6.2. 2-[2-(2-aminoethoxy)ethoxy]ethanol ***(7)***

2-[2-(2-azidoethoxy)ethoxy]ethanol (4g, 0.025 mmol) and Pd/C (1.3 g) in methanol was srirred 48 h at room temperature under hydrogen. The Pd/C was filtered off and solution was evaporated to give 3.2 g 96 % (yield) as yellow oil. ^{1}H NMR (300 MHz, $CDCl_3$) δ 3.77-3.73 (m, 3H), 3.70-3.67 (m, 5H), 3.65-3.61 (m, 3H), 3.58-3.54 (t, 2H). MS (ESI): m/z (%) = 157 $[M+Na]^+$.

8.2.6.3. 5-({2-[2-(2-hydroxyethoxy)ethoxy]ethyl}amino)-5-oxopentanoic acid ***(8)***

2-[2-(2-Aminoethoxy)ethoxy]ethanol (3.2 g, 0.02 mmol) and glutaric anhydride (2.7 g, 0.02 mmol) were mixed in THF overnight at room temperature. After the solvent was removed by using vaccum evaporator to obtain 5.2 g of yellow oil. ^{1}H NMR (300 MHz, $CDCl_3$) δ 7.35-7.02 (broad, *J* = 49.9, 1H), 6.81-6.69 (t, *J* = 34.4, 1H), 3.80-3.57 (d, *J* = 70.2, 9H), 3.48-3.43 (m, *J* = 15.0, 1H), 2.79-2.74 (t, *J* = 13.4, 2H), 2.47-2.38 (m, *J* = 26.4, 3H), 2.34-2.29 (t, *J* = 16.0, 1H), 2.08-1.96 (m, *J* = 35.6, 3H), 1.87-1.84 (t, *J* = 6.6, 1H). MS (ESI-): m/z (%) = 262 $[M-H]^-$.

8.2.6.4. 5-[(2,5-dioxopyrrolidin-1-yl)oxy]-N-{2-[2-(2-hydroxyethoxy)ethoxy]ethyl}-5-oxopentan amide ***(9)***

Acid **8** (4.6 g 0.0174 mmol) and DCC (3.63 g, 0.0175 mmol) were mixed in the DCM. Later NHS (2.02g, 0.0175 mmol) was added and the reaction mixture was stirred overnight at room temperature. Then the reaction mixture was filtrated and the solvent was evaporated to obtain yellow oil (**9**). This crude product was used in the next step of synthesis without purification. ^{1}H NMR (300 MHz, MeOH) δ 4.4.29-4.21 (s, 1H), 3.76-3.36 (m, 8H), 2.88 (s, 4H), 2.79-2.7 (m, 2H), 2.58-2.52 (m, *J* = 19.8, 1H), 2.47-2.27 (m, 3H), 2.09-2.00 (m, 2H), 1.92-1.85 (m, 1H). ^{13}C NMR (75 MHz, MeOH) δ 170.50 (d), 168.60 (d), 70.17 (s), 68.77 (s),

63.35 (s), 39.00 (s), 34.09 (s), 32.72 (s), 29.49 (s), 25.16 (s, succinic C-C), 20.55 (s), 19.69 (s). MS (ESI): m/z (%) = 367 $[M+Na]^+$.

*8.2.6.5. N1-(3,4-dihydroxyphenethyl)-N5-{2-[2(2hydroxyethoxy)ethoxy]ethyl}pentanediamide (**10**), dop-PEG*

To the solution of dopamine hydrochloride (104.7 mg, 0.76 mmol) and TEA (0.137 ml, 0.98 mmol) in MeOH, compound **9** (200 mg, 0.76 mmol) was added. The mixture was stirred at room temperature for 24 h under argon. Later, the solvent was evaporated and the obtained crude compound was purified by flash column chromatography using EtOAc:MeOH:H_2O = 5:1:0.5 as eluent that gives brown-yellow oil. ^{1}H NMR (300 MHz, MeOH) δ 6.70-6.67 (m, *J* = 4.8, 11.6, 2H), 6.56-6.53 (d, *J* = 8.1, 1H), 4.26-4.17 (m, *J* = 26.1, 1H), 3.75-3.51 (m, *J* = 70.8, 6H), 3.42-3.27 (m, *J* = 43.6, 6H), 2.69-2.59 (t, *J* = 30.3, 2H), 2.37-2.13 (m, *J* = 73.5, 6H), 1.94-1.84 (d, *J* = 28.7, 2H). ^{13}C NMR (75 MHz, MeOH) δ 173.60 (s), 145.95 (s), 144.13 (s), 130.66 (d), 119.69 (s), 115.53 (s), 114.99 (s), 70.12 (s), 69.83 (s), 69.17 (s), 68.76 (s), 63.17 (s), 40.76 (s), 38.92 (s), 34.50 (s), 32.69 (s), 24.88 (s), 21.84 (s), 21.02 (s). MS (ESI): m/z (%) = 421 $[M+Na]^+$.

8.2.7. Silica particles

8.2.7.1. Silica-NH_2

Amine-terminated silica particles (Silica-NH_2) were prepared by sonicating Silica-NPs (60mg) for 30 min. in anhydrous ethanol (20 mL), then APTMS (6 µL) was added and the suspension was stirred for 24 h at room temperature under nitrogen. Silica-NH_2 was obtained by three consecutive wash/ centrifugation cycles at 12,300 rcf (Scanfuge Mini, ORigio). The purified particles were dried in oven at 50 °C overnight.

8.2.7.2. Silica-N_3

4-Azidobenzoic acid (0.20 mmol), DCC (0.22 mmol) DMAP (0.066 mmol) were dissolved in 5 mL anhydrous DMF. A suspension of silica-NH_2 in anhydrous DMF (10 mg in 5 mL) was added to the solution and the mixture stirred at room temperature for 24 h under nitrogen. The azido-terminated silica particles (Silica-N_3) were isolated through consecutive wash/centrifugation at 12,300 rcf with DMF (twice) and ethanol (twice) and finally oven dried at 50 °C for overnight.

8.2.7.3. Silica-BA

The Silica-N_3 (15 mg) were dispersed in 15 mL of anhydrous DMF and sonicated for 40 min. The "click" reaction was carried out by addition of 4-[(1-oxo-4-pentyn-1-yl) amino]phenylboronic acid **(1)** (4 mM) and CuI(PPh_3) (0.4 mM) to the Silica-N_3 suspension and stirred for 48 h at 80 °C. The resulting nanoparticles were separated by centrifugation at 12,300 rcf, purified through consecutive wash/centrifugation cycle at 12,300 rcf with DMF (twice) and 1 mM EDTA water solution (twice), and finally oven dried at 50 °C overnight.

8.2.8. Magnetic particles

8.2.8.1. MP-NH_2

Water dispersion of bare iron magnetic nanoparticles (10 mg/mL, 1 mL), formed as reported previously [3], was mixed with 2-nitrodopamine (7 mg) and sonicated for 1 h at room temperature. The modified particles (MP-NH_2) were isolated by means of a magnet and purified through six consecutive wash/precipitation cycles at 12,300 rcf with water to ensure complete removal of unreacted 2-nitrodopamine.

8.2.8.2. MP-N_3

4-Azidobenzoic acid (0.20 mmol), DCC (0.22 mmol) and DMAP (0.066 mmol) were dissolved in 5 mL of anhydrous DMF and stirred for 1 h at room temperature. A suspension of MP-NH_2 was added and the resulting mixture was stirred overnight at room temperature. The azido-terminated iron magnetic nanoparticles (MP-N_3) were isolated by centrifugation at 12.300 rcf and purified through four consecutive wash/centrifugation cycles at 12.300 rcf with DMF.

8.2.8.3. MP-BA

MP-N_3 (6 mg in 1 mL DMF), 4-[(1-oxo-4-pentyn-1-yl) amino]phenylboronic acid (**1**) (10 mg, 0.0433 mmol), triethylamine (300 µL, 4.3 molar excess) and CuI (1 mg, 0.0052 mmol) were dissolved in 3 mL of DMF and left to stir over week-end at room temperature. The boronic acid-terminated iron magnetic nanoparticles (MP-BA) were isolated by centrifugation at 12,300 rcf and purified through consecutive wash/centrifugation cycles at 13.500 rpm with water (twice), 1 mM EDTA (thrice) and water (thrice).

8.2.9. Nanodiamonds (NDs)

8.2.9.1. ND-N_3

4-Azidobenzoic acid (0.20 mmol), DCC (0.22 mmol) and DMAP (0.066 mmol) were dissolved in 5 mL anhydrous DMF. A suspension of ND-OH particles in anhydrous DMF (10 mg in 5 mL) was added to the solution and stirred at room temperature for 24 h under nitrogen. The azido-terminated ND particles (ND-N_3) were isolated through consecutive wash/centrifugation at 12.300 rcf with DMF (twice) and ethanol (twice) and finally oven dried at 50 °C for overnight.

8.2.9.2. ND-BA

The ND-N_3 (15 mg) were dispersed in 15 mL of anhydrous DMF and sonicated for 40 min. The "click" reaction was carried out by addition of 4-[(1-oxo-4-pentyn-1-yl) amino]phenylboronic acid **(1)** (4 mM) and CuI(PPh_3) (0.4 mM) to the ND-N_3 suspension and stirring the mixture for 48 h at 80 °C. The resulting ND-BA's were separated by centrifugation at 12 300 rcf, purified through consecutive wash/centrifugation cycle at 12 300 rcf with DMF (twice) and 1 mM EDTA water solution (thrice), and finally oven dried at 50 °C overnight.

8.2.10. Lipid nanocapsule

8.2.10.1. Preparation of LNCs

LNCs were formulated at nominal size of 25 nm using a phase inversion method of an oil/water system [4]. Briefly, the oil phase was mixed with the appropriate amounts of Solutol, Phospholipon 90G, NaCl and distilled water, and heated under magnetic stirring up to 85 °C. The mixture was subjected to 3 temperature cycles from 70 to 90 °C under magnetic stirring. Then, it was cooled to 78 °C, 3.3 mL of distilled cold water (0 °C) were added, and the suspension was still stirred at room temperature for another 10 min before further use. The composition of the formulation is summarized in **Table 8.1**. The percentage composition is just the mass percentage of the components for the lipid nanocapsules (a total initial mass of 1.26 g). LNCs were purified from supernatant using disposable PD-10 desalting columns (Sephadex® G-25 for gel filtration as stationary phase, Amersham Biosciences). A column was stabilized with 25 mL of distilled water.

Table 8.1. Composition of the components for the lipid nanocapsules preparation for a total initial mass of 1.26 g

	Labrafac (%)	Solutol (%)	Phospholipon 90G (%)	NaCl (%)	Water (%)
LNC	20.0	32.4	3.0	1.7	42.9

Then 2 mL of a suspension of LNCs were deposited on the column, 0.5 mL of water was added to complete the dead volume of the column, then 4 mL of distilled water eluted and the LNCs were collected in this eluant. The suspension was then dialyzed (pore size: 6000-8000 Da) against deionized water overnight. The solution was freeze-dried and weighed in order to estimate the concentration.

8.2.10.2. Formation of boronic-acid LNCs (BA-LNCs)

BA-coated nanocapsules were obtained by post-insertion method at room temperature. An excess of the amphiphilic compound compared to LNCs was used to reach the highest density of active boronic molecules at the surface (mass ratio of ABA/LNC 1:2). Briefly, preformed nanocapsules (4 mg/mL) were incubated for 24 h with aqueous suspension of ABA (2 mg/mL) under planetary stirring (200 rpm) at room temperature in a final volume 600 µL. After 24 h, the suspension of LNCs decorated by boronic acid molecules was removed and the precipitant composed of the non-incorporated compounds was quantified.

8.2.11. Preparation of dopamine-derived nanodiamonds

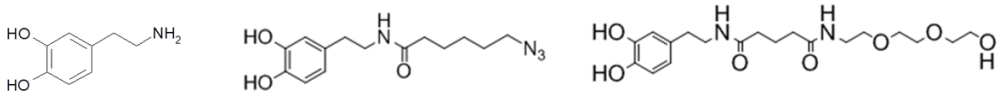

DOP-NH_2 DOP-N_3 DOP-PEG

Figure 8.5. Chemical structure of different dopamine derivatives used for the surface modification of NDs.

Dop-NH_2 (1), Dop-N_3 (2) or a mixture of Dop-N_3 (2) /Dop-PEG (3) and in equal molar mass (6 mM) were addded to a suspension of ND-OH particles in dry acetonitrile (ACN) (5 mg mL^{-1}), sonicated in a ice bath with a horn-type sonotrode (3 x 10 min, amplitude: 70%) for 8 hours in dry ACN and then stirred at room temperature for 12h. The functionalized ND particles were separated by centrifugation at 10.000 rpm, purified through four consecutive wash/centrifugation cycles at 10.000 rpm with ACN and finally oven-dried

(50 °C). Later azide terminated mixed NDs were further preceded for the 'click' chemistry protocol that had been used for the preparation of ND-BA. Alkynyl dimeric amine compound was used to 'click' the azide terminated NDs and the compound was kindly provided by Dr. Aloysius Siriwardena.

8.2.12. Preparation of amine terminated NDs from silanization method (ND-sil-NH_2)

Commercially available hydroxylated NDs (ND-OH) were dispersed in MQ water and sonicated for 6 hours and it was centrifuged and dried overnight at 50 °C. Next day, the ND-OH particles (5 mg) are suspended in dry acetone (2 mL) and sonicated for an hour. 10 % of APTES was added on the suspension and stirred for 48 hours at room temperature. Following three washes with acetone, particles were dried overnight at 50 °C.

8.3. Determination of the amount of active boronic acid on the NPs-BA

8.3.1. ND-BA, MP-BA and Silica-BA

The boronic acid modified particles (2 mg) were mixed with 5.5 mM solution of mannose (total volume 1 mL) for 1h to link the mannose to the boronic acid functions. The amount of linked mannose was determined by treatment with a phenol/H_2SO_4 solution as described previously [4]. First, a calibration curve for mannose in solution was established using a phenolic aqueous solution (5 wt%, 60 µL), concentrated H_2SO_4 (900 µL) which was added to an aqueous mannose solution (60 µL), stirred for 10 min and then an absorption spectrum was recorded (Perkin Elmer *Lambda 950 dual beam) against a blank sample (without mannose)*. The absorbance of the solution was measured at two wavelengths: λ_1=485 and λ_2=570 nm and the absorbance difference (A_{485}–A_{570}) plotted against the concentration of mannose. The quantity of surface-linked mannose was determined with 60 µL of the corresponding particles solution in water (2 mg mL^{-1}), treated with phenol/H_2SO_4 following the same protocol as described above.

8.3.2. BA-LNCs

UV/vis spectroscopy was used to detect the phenylboronic acid moieties incorporated into LNCs. UV-vis spectroscopic measurements were carried out on a Perkin-Elmer Lambda 950 dual-beam spectrophotometer operating at a resolution of 1 nm in the region 230-310 nm. Amphiphilic boronic acid compound (ABA) in dichloromethane shows an absorption band with a

maximum at 259 nm. A calibration curve of different concentrations of ABA in dichloromethane (12.5 to 100 µg/mL) versus the intensity of the absorption at 259 nm was established. The amount of incorporated boronic acid was calculated by measuring the concentration of the non-incorporated ABA in dichloromethane and substracted from the initial ABA concentration of 2 mg/mL.

8.4. Stability study of NDs in MQ water

1 mg/mL of NDs suspension was prepared in MQ water. After 1 hr of sonication, 500 µL of the suspension was transferred in a vial and photographs were taken in each 0, 1, 2, and 24 h. Likewise, particle size was measure using zetasizer nano in 0, 1, 2, 3, 4 and 24 h.

8.5. Preparation of NDs/pDNA complexes

Different NDs/pDNA complexes were prepared by adding increasing amount of NDs into 1 ug/ mL of pDNA solution in MQ water. After incubating for 30 minutes at room temperature, particle size and zeta potential were measured at 25 °C with an equilibration time of 2 minutes using zetasizer nano. Three independent experiments were done for each condition.

8.6. Gel retardation

The condensation ability of modified and commercial NDs with pDNA was assessed by gel retardation assay. The complexes containing pDNA (1 µg in a final volume of 20 µL) were prepared in water at NDs/pDNA ratio of 60 to 1. After 30 min of incubation at room temperature, electrophoresis was carried out with 1% agarose gel (w/v) containing ethidium bromide in 1X Tris–acetate–EDTA (TAE) buffer at 90 V for 50 min. The retardation of complexes was visualized on a UV trans-illuminator using a Gel Doc System. The values represent the weight ratios of NDs/pDNA in a 20 mL volume.

8.7. Biological assays

8.7.1. Cell culture

HEK293 and Huh-7 cells were cultured in Dulbecco modified Eagle medium (DMEM) supplemented with 10 % heat-inactivated fetal calf serum (FCS), 100 U/mL penicillin, and 100 µg/mL streptomycin**.**

8.7.2. Cytotoxicity assay

Huh 7 cells were seeded in 96 wells plate at a density of 7.10^3 cells per well a day before assay. The medium was replaced with fresh medium containing the particles of desired concentrations and incubated for 48 h. After, MTS assay was performed as described by the company (CellTiter 96 AQueous One Solution cell proliferation assay; Promega). First the cells were washed with PBS once then, cell medium was changed with 20 % of MTS solution prepared in fresh medium and incubated for 30 to 45 min. The optical density of each well was measured using a microplate reader, with absorbance detection at 490 nm. Each condition was replicated for four times and wells without particles were taken as negative control**.**

Similarly, in case of transfection study cytotoxicity was performed by using MTT assay. For this, HEK293 cells were seeded in 96 wells plate at density of 7.10^3 cells per well a day before assay. Cells were incubated with particles and particle/DNA complexes for 4 hours in serum free medium and later particles and particle/DNA complexes were washed off and cells were further incubated with complete medium for 24 hours before performing MTT assay. Later, the medium was replaced and10 µL of MTT solution (12 mM in sterile PBS) was added in each well and incubated for 4 h at 37°C. Then medium was carefully removed and formed formazan crystals were solubilized with DMSO (50 mL). The absorbance of each well was read on a microplate reader (PHERAstar FS, BMG LABTECH) at 540 nm. Wells without particles were taken as negative control. Each condition was performed in triplicates and average and standard deviation were calculated from three independent experiments.

8.7.3. Virus entry inhibition assay

For experiments with HCV, we used a modified JFH1 virus containing mutations at the C-terminus of the core protein leading to amino acid changes F172C and P173S, which have been shown to increase the viral titers [5] and mutation in E1 glycoprotein to reconstitute the A4 epitope (SSGLYHVTNDC) as described previously [6]. JFH1 virus was pre-incubated with different concentrations of nanoparticles for an hour at room temperature. Then the virus/particle complexes were incubated with Huh-7 cells [5] that were seeded at a density of

3.10^4 cells/well a day before in 24-well plates containing microscopy coverslip. Two hours later, infected cells were washed 2 times with PBS to remove complexes completely, and they were further incubated for 48 h with fresh medium. After 48 h cells were fixed with 100 % methanol (-20°C) and the percentages of infected cells were determined by immunofluorescence using a monoclonal antibody (primary) recognizing HCV glycoprotein E1 (A4 epitope) and likewise secondary antibody carrying fluorophore (CY-3 tagged goat anti-mouse) that recognizes primary antibody [7]. Nucleus was labeled by using 4'-6-diamidino-2-phenylindole (DAPI), a DNA-specific fluorochrome. Infected cells were labeled by CY-3. Five images (for both nucleus and infected cells) were collected from different area of each coverslip by using a fluorescent microscopy (Zeiss Axiophot 2). Further, total number of cells and infected cells from each image were counted by using Image J. Percentage of infected cells were calculated by using formula below,

$$\%\ \text{infected cells in each conditions} = \frac{\text{total number of infected cells}}{\text{total number of cells}} \times 100$$

$$\%\ \text{infected cells compared to negative control in each conditions} = \frac{\%\ \text{infected cells in each tested conditions}}{\%\ \text{infected cells of negative control}} \times 100$$

All the conditions were tested in duplicate. Conditions without particles were taken as negative control.

To determine the nanostructured boronic acid specifically acts on the entry of virus, lipid nanocapsule decorated with boronic acid was added at different time points before, during and after inoculation of Huh-7 cells with JFH1.

8.7.4. Competitive assay with mannose and Man-9

BA-LNCs containing 620 µM of BA moieties was incubated with 520 µg/mL of mannose (2889 µM) in excess, likewise BA-LNCs containing 382 µM of BA moieties was incubated with 190 µg/mL of N-linked high mannose oligosaccharides mannonanose-di-(*N*-acetyl-D-glucosamine) (Man-9, 162 µM) at room temperature for one hour and later further required dilutions were carried out to pre-incubate this sugar coated-BA-LNCs with HCVcc at room temperature. 1 h later, Huh-7 cells were infected for 2 hours at 37 °C with these nanoparticles/virus complexes. After 2 h of infection, the complexes were washed away and

replaced with fresh cell culture medium. Immunofluorescent assay was carried out 48 h later to score the infected cells.

8.7.5. HCV pseudotyped particles (HCVpp)

The luciferase-based HCV pseudotyped (HCVpp) retroviral particle infection assay was used to further confirm the effect of BA-LNCs on the HCV entry. These are retroviral cores carrying HCV glycoproteins in their envelope [8]. In this context only the early steps of the viral life cycle, i.e. virus interaction with receptors, uptake and fusion, are HCV specific, whereas all later steps are dependent on the retroviral nucleocapsid elements, and luciferase expressed from the retroviral genome is measure to determine HCVpp entry efficiency. The following plasmids encoding HCV envelope glycoproteins of different genotypes kindly provided by J Ball (Nottingham University, UK) were used in this work: UKN2B-1.1 (genotype 2b), UKN4-11.1 (genotype 4), UKN6-5.340 (genotype 6) [9]. In addition, the plasmid encoding HCV envelope glycoproteins from genotype 2a (strain JFH-1) was kindly provided by T. Pietschamnn and R. Bartenschlager (University of Heidelberg, Germany). The plasmid encoding HCV envelope glycoproteins from genotype 1a (H77) has been described previously [8]. As a control, retroviral particles pseudotyped with vesicular stomatitis virus glycoprotein G (VSVg) was used. The level of infection was determined by using luciferase assay. Briefly, the particles at different concentrations were incubated with the pseudoparticles for 1 h at room temperature then the Huh 7 cells were infected by the particle/virus complex. Infection time was set for 2 h in case of HCVpp and 1 h for VSVg. Later, the complex was replaced with fresh cell culture medium and intracellular firefly luciferase signal was measured after 72 h of incubation and normalized to untreated conditions.

8.7.3. *In vitro* transfection studies

HEK293 cells were maintained in DMEM supplemented with 10% FBS and penicillin/streptomycin in a 5% CO_2 atmosphere at 37 °C. Cells were seeded into 12-well plates (2.10^5 cells per well) 48 h before experiments. Cells were washed with PBS, maintained in serum-free medium and incubated for 4 h in a CO_2 atmosphere at 37°C in the presence of NDs/pDNA complexes. After incubation, cells were washed three times with PBS and then maintained in DMEM supplemented with 10% FBS for 24 h. GFP expressed cells were observed by confocal microscopy and the quantified with flow cytometry.

8.8. Instrumentations

8.8.1. Fourier transformed infrared spectroscopy

Fourier transform infrared (FT-IR) spectra were recorded using a ThermoScientific FTIR instrument (Nicolet 8700) with a resolution of 4 cm^{-1}. Dried nanoparticles (1 mg) were mixed with KBr powder (100 mg) in an agate mortar. The mixture was pressed into a pellet under 10 tons load for 2-4 min and the spectrum was recorded immediately. Sixteen accumulative scans were collected. The signal from a pure KBr pellet was subtracted as a background.

8.8.2. X-ray photoelectron spectroscopy

X-ray photoelectron spectroscopy (XPS) measurements were performed in a Specs analysis chamber, equipped with a monochromatized Al K_α X-ray source ($h\nu$ = 1486.74 eV) and a Phoibos 150 mm radius hemispherical electron energy analyzer. The analyzer (constant) pass energy was set to 100 eV for survey spectra and at 20 eV for high resolution scans, with an estimated total (source + analyzer + core hole width) resolution of 0.85 eV for the latter case (for the N 1s spectra). The pressure in the analysis chamber was in 10^{-8} Pa vacuum range, and an electron flood gun operating at 1 eV energy and 100 µA electron current was used to ensure sample neutralization. Electrons are recorded at normal emission in "Large Area Mode" of the Phoibos analyzer. The data are deconvoluted by using mixed Lorentz/Gauss profiles with the CasaXPS software.

The samples were prepared by casting 50 µL aqueous suspensions of nanoparticles on a clean silicon wafer and followed by drying under room temperature.

8.8.3. Particle size measurements

Particle suspensions (40 $\mu g.mL^{-1}$) in water were sonicated. The particle size of the nanoparticles suspensions was measured at 25°C using a Zetasizer Nano ZS (Malvern Instruments S.A., Worcestershire, U.K.) in 173° scattering geometry and the zeta potential was measured using the electrophoretic mode.

8.8.4. Confocal microscopy

Transfected cells were washed with warm PBS, and fixed with 4% paraformaldehyde at room temperature for 15 min. Cells were then washed three times with PBS, mounted and

observed using a Nikon A1-R (Nikon Instruments, Tempe, AZ) laser confocal microscope (Nikon Ph1 DLL 10_/0.30 Plan Fluor objective) excited at 488 nm.

8.9. References

1. Wang, Y., et al., *Click chemistry for facile immobilization of cyclodextrin derivatives onto silica as chiral stationary phases.* Tetrahedron Letters, 2008. **49**(35): p. 5190-5191.
2. Kanayama, N.K., H., *Interfacial Recognition of Sugars by Boronic Acid-Carrying Self-Assembled Monolayer.* Langmuir, 2000. **16**: p. 577-583.
3. Mazur, M., et al., Nanoscale, 2013. **5**(7): p. 2692-2702.
4. Heurtault, B., et al., *A novel phase inversion-based process for the preparation of lipid nanocarriers.* Pharm Res, 2002. **19**(6): p. 875-80.
5. Delgrange, D., et al., J Gen Virol, 2007. **88**: p. 2495-2503.
6. Goueslain, L., et al., J Virol, 2010. **84**: p. 773-787.
7. Dubuisson, J., et al., J Virol, 1994. **68**: p. 6147-6160.
8. Bartosch, B.D., J.; Cosset, F. L., *Infectious hepatitis C pseudo-viruses containing functional E1E2 envelope protein complexes.* J. Exp. Med., 2003. **197**: p. 633-642.
9. Lavillette, D., et al., *Characterization of host-range and cell entry properties of the major genotypes and subtypes of hepatitis C virus.* Hepatology, 2005. **41**(2): p. 265-74.

LIST OF PUBLICATIONS

- Khanal M, Vausselin T, Barras A, Bande O, Turcheniuk K, Benazza M, Zaitzev V, Teodorescu CM, Boukherroub R, Siriwardena A, Dubuisson J, and Szunerits S; (2013) Phenylboronic-acid-modified nanoparticles: Potential antiviral therapeutics. ACS Appl Mater Interfaces, 5(23), 12488-12498.

- Turcheniuk K, Khanal M, Motorina A, Subramanian P, Barras A, Zaitsev V, Kuncser V, Leca A, Martoriati A, Cailliau K, Bodart JF, Boukherroub R and Szunerits S; (2014) Insulin loaded iron magnetic nanoparticle–graphene oxide composites: synthesis, characterization and application for *in vivo* delivery of insulin: RSC Advances, 4, 865-875.

- Khanal M,, Barras A, Vausselin T, Fénéant L, Boukherroub R, Siriwardena A, Dubuisson J, and Szunerits S; (2014) Boronic acid-modified lipid nanocapsules: novel platform for highly efficient inhibition of hepatitis C viral entry. Nanoscale (revision submitted)

- Khanal M, Larsonneur F, Raks V, Barras A, Baumann J-S, Martin FA, Boukherroub R, Ghigo J-M, Mellet CO, Zaitsev V, Fernandez JMG, Beloin C, Siriwardena A, Szunerits S; (2014) Inhibition of type 1 fimbriae-mediated *Escherichia coli* adhesion and biofilm formation by trimeric cluster thiomannosides conjugated to diamond nanoparticles. (submitted)

- Siriwardena A, Khanal M, Barras A, Bande O, Mena-Barragan T, Mellet CO, Fernandez JMG, Boukherroub R, Szunertis S; (2014) Unpreceented functional switch from substrate to inhibitor of glycosyl hydrolases, engineered through multivalent presentation of simple *O*-glycosides on nanodiamond edifices. (submitted)